NASA CONTRACTOR REPORT

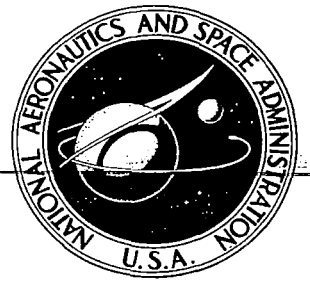

NASA CR-1695

A STUDY OF THE USE OF LIQUID BASE FOAMS FOR JET NOISE REDUCTION

by L. Manson, S. Lieberman, and H. L. Burge

Prepared by
TRW SYSTEMS GROUP
Redondo Beach, Calif. 90278
for Langley Research Center

NATIONAL AERONAUTICS AND SPACE ADMINISTRATION • WASHINGTON, D. C. • FEBRUARY 1971

1. Report No.	2. Government Accession No.	3. Recipient's Catalog No.
NASA CR-1695		

4. Title and Subtitle	5. Report Date
A STUDY OF THE USE OF LIQUID BASE FOAMS FOR JET NOISE REDUCTION	February 1971
	6. Performing Organization Code

7. Author(s)	8. Performing Organization Report No.
L. Manson, S. Lieberman, and H. L. Burge	NA
	10. Work Unit No.

9. Performing Organization Name and Address	11. Contract or Grant No.
TRW Systems Group One Space Park Redondo Beach, California	NAS1-9426
	13. Type of Report and Period Covered
12. Sponsoring Agency Name and Address	Contractor Report
National Aeronautics and Space Administration Washington, D. C. 20546	14. Sponsoring Agency Code

15. Supplementary Notes

16. Abstract

The results presented are of an experimental investigation of the acoustical properties of liquid base foams and of jet noise reduction through foam injection. Results are given for an analytical effort to build a mathematical model of the sound propagation and absorption of foams. The experimental investigation showed attenuation constants on the order of 3 nepers/inch (118 nepers/m). Jet noise reduction values up to 10 PNdB were recorded. The analytical effort confirmed the hypothesis of a resonant response of foams to sound waves. The overall results indicate foam has a high potential as a sound attenuation medium.

17. Key Words (Suggested by Author(s))	18. Distribution Statement
Jet Exhaust Noise Jet Noise Attenuation Foam Injection	Unclassified - Unlimited

19. Security Classif. (of this report)	20. Security Classif. (of this page)	21. No. of Pages	22. Price*
Unclassified	Unclassified	144	$3.00

*For sale by the National Technical Information Service, Springfield, Virginia 22151

FOREWORD

This report was prepared by the Science and Technology Division of TRW Systems Group at One Space Park, Redondo Beach, California, under Contract NAS 1-9426. The contract was administered by the Langley Research Center of the National Aeronautics and Space Administration, Hampton, Virginia. The NASA project manager was J. W. Cawthorn.

Peter Verenkoff collected and reduced the acoustical data in the standing wave experiments. Larry Hynek and Joe Mark built the foam generators and assembled the nitrogen flow systems.

Discussions with Dr. C. T. Molloy on acoustical measurements were interesting and helpful.

The acoustic measurements in the reverberation chamber and in the jet noise experiments were made and the data reduced by

J. P. Ortega and P. Gonzales
of Western Electro-Acoustic-Laboratory, Incorporated
1711 Sixteenth Street, Santa Monica, California

SUMMARY

An experimental investigation has been made of the sound absorbing properties of liquid base foams and of their ability to reduce jet noise. An analytical study was also conducted of the sound absorption mechanisms in foam, based on the foam's measured acoustic properties.

The investigation included measurements of absorption coefficients with plane waves and in diffuse sound fields. Liquid foams showed excellent sound absorption qualities, especially in the high audible range of frequencies; absorption coefficients up to 0.9 were measured. The intrinsic acoustic properties of foams, e.g., the characteristic impedance and the propagation constant, were also measured. The attenuation constants were on the order of 118 nepers/m (3 nepers/inch).

A mechanical analog of the behavior of foam under the action of plane sound pressure waves was developed and a corresponding electric transmission line type network was established. Analysis of the analogs showed that a resonant response of individual bubbles coupled to neighboring bubbles by a damped spring-like mechanism accurately describes the sound propagation and absorption mechanism in foams.

The sound emitted by a 1-inch diameter (0.0254 m) cold nitrogen jet was measured for a subsonic (300 m/sec, 985 ft/sec) and a supersonic (442 m/sec, 1450 ft/sec) jet. Noise reduction up to 10 PNdB was measured. The principal results were:

- Foam injection reduces noise under all conditions.
- Noise reduction is greater the higher the noise level.
- The effects are most pronounced in the high frequencies.
- Directivity is affected by the foam injection.
- Foam injection attenuates high frequency sound in all directions; in some instances low frequency sound emission is increased in the direction of small angles with the jet axis.

CONTENTS

CONTENTS (Continued)

LIST OF SYMBOLS

A	area (m^2)
B	Rayleigh's dissipation function
b	dissipation coefficient (N-sec/m)
c, C	sound velocity (m/sec)
C'	mechanical compliance per unit length [(m/N)/m]
C	capacitance
D	diameter
EXP	expansion ratio ($\rho_{liquid}/\rho_{foam}$)
f	frequency (Hz)
F	thrust (N)
k_1, k	spring constant (N/m)
K'_m	spring constant per unit length [(N/m)/m]
L	length (m)
L	inductance
L	Langrangian
m	mass (kg)
M'_m	mass per unit length (kg/m)
M	Mach number
M_c	convection Mach number
n	ratio of sound pressure maxima to minima
N	noisiness (noys)
P, p	pressure (N/m^2)
R	radius (m)
R	resistance
R_m	mechanical responsiveness per unit length
r	reflection coefficient

t	time (sec)
U	$= \alpha'^2 - \beta^2$
V	velocity (m/sec)
v	particle velocity (in/sec)
v	elementary volume change
V	volume
V	$= 2\alpha'\beta$
$\dot{w}$	flow rate (kg/sec)
X_o	real part of Z_o
y_1, y_2	distance from sample surface of first and second pressure minima
Y_o	imaginary part of Z_o
Y	impedance
Z_1	surface impedance (ρC units)
Z_o	characteristic impedance (ρC units)
Z_{air}	characteristic impedance of air (ρC x area)

Greek Letters

α	absorption coefficient
α'	attentuation constant (nepers/m)
α	eddy lift time factor
β	phase constant (radians/m)
γ	propagation constant (m^{-1})
γ	ratio of specific heats
Δ	phase angle of r
δ	damping coefficient
Σ	error
θ	angle (rad)
θ	volume ratio

θ	mass ratio
λ	wavelength (m)
μ	dynamic viscosity (N-sec/m^2)
ν	μ/ρ Kinematic viscosity (m^2/sec)
ρ	density
ρ_o	density of air
σ	surface tension (N/m)
σ	real part of tanh γL
τ	imaginary part of tanh γL
Φ_{Z_1}	phase of Z_1
ω	angular velocity (rad/sec)

Subscripts

f	foam
g	gas
i	incident
j	jet
l	liquid
r	reflected
r	at resonance
o	undisturbed value
o	stagnation
o	in air

A STUDY OF THE USE OF LIQUID BASE FOAMS FOR JET NOISE REDUCTION

by L. Manson, S. Lieberman and H. L. Burge

TRW Systems Group

1. INTRODUCTION

1.1 BACKGROUND

Increasing aviation requirements in terms of usage, larger aircraft, and/or higher powered engines have resulted, in general, in an increased aerodynamic related noise problem, to the point that it has attracted concerted public attention. Though the problem has existed for many years, its complexities have made progress for jet engine noise alleviation relatively slow. Concerted research efforts to provide a basis for engine design have lagged actual engine development. During the past two decades, excellent progress has been made in the theoretical understanding of the sources of such noise. Attempts to alleviate the problem have taken essentially two major directions, mechanical and fluid dynamic. In the mechanical area the use of multiple nozzles, spike nozzles, slit nozzles and internal acoustically treated ducts are primary examples. The bypass fan is a notable achievement of the fluid dynamic approach as is the use of secondary ingestion to affect mixing shear layers. The fluid dynamic approach has indicated that machinery component design based upon acoustic fluid mechanics can be promising in the reduction of noise associated with jet engines.

The use of other means of nearly passive techniques in alleviating jet engine noise, such as by the injection of water and solid particles, has been suggested; experimental investigations have been made of water injection into jet exhausts. The results have not indicated sufficient noise reduction for the amount of injectant required.

The use of foamed liquids as a means of attenuating noise associated with jet engines has apparently not been investigated. In this concept a foamed liquid is injected into the periphery of the exhaust jet to envelop it and provide a means of sound absorption as well as shear gradient moderation. The concept may also be considered for internal duct flow wherein it is envisioned to behave like a mechanically treated acoustic liner. The use of the foamed liquids as a means of noise control is in the general category of fluid dynamic treatment.

Early in 1968 TRW Systems began investigations of the use of foamed liquids and foamed propellants as potential means of cooling rocket engines. In this concept a separate fluid or one of the propellants is introduced onto the rocket combustion internal wall as a foamed liquid. The foamed liquid is then allowed to be aerodynamically shear dragged along the wall to provide a continuous liquid foam surface coverage. Superior insulating properties of the foam provide excellent thermal protection to the wall.

Both water and amine base foams were found to perform satisfactorily in the rocket evaluations (Reference 1). These investigations led to means of generating foamed liquids with ultrahigh bulk viscosity, low thermal conductivities, and controllable densities.

Examination of the combustion noise levels in the experimental rocket engines with and without foam on the wall revealed that the apparent peak-to-peak pressure oscillations were appreciably reduced in the liquid foam tests. These observations led to the formulation of the hypothesis that foamed liquid barriers should be excellent acoustic energy absorbers in high sound fields. Brief laboratory jet experiments confirmed that this hypothesis was correct. The exact nature of the dissipation mechanism was not formulated; however, it was felt that the foam bubble matrix had available in it several potential dissipating mechanisms; i. e., gas pump work in bubble dilation, surface tension work in dilation, viscous dissipation, reradiation of sound and mass transfer. Further, this matrix should exhibit resonance behavior and be tuneable through control of the bubble size in the matrix.

The reported effort provides a summary of detailed investigations of the use of foamed liquids as a potential fundamental means of noise attenuation. The properties of foamed liquids, which may affect the potential of control of jet engine generated noise, are briefly reviewed; a discussion of the TRW Systems experience in generating applicable foams is included.

1. 2 PROGRAM OBJECTIVES

No prior work on the acoustical properties of liquid base foams was found in the literature. Therefore, the first objective of the present program was to determine experimentally the absorption coefficients of various foams, as measured by classical methods.

Secondly, a better understanding of the ways in which foams absorb sound was needed to develop the concepts basic to an abatement technology. For this effort it was found that classical sound absorption coefficients are not sufficient. A more complete characterization of foams, e. g., their characteristic impedances and propagation constants, were needed.

One of the most promising sound abatement applications is to jet noise suppression. Hence, a series of experiments on a small cold jet were conducted as possible preliminary work on larger, hot jets. The influence of foam type and injection geometry, as well as that of foam flow rate, were explored; insight to the sound suppression mechanisms was sought.

The experimental determination of the acoustic properties of foam is described in Section 2 of this report. Section 3 is devoted to the investigation of a model for the sound absorption mechanisms. The jet noise reduction experiments are described in Section 4.

1. 3 PROPERTIES OF FOAMS

The types of foams considered in this work are those in which the foam in a gross sense appears to be homogeneous, i. e., gas bubbles are small and "smoothly" dispersed throughout the liquid. As such, these foams are an aglomeration of gas bubbles separated from each other by thin liquid films (Reference 2). The scientific aspects of foamed liquids have been studied for many years and are set forth in several books and review articles (References 2 through 6). Discussions pertinent to the program are summarized below.

1. 3. 1 Foaming Parameters

The structure of foam and its physical properties depend on the mode of gas dispersion as well as on the following parameters

- Type of foaming agent
- Concentration of foaming agent
- Volumetric ratio of gas and liquid
- Gas constituent

During the past 20 to 30 years, foam agent technology has made great strides. The predominant type of foaming agent that has evolved as the best is a protein hydrolysate made from, for example, hoof and horn meal, soybeans, animal blood, or fish meal (Reference 7). The finished product, which contains additives such as a bactericide to forestall putrefication, freezing point depressants for temperature as low as -40°F, or metal salts to increase bubble strength, becomes a concentrated liquid to be added to water at a rate of 3 or 6 percent. An excellent review of storage life and utility of protein type foaming agents under various environments is given in Reference 8. Most agents meet certain military specifications and in one instance liquids were in good condition after 15 years or more.

In the past several years many new types of foaming agents have been developed and marketed. National Foam System, Inc. (References 9 and 10) perfected a foamed polymeric film produced by agitating a solution of water and a linear low molecular weight polymer with air which is further reacted by a catalyst in the presence of air. The foam was specifically developed to combat alcohol and amine type fires. The protective inert polymeric film is resistant to solvent attack whereas the protein films are not. The foaming agent is marketed in two separate containers – a 100 percent concentrate and a 3 percent catalyst.

Another industrially important foaming agent is a synthetic detergent type which, when added to water, is capable of forming a truly high expansion foam of approximately 1000 parts of air by volume to 1 part of liquid. This represents an increase in expansion of approximately two orders of magnitude over the conventional protein or polymeric formula. The above three types of foaming agents have been used in this investigation. No additional surface chemistry efforts were accomplished in this program.

The concentration of the foaming agent affects the stability and heat resistance of the foam if concentrations less than those specified in the preceding paragraphs are used. The basic effect of the foaming agent is to reduce dramatically the surface tension of the water until the optimum concentration is reached. A rapid variation of surface tension with surface active agent concentration is fundamental to the ability of a liquid to foam.

The ratio of the volume of foam (gas + liquid) to the volume of the liquid is another fundamental foam parameter and is called the expansion ratio. Expansion ratio can also be expressed as foam density and primary effects of temperature and pressure on expansion ratio or foam density can be estimated from the ideal gas law. Laboratory studies (References 11, 12, 13, and 7) show that physical properties such as thermal conductivity, viscosity, and drainage (stability), vary widely with expansion ratio as discussed below.

1. 3. 2 Foam Density

The expansion ratio is defined as

$$EXP = \frac{V_{foam}}{V_{liquid}}$$

The density of foam is, therefore,

$$\rho_f = \frac{\rho_L}{EXP}$$

The density may decrease somewhat at first because of the growth of large bubbles at the expense of smaller bubbles (Section 1. 3. 7); it will eventually increase because of bubble collapse. Density as a function of expansion ratio was obtained in this study by weighing freshly generated samples of foam.

An interesting method for measuring density was proposed by N. O. Clark (Reference 14) who found that the ratio of electrical resistivity of the foam to that of the liquid was linearly related to the foam/liquid density ratio. Since the electrical conductivity measurement can be made continuously near the point of foam production, it should be far superior to weighing foam samples to obtain foam density.

1. 3. 3 Ultimate Shear Stress and Viscosity

The ultimate shear stress (stress for no flow condition), as well as bubble size distribution, are determined by the amount of mechanical work done in the foam. Hence for a given expansion ratio, bubble size governs the ultimate shear stress. It is not known how bubble size affects viscosity or other physical properties of the foam, but one can conjecture that the effect will be substantial.

The effect of pressure (in other words, expansion ratio or foam density) on viscosity is shown in Figure 1.1 as taken from Grove, Reference 11. At an expansion ratio of approximately 6, the viscosity of the foam is approximately 24 times greater than that for water. Grove studied only one foaming agent type and one concentration level. He did not report varying the bubble size (ultimate shear stress) which may be a primary variable. French (Reference 12) does not explain how he measured ultimate shear stress.

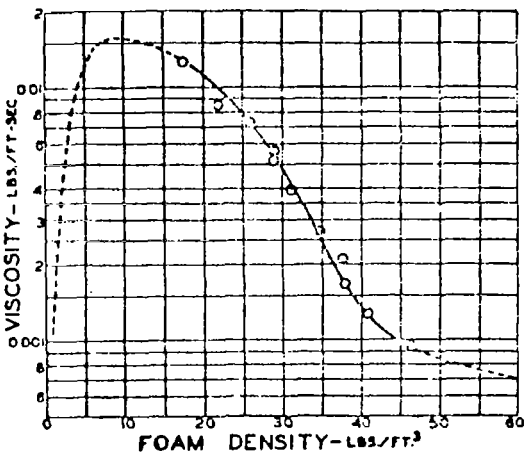

Figure 1-1. Effect of Pressure on Foam Viscosity

Foam viscosity was not measured in the present investigation.

An attempt was made to measure ultimate shear stress by means of an inclined plane of variable inclination angle on which a slab of foam could slide. It became rapidly evident that such a measurement was not useful, since fresh foam would not slide at first; it started to move easily after a short interval of time during which some liquid drained to the surface of the foam in contact with the plane. At that time, the motion of the foam was characterized by the liquid in the boundary layer rather than by any foam property.

1.3.4 Insulating Qualities of Foams

Foams are extensively used in fire fighting because they offer a unique combination of properties:

- Low thermal conductivity
- High resistance to destruction by heat radiation
- Ability to cling and spread
- Resilience towards mechanical disturbance

The thermal conductivity of a foam increases with the expansion ratio, as shown in Table 1-1 taken from Reference 15.

The resistance of foams to destruction by heat was measured by French (Reference 12) and correlated by Thomas (Reference 13). The relative heat resistance of foam was defined as the measured ratio of the time for fixed radiative heat flux to destroy a given quantity of foam to that calculated to vaporize an equivalent quantity of water. This ratio correlated with the product of the expansion ratio and the shear strength and was found to increase with that product reaching measured values of 1.5. The increase in heat resistance of foams can be attributed to an increase in reflectivity.

Table 1-1. Thermal Conductivity of Foams

EXP	K (Btu/hr. F. ft)	
	Experimental	Theoretical
1 (water)	0. 35	--
7. 5	0. 12	1. 15
11. 0	0. 113	0. 094
19. 0	0. 080	0. 046
∞ (air)	0. 0156	--

1. 3. 5 Foam Resilience

Another beneficial and unique property of a foam is its ability to cling and spread while retaining excellent thermal resistance. The ability of a foam to spread and cling is primarily caused by its reduced external surface tension.

Adamson (Reference 16) discusses the resilience of foams noting that the elasticity of the surface film, defined as the increase in surface tension per fractional increase of the film area, gives a measure of the ability of a surface film to adjust its surface tension to an instant stress, i. e., to accept a stress increase without rupture. Another related cause of resilience is the fact that, when a surfactant (foaming agent) is present, the instantaneous surface tension of a fresh surface is greater than the equilibrium value. Any incipient rupture of film will be resisted as soon as damage exposes interior material.

The very high apparent viscosities and surface tensions of foamed liquids suggests the possibility of foam surface survival, even when subjected to the high shearing stresses of high velocity gas flow. This was observed in internal duct flow in subsonic, transonic, and supersonic flow (References 1, 2, 3).

1. 3. 6 Foaming Agents and Their Concentration

The foaming agents utilized in this investigation were

- Protein hydrolysate (3 percent Regular Protein)
- Detergent (High Expansion Foam)
- Polymer with a catalyst (100 percent Aero-o-Foam and a protein catalyst)

The most stable foams in the widest range of densities were obtained with the protein foaming agent. The High Expansion foaming agent, which was specifically developed to form large bubbles and to produce very light foams with small pressure drops in the generator, formed fairly stable foams in our generator only in the expansion ratio range 11 to 20. A modification of the foam generator had to be made to obtain lighter foams and these contained some very large bubbles, making acoustical measurements difficult. However, detergent foams showed good sound reducing capability in the model jet noise reduction tests.

The polymer foams drained too fast, so that acoustical measurements were difficult. This agent was not available for the jet noise reduction tests.

The concentration of the foaming agent affects the stability of the foam only if the concentration is low. Clark (Reference 17) states that at low concentrations expansion is proportional to concentration, while at sufficiently high concentrations expansion is proportional to the energy level, i. e., the energy expanded in forming the foam. These observations matched our own experience which is discussed later.

1. 3. 7 Drainage of Foams

The foam structure continuously changes from the moment it is formed by mixing of the liquid solution and the gas inside a foam generator until the liquid and the gas phases are completely separated again through drainage and bubble collapse. There are two types of foam structure. In the first the foam consists of nearly spherical bubbles separated by rather thick films. The other type, which may develop from the first as a result of drainage or may be formed directly with low-viscosity liquids, consists of gas cells separated by thin films or laminas. The cells are polyhydral in shape, as shown in the sketch below taken from Reference 16. The over pressure in each cell is given by Laplace's equation

$$\Delta P = \sigma(1/R_1 + 1/R_2)$$

where σ is the surface tension and R_1 and R_2 are the radii of curvature. The Channel A of the junction of three or more cells is known as the Plateau border. The high curvature at the boundaries of the Plateau border means that a considerable pressure difference exists between the liquid and gas phases. The pressure in the gas cell must be uniform, hence large pressure gradients must exist in the liquid phase. The Plateau border is a region of low pressure so that liquid flows from the thin plane walls toward the curved Plateau border (see sketch).

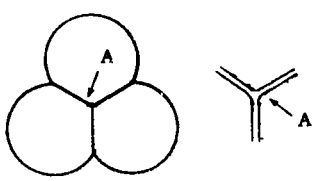

Plateau's Border

Thus, draining may be mainly caused by gravity in a new foam, but capillary forces soon become important.

A further change in foam structure with time is caused by bubble coalescence and gas migration. The pressure inside small bubbles is higher than in large bubbles, as indicated by the Laplace equation. Thus, there is a tendency to rupture the walls separating bubbles of unequal size. Moreover, the thin liquid walls are not impermeable to gas so that big bubbles grow at the expense of the smaller ones (Reference 18) even when the walls are strong enough to withstand a pressure difference. The final result of drainage is, of course, bubble collapse, resulting in foam destruction. The whole process may take hours and even days in a static environment.

In addition, if the temperature of the liquid and gas from which the foam is generated is not equal to ambient, the foam will grow or shrink because of gas expansion or contraction inside the bubbles. Even when the foam is generated from liquid and gas at ambient temperature, its volume will increase at first because small bubbles feed bigger ones; the volume will then decrease when bubble walls are weakened by drainage and collapse.

In general, however, the effective time constant for these processes to take place is much larger than that associated with flow phenomenon in a jet engine; consequently, foamed liquids can be of interest to the problem of jet engine noise control if they possess favorable acoustic properties.

1. 3. 8 Methods of Producing Foams

Methods of producing foams may be classified as chemical or mechanical. Foams may be produced by the chemical reaction of two solutions, one containing a foaming agent to form a gas which fills each tiny bubble. Commercially, chemical foam making techniques have been replaced almost completely by simpler and cheaper mechanical methods of making foam. Gas-liquid proportioning/mixing/agitating may be accomplished by aspiration or pumping as described in Reference 19. Fry and French, Reference 20, describe a simple laboratory mechanical foam generation method which permits easy variation of foam parameters. In this method, a liquid and foaming agent are premixed and stored in a suitable pressure vessel. Compressed air serves as a pressurizing gas and as the foaming gas. Liquid and gas flow rates were indicated by rotometers and metered by needle valves and impinged in a tee arranger; the outlet was connected to a union containing a series of screens. The size and number of screens could be varied to obtain any desired bubble size and, hence, ultimate shear stress. The bubble size was also shown to vary with liquid flow rate and ratio of air flow to liquid flow through the screen improver. This method was found to be satisfactory by a later investigator (Reference 7). The foam generator assembled at TRW closely resembles the model described by French and Fry (Reference 20) except that mixing of gas and liquid was done inside a B-B bed improver while subsequent mechanical energy input to the foam took place in lengths of tubing or flex lines.

1. 3. 8. 1 Flow System

A flow schematic of the foam generator is shown in Figure 1-2. A water solution of the foaming agent is stored in the central tank. That tank is pressurized from one of the nitrogen bottles and the pressure is controlled by a regulator. Liquid flows from the tank through a filter and a rotometer to the improver where it is mixed with nitrogen flowing from the second compressed gas bottle. The flow of gas is controlled by a pressure regulator and read on a gauge. To vary foam density, the gas flow rate was varied by adjusting the regulator at the nitrogen bottle, while the liquid flow rate was maintained constant. Repeatable foam densities were obtained over a range of gas flows, limited by the appearance of slug flow for high gas flows.

A small water heat exchanger was inserted into the nitrogen line immediately upstream of the improver, in order to insure equality of liquid and gas temperatures at all times. As noted earlier foams tend to grow or shrink if the two temperatures are not equal.

1. 3. 8. 2 The Improver

The improver is essentially a packed bed in which gas and liquid are mixed and interspersed. Several packing materials were investigated, i. e., coarse and fine steel wool, 0.175-inch diameter B-B's. 0.100-inch diameter B-B's, and combinations of B-B's and steel wool. All of these materials were held between two metal screens in a 1-inch diameter A-N fitting. The liquid and gas entered the improver from a small plenum located above the upper screen, while the foam left the improver through a 1/4-inch fitting and a flex line.

The fine steel wool was not as effective as the other packing materials; removal of all packing resulted in a soupy foam. There was no

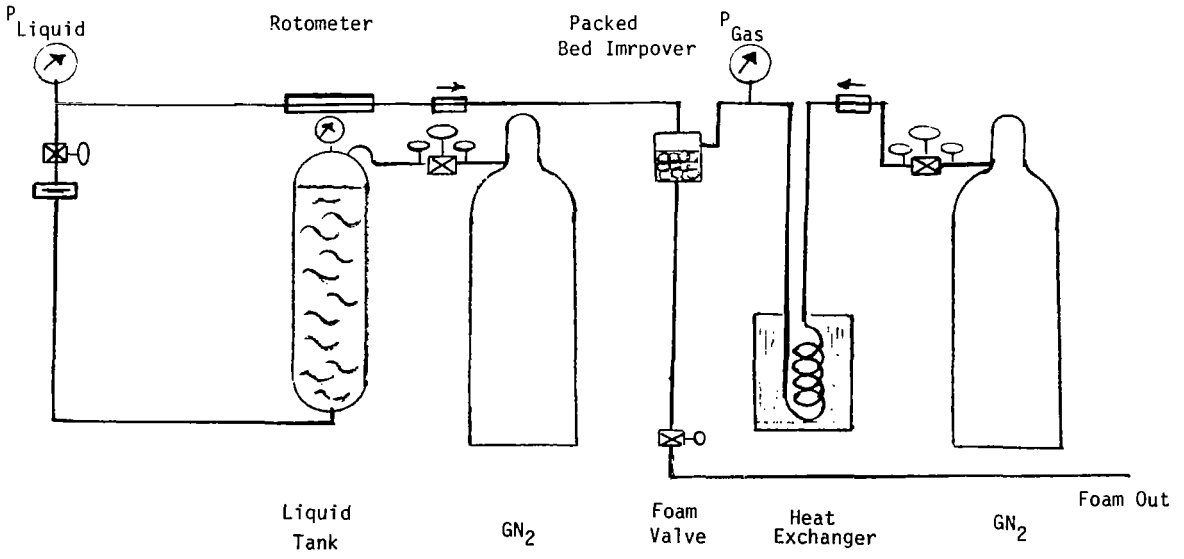

Figure 1-2. Flow Schematic of the Foam Generator

visible difference in the foam quality obtained with all of the other packings. However, a long line after the improver was found to be essential in the production of even-textured, shear-resistant foams in a wide range of expansion ratios.

Similar results were found when the packed bed improver was replaced by a porous plate made of sintered flat metal screens ("Rigimesh"). Three such plates were tried:

- Tight, low porosity plate (5 layers of 50 x 250 mesh screens)
- High porosity plate made from fine wire screens
- Wide mesh, coarse wire plate (2 layers of 12 x 64 mesh screen)

The plates were mounted in a holder and the liquid was dropped in a shower into the Rigimesh plate while the gas was fed into a plenum above the plate. Good foams were formed with the lowest porosity plate. The two other plates let the liquid dribble through and the foam was not even textured.

High expansion foams (EXP > 20) could not be obtained with the detergent foaming agent from either the packed bed or the porous plate improver as long as there was any obstruction to foam flow beyond the improver. Expansion ratios of 50 to 150 were obtained in either device by removing the back plate from the Rigimesh holder, and by replacing the back plate and lower screen of the packed bed with loosely woven cotton cloth. The flow rates per unit area of improver were very low and the foam texture nonhomogeneous.

1.4 ACOUSTICAL PROPERTIES OF FOAMED LIQUIDS

The use of foamed liquids for acoustic energy absorption can properly be placed in the general category of two-phase fluid behavior. Two-phase fluids have been recognized for some time to exhibit peculiar characteristics with respect to their apparent propagation of pressure waves. The first investigation of sound speeds in two-phase flow was reported by Mallock (Reference 21) for a bubbly water-air system. Through the assumption of no mass transfer, isothermal gas and homogeneous mixing, Mallock observed that the mixture sound speed was apparently much lower than that of either the air or water. Ackeret (Reference 22), Spitzer (Reference 23), and Foldy (Reference 24) extended these early results, primarily with interest in the underwater problems of sound propagation with bubbles present in the water, either induced by cavitation or introduced by extraneous noncondensable gases. In the 1950 decade the phenomenon of two-phase flow received new interest from requirements brought on by chemical processes, high speed underwater devices, high energy release boiler systems, and vapor driver MHD

cycles. This was followed in the 1960 decade by intense research in high combustion intensity systems with instability; it was found that solid particles had appreciable attenuation effects in an oscillating pressure field.

An excellent summary of two-phase flow liquid systems is given by Gouse in Reference 25. Perhaps one of the most significant understandings of the nature of propagation of a pressure wave in a two-phase liquid-gas fluid, including the effects of mass transfer, is that of Karplus and Clinch (Reference 26). The earliest reported analytical findings for the two-phase flow of gas solids is that of Epstein (Reference 27). This work was later extended to fogs (Reference 28). These efforts were later extended to a variety of problems, including rocket engine instability control by particulates. The work of Temkin and Dobbins (References 29 and 30) is notable here. Lire (Reference 31) provides an excellent summary of pertinent references in this area.

Arnold and Slutsky (Reference 32) reported on a sponsored project for the attenuation of plane waves of sound by suspension of the resonating particle. In this effort flexible rods or filaments for dissipation of acoustic energy are being considered, wherein the energy absorption occurs by providing deformable bodies which are capable of taking up a number of modes of motion in a resonant manner. A complete summary listing of pertinent reports and papers in this general area are included in the Bibliography of this report.

1. 4. 1 General Comments on Pressure Propagation in Two-Phase Liquid, Noncondensable Gas System

To fully appreciate the concept of sound attenuation by liquid foams, it is necessary to understand the nature of wave propagation in a two-phase liquid-gas system. A number of papers on derivations of sound speeds within such mixtures are included in the reference list. The following is a condensation of a number of these papers and is an effort to provide limits of the sound speed as a function of mixture properties. The Karplus reference is recommended for detailed study here.

It is, perhaps, most rigorous to speak of a propagation constant in the two-phase fluid rather than the sound speed. It is expected that the sound speed in a thermodynamic sense must be associated only with low frequency in order that equilibrium can in fact exist. In this region, the sound speed may then be expected to be only a function of the relative masses of the two fluids in the two-phase mixture. In the intermediate frequency range certain relaxation phenomenon may be expected and the propagation constant will probably be a function of frequency and size distribution of the local bubble matrix. At high frequencies, it would not be unexpected for a given mass and size distribution to have one of the phases not respond to the local passage of a wave and, consequently, the propagation constant would only depend upon the predominant phase. Furthermore, in the intermediate range it would not be unusual to have relaxation phenomenon take place somewhat analogous to relaxation phenomenon in gases, wherein internal degrees of freedom become involved in the propagation constant.

1. 4. 2 Thermodynamic Equilibrium

It is asserted that in the foamed liquid matrix the gas bubble dilation tends to be isothermal and the liquid water mass high heat capacity is capable of absorbing and giving up sound wave energy without appreciable temperature change. Further it is assumed that mass transfer associated with equilibrium pyschometrics is negligible, thus the mass ratio of gas and liquid remains constant. Finally, the gas bubbles are assumed to be homogeneously dispersed and small with respect to the wavelength of a regular disturbance.

Consider an element of such a medium with particle velocity and pressures as shown below and a disturbance passing at velocity $\bar{C}$.

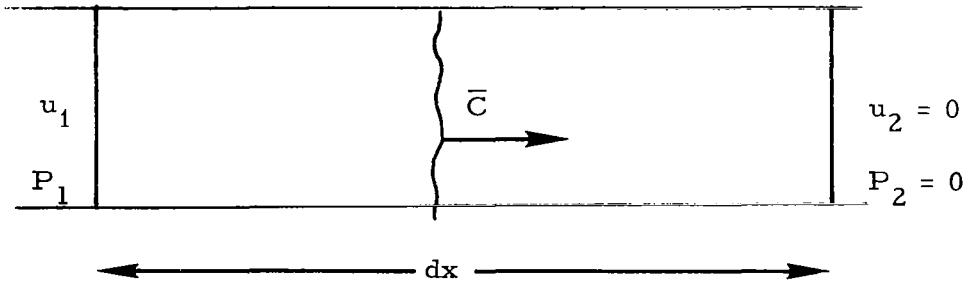

The mass ratio is taken as

$$\eta = \frac{M_a}{M_b} \tag{1}$$

Now

$$M_a = \rho_a V_a \text{ for fluid a} \tag{2}$$

$$M_b = \rho_a V_b \text{ for fluid b}$$

The volume ratio is

$$\theta = \frac{V_a}{V_a + V_b} = \frac{\frac{M_a}{\rho_a}}{\frac{M_a}{\rho_a} + \frac{M_b}{\rho_b}} \tag{3}$$

$$\vartheta = \frac{\eta \frac{\rho_b}{\rho_a}}{\eta \frac{\rho_b}{\rho_a} + 1} \tag{4}$$

Now, assuming the particle velocities and pressures ahead of the wave to be zero and those behind the wave to be u_1 and P_1, application of the momentum equation gives

$$(P_1 - P_2)\, dt = \{\theta \rho_a + (1-\theta)\, \rho_b\}\, u_1\, dx \tag{5}$$

The displacement, dx, is taken as

$$dx \equiv \bar{C}\, dt$$

The change in volumes behind and in front of the wave are

$$dV_1 = u_1\, dt \tag{6}$$

$$dV_2 = (P_1 - P_2)\left[\beta_a \theta + \beta_b\, (1-\theta)\right] dx \tag{7}$$

where β_a and β_b are the bulk compressibility coefficients of fluids a and b.

It is recognized that the two volume changes must be equal.

$$\therefore\ \bar{C}^2 = \frac{1}{[\beta_a \theta + \beta_b\, (1-\theta)]\, [\rho_a \theta + \rho_b\, (1-\theta)]} \tag{8}$$

The bulk compressibility coefficients are given by

$$\beta = \frac{1}{\rho}\left(\frac{d\rho}{dP}\right)_s$$

If the gaseous constituent is a perfect gas

$$C_g^2 = \left(\frac{dP}{d\rho}\right)_s = \gamma RT$$

The compressibility coefficient for the gas is

$$\beta_g = \frac{1}{\rho_g C_g^2} \tag{9}$$

For the liquid the factor is

$$\beta_\ell = \frac{1}{\rho C_\ell^2} \tag{10}$$

$$\bar{C}^2 = \left\{\left[\frac{\theta}{\rho_g C_g^2} + \frac{1-\theta}{\rho_\ell C_\ell^2}\right]\left[\rho_g\theta + \rho_\ell(1-\theta)\right]\right\}^{-1} \tag{11}$$

which can also be written as

$$\bar{C}^2 = \left\{\left[\frac{\theta}{\gamma P} + \frac{1-\theta}{\rho_\ell C_\ell^2}\right]\left[\frac{P}{RT}\theta + \rho_e(1-\theta)\right]\right\}^{-1} \tag{12}$$

It is noted that in the case of isothermal propagation the first term in the demoninator on the left of Equation (12) tends to θ/P as $\gamma \rightarrow 1.0$.

For water-air mixtures at ambient pressure values of $\bar{C}$ as low as ~22 m/sec (~60 ft/sec) are possible. Figure 1-3 shows a sound speed dependence with reduced sound speeds from those of the individual constituents over a wide range of mixture ratios. In the limits as θ goes to zero or unity the sound speeds approach those of the constituents.

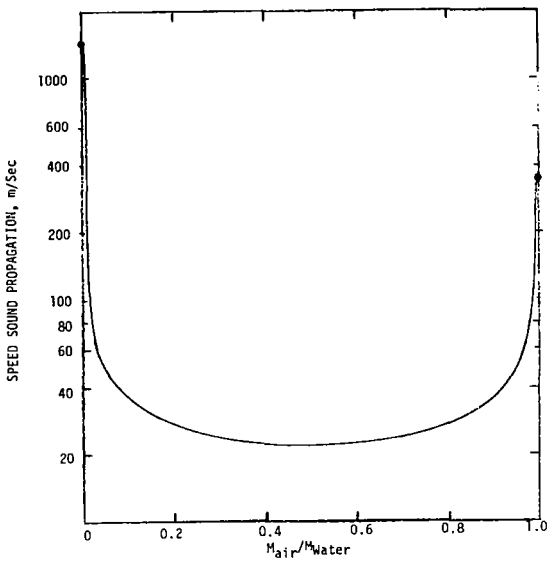

Figure 1-3. Speed of Sound Propagation in Two-phase Mixture of Air and Water

It is noted that the sound speed for a two-phase mixture of liquid and gas is quite pressure dependent. Of particular interest is the fact that the propagated wave cannot be maintained, in general, in its original form; i. e., the wave must steepen and distort or flatten and distort. An initially sinusoidal wave will be distorted, because the larger the negative ΔP, the slower the wave phase velocity. As the two-phase system becomes essentially gas, the assumption of isothermal propagation must be modified to that of adiabatic propagation in the predominant phase.

For intermediate frequencies the results of Spitzer (Reference 23) are recommended for void fractions wherein the interface matrix structure is continuous. When the void fraction becomes quite large, the results of Temkins and Dobbins are recommended (Reference 30). Silberman's (Reference 33) carefully conducted experiments have shown that the Spitzer results qualitatively give good estimates of the phase velocity and attenuation constant for bubbly mixtures containing larger bubbles (>0. 012 inch) and small concentrations. From standing wave tube experiments he demonstrated bubble resonance when its natural frequency was applied. Further, maximum attenuation occurs near resonance. It should be expected that at frequencies far removed from resonance on the low side that the bubble contraction and expansion displacement should be very nearly in phase with the applied sound field. Far above resonance the bubble displacement will lag by nearly 180 degrees, and the attenuation should be small in both extremes.

In this study two classical methods for measuring sound absorption coefficients were used to characterize a wide variety of foams. The standing wave tube measurements were used to yield an absorption coefficient for sinusoidal plane waves at normal incidence and the surface impedance of the foam for normal plane waves. Reverberation chamber measurements yielded an absorption coefficient for three-dimensional pressure waves of random incidence. These tests are described in Section 2 of this report.

Neither of these absorption coefficients is an intrinsic property of the foam. Acoustic properties of a medium are fully defined when their characteristic acoustic impedance and propagation constant are known for all frequencies. In theory standing wave tube measurements can yield

these two properties. However, the accuracy of the method is not high, especially when the continuously changing structure of draining foams limits the time available to perform the measurements. Better accuracy could be achieved by measuring characteristic impedance in a standing wave tube and the propagation constant in a traveling wave apparatus.

1.5 JET EXHAUST NOISE CHARACTERISTICS AND LIQUID FOAM INJECTION

Sound generation by turbulent jets has been the object of extensive studies since the advent of the turbojet engine. Excellent review papers, including extensive bibliographies, are available in the literature (References 34 and 35). Only the jet noise emission characteristics which may be of importance in understanding the effect of foam injection will be briefly reviewed here.

The gas jet starts mixing with still air as soon as it leaves the nozzle. The mixing zone surrounds the core of the jet and grows linearly with axial distance until the core disappears entirely. The core extends for several nozzle diameters from the nozzle and most of the sound is generated in the highly turbulent mixing region surrounding the core. Several sound generation mechanisms involving inertial forces associated with fluctuation of momentum flux have been proposed. A general agreement exists for the overall sound emission as expressed by Lighthill's V_j^8 power law

$$P \sim \rho_o V_j^8 D^2 / C_o^2$$

which holds from subsonic to supersonic jet speeds, V_j, up to about twice the ambient speed of sound, C_o.

It has been shown (Reference 34) that sound emission for subsonic jets is independent from axial distance in the mixing region and drops off with the seventh power of distance in the developed jet region.

Nagamatsu and Sheer (Reference 36) have shown that for supersonic jets sound emission grows linearly with axial distance in the mixing region until the supersonic core tip is reached. Beyond that point the sound emission drops off like that of subsonic jets. The supersonic core, i. e., region in which velocities equal to the velocity at nozzle exit still exist, is shorter than the supersonic core region; thus sound emission in supersonic jets peaks beyond the mixing region as defined in subsonic jet work.

Convection of eddies causes a crowding of sound waves in the downstream direction resulting in a sound amplification in the ratio of C^{-4} where

$$C = [(1 - M_c \cos \theta)^2 + \alpha^2 M_c^2]^{1/2}$$

where M_c is the convection speed-to-sound velocity ratio, θ is the polar angle centered on jet axis, and α varies inversely as the lifetime of an eddy. Convection also causes a Doppler shift of frequency in the ratio of C^{-1}, thus explaining the differences in polar distribution for high and low frequency sound found by Lassiter and Hubbard (Reference 37, Figure 10).

Because of the directivity of sound emission, noise reduction can be achieved by use of multiple nozzles or corrugated nozzles, but only at the expense of thrust reduction. In ground applications, direct removal of kinetic energy is also possible. The largest advance in jet noise reduction was achieved by the introduction of the fan jet engine in which the mean jet velocity is lowered by the addition of a large volume of slower bypass air. Unfortunately the fan engine itself is a powerful source of sound.

Removal of sound energy at the source is the principle used in jet noise suppression through foam injection. Sound energy is dissipated by resonance of the foam structure in the ingested foam particles. There are indications in the recently obtained data that some favorable change in the turbulence characteristics of the jet mixing region is also taking place.

2. DETERMINATION OF ACOUSTICAL PROPERTIES OF FOAMED LIQUIDS

Both the standing wave and reverberation room methods were used in the fundamental investigations of the acoustical properties of foamed liquids. These methods and their results are discussed below, followed by a presentation of a tentative model of the sound absorption mechanisms.

2.1 STANDING WAVE TUBE MEASUREMENTS

2.1.1 Method and Apparatus

The standing wave method for the determination of the absorption coefficient is conceptually simple and well known. A loudspeaker at one end of a tube emits a sinusoidal wave of the desired frequency. The sound wave is then partly reflected at the surface of the sample located at the opposite end of the tube. The resultant of the incident wave of amplitude 1 and the reflected wave of amplitude r is a standing wave pattern with alternate sound maxima (1 + r) and minima (1 - r). The reflection coefficient r follows directly from the ratio, n, of the sound pressure maxima and minima

$$r = \frac{n - 1}{n + 1}$$

The absorption coefficient α is by definition the ratio of absorbed to incident energy

$$\alpha = 1 - |r|^2$$

The reflection coefficient, r, is a complex number and its phase angle, Δ, with respect to the incident wave can be determined by measuring the distance from the surface of the sample to the first and second minima, y_1 and y_2. These minima are one-half wavelength apart

$$\Delta = \left(\frac{y_1}{\lambda/4} - 1\right)\pi = \left(\frac{2y_1}{y_2 - y_1} - 1\right)\pi$$

The surface impedance Z_1 of the sample can be calculated from the above measurements. The surface impedance is the ratio of pressure to particle velocity on the surface of the sample

$$Z_1 = \frac{p_i + p_r}{v_i + v_r}$$

where p_i and p_r are the incident and reflected pressures; v_i and v_r are the corresponding particle velocities. The relations for the incident and reflected pressures to the particle velocities are $p_i = \rho_o C v_i$ and $p_r = -\rho_o C v_r$, where $\rho_o C$ is the impedance of air. The ratio of the reflected pressure to the incident pressure is the reflection coefficient

$$r = |r| e^{j\Delta}$$

The real and imaginary parts of the surface impedance can be obtained from $|r|$ and Δ by use of Smith' s charts, or calculated directly on a computer as was done in this study.

The sound field inside the tube is explored by a moveable probe microphone traveling on a track equipped with a scale on which the distance between probe entrance and the sample surface can be read. An electronic analyzer permitted the direct reading of the absorption coefficient, α, though the reflection coefficient, r, was the basically measured value.

A standard Brüel and Kjaer standing wave tube apparatus Model 4002 with a type 2107 frequency analyzer was used in most tests. A few foam distruction tests were made with the more powerful 4002S model.

The standing wave tube was mounted vertically in order to obtain a stable foam surface, perpendicular to the axis of the tube, as shown in Figure 2-1. A block diagram of the associated equipment is shown in Figure 2-2. The high intensity apparatus is shown in Figure 2-3.

The sine wave generator was used to select test frequencies. The amplitude was adjusted to 10 watts rms at the standing wave tube speaker. A 10-cm diameter tube was used with frequencies below 1600 Hz, and a 3-cm diameter tube for frequencies between 1600 and 6400 Hz. The narrow band analyzer (1/3 octave) was used to measure the coefficient of absorption.

Prior to conducting the standing wave tube experiments on foams, a test was conducted in the empty tubes to determine the sound level to which the foam would be subjected. A calibrated condenser microphone was placed at the sample plane in the tube. The drive power was adjusted to 10 watts rms and the sound level was measured in decibels for all test frequencies. The sound level variation with frequency was on the order of ±12 percent. Because the time consumed in normalizing the sonic intensity was long enough to allow excessive foam aging, it was decided merely to hold the drive power constant. This in no way affects the acoustic properties being measured. The sound level seen by the foam was in the 60 to 80 db range - low enough to minimize direct foam destruction by the sound waves.

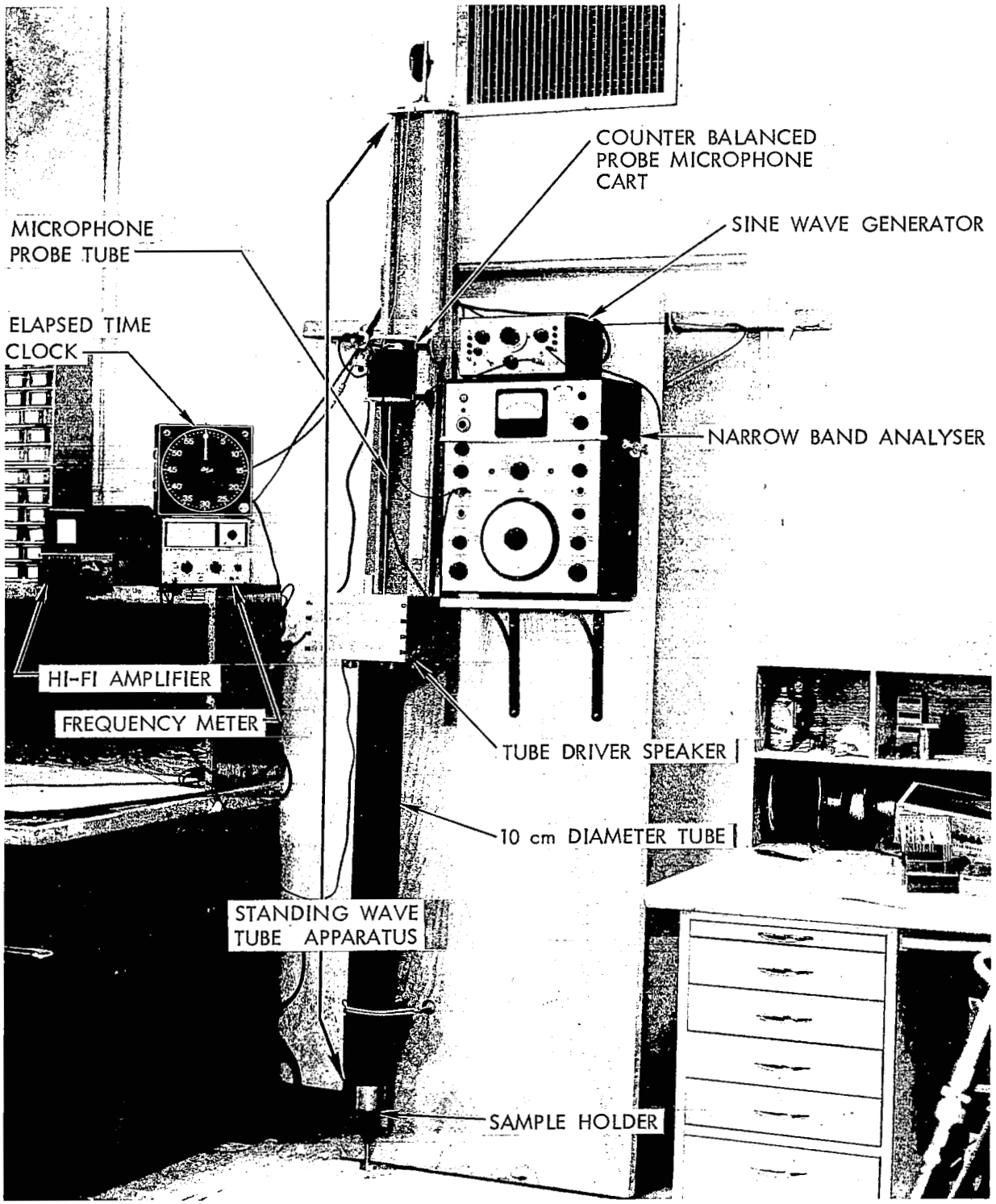

Figure 2-1. Standing Wave Tube Apparatus and Associated Equipment

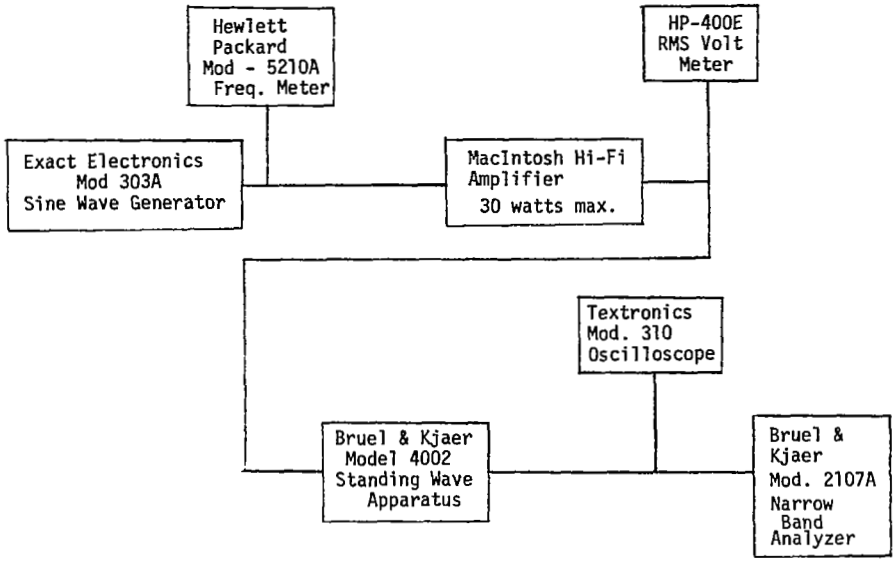

Figure 2-2. Block Diagram of Standing Wave Tube Apparatus and Associated Equipment

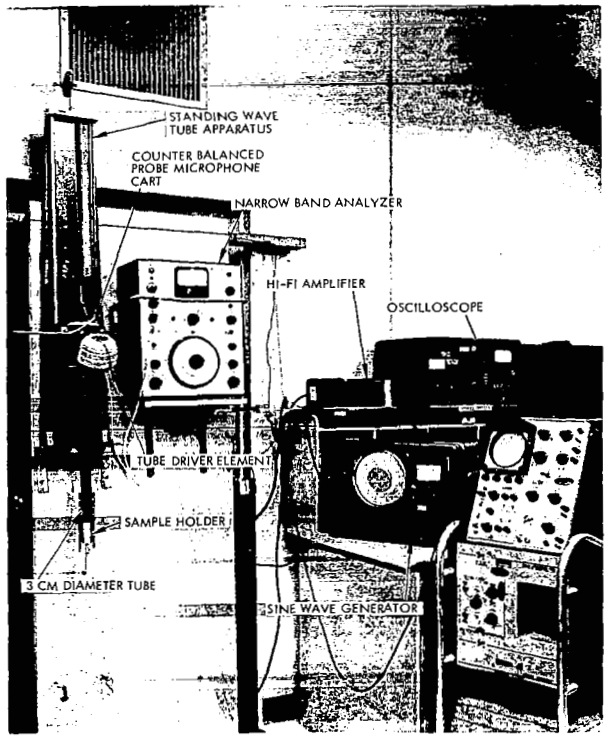

Figure 2-3. High Intensity Standing Wave Tube Apparatus

An oscilloscope was used to check the integrity of the standing wave, i.e., observe resonances in the apparatus. This was particularly important when the high-intensity apparatus (Figure 2-3) was used. Sound levels were limited by wave distortion to about 120 db, depending on frequency.

2.1.2 Test Procedures, Results, and Accuracy

Approximately 50 tests were made as shown in Table 2-1. Most of the tests were made for a foam sample of 1-inch depth. Some typical results are shown in Figures 2-4 through 2-14. Three concentration levels were selected for the High Expansion and the hydrolized Protein foaming agents; the expansion ratio (i.e., foam density) varied from about 12 to the highest attainable value. Low expansion ratio foams (below 11 or 12) drained too rapidly to permit measurement.

Very light foams could only be obtained with high foaming agent concentrations. The amount of gas that could be incorporated into the liquid without alternate slugs of gas and foam leaving the foam line increased with concentration and pressure drop in the foam line (i.e., length of line and pressure at the improver).

For the High Expansion foaming agent a very light foam (EXP-100) could also be obtained without any foam pressure drop at very low flow rates; the bee-bee bed of the improver was covered with a cloth instead connecting it to a line. These foams were not, however, reproducible enough for acoustic experiments.

A test consisted of measurements of α, y_1, and y_2 at five frequencies in the large diameter, low frequency tube, followed by measurements at seven frequencies in the small diameter, high frequency tube. Measurements made on a given foam sample took 6 to 8 minutes, and a freshly generated foam sample was needed for each frequency range.

Foams produced from the polymer foaming agent with a catalyzer (Aerofoam 100 plus 3 percent of 3% Regular Protein) drained too rapidly even when a high concentration of foaming agent was used. Only one foam of this type (#300) was tested. The general aspects of the absorption coefficient and surface impedance graphs were similar for both Protein and High Expansion foams.

Several factors limit the accuracy of the test results. High precision measurements are needed to obtain accurate surface impedance values. In order to obtain a 2 percent accuracy on the resistive and the reactive parts of the surface impedance R. A. Scott (Reference 38) measured the location of pressure minima to 0.1 millimeter precision. Such precision is hard to match on the Bruel and Kjaer instrument in which the scale is graduated in centimeters and the microphone carriage carries a millimeter scale but has no vernier. An attempt at greater accuracy would result in a lengthening of the time needed for a reading and hence would increase the influence of foam aging. An indication of the foam aging influence was obtained by repeating a measurement, usually at

Table 2-1. Characteristics of Foams Tested by the Standing Wave Tube Method

Percent Foaming Agent	EXP Nominal	Run No.	Percent Foaming Agent	EXP Nominal	Run No.
3% Regular Protein Foaming Agent			High Expansion Foaming Agent		
3	15	134	3	11	106
3	22	135	3	13	107
3	28	136	3	15	105
3	39	137	3	17	104
3	53	141	3	68/118	108
6	17	132	4	79/46	101[2]
6	23	131	4	15	102[2]
6	32	130	4	22	103[2]
6	43	129	4 1/2	12	115
6	46	302[4]	4 1/2	18	117
6	37	303	4 1/2	26	118
6	38	304[5]	4 1/2	26	145
6	38	305[5]	4 1/2	47	139
6	38	306[5]	6	13	110
10	16	121	6	20	113
10	22	120	6	31	114
10	33	122	6	44	112
10	40	140	6	44/57	109
10	81	119			
20	78	138			
Styrofoam			Aero-O-Foam 100 + Catalyst Foaming Agent		
Flat		142	50	40	300[4]
Grooved		143	50	30	301[3]

1. EXP = Expansion Ratio = Liquid-to-foam density ratio
2. Preliminary test, included aging
3. High intensity apparatus used at low db
4. High intensity apparatus used at 95 db
5. Three sample depth measurements

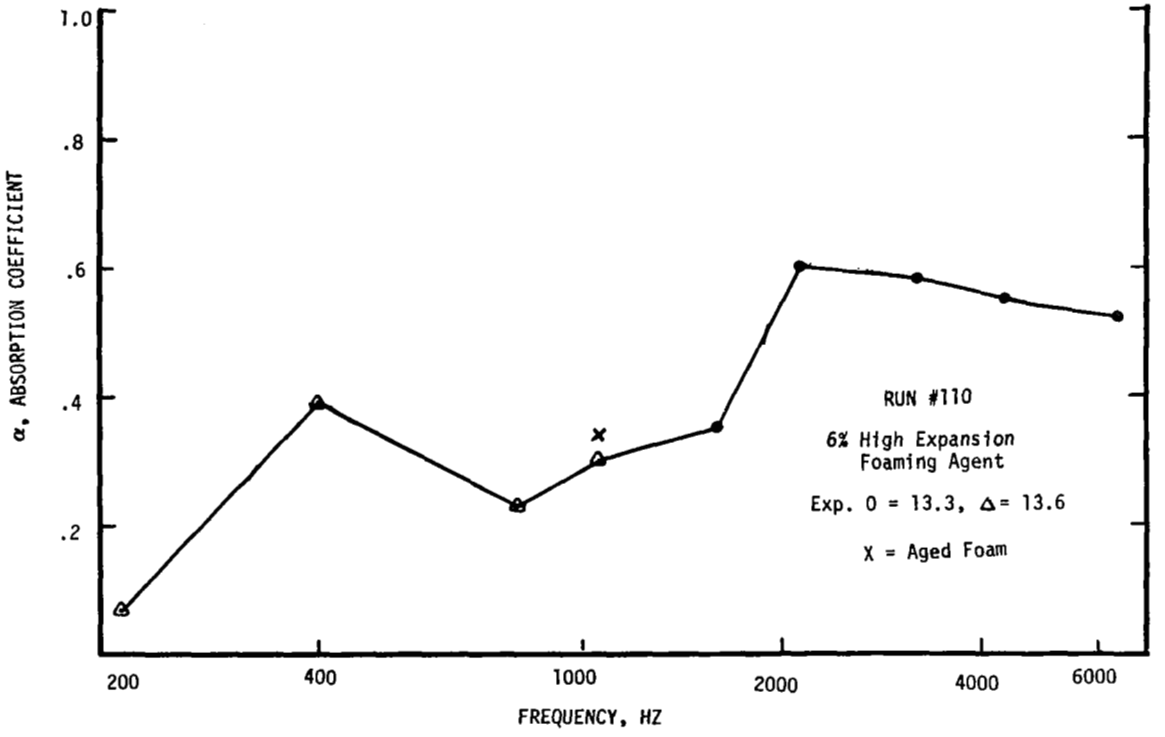

Figure 2-4. Absorption Coefficients, Standing Wave Tube Run 110

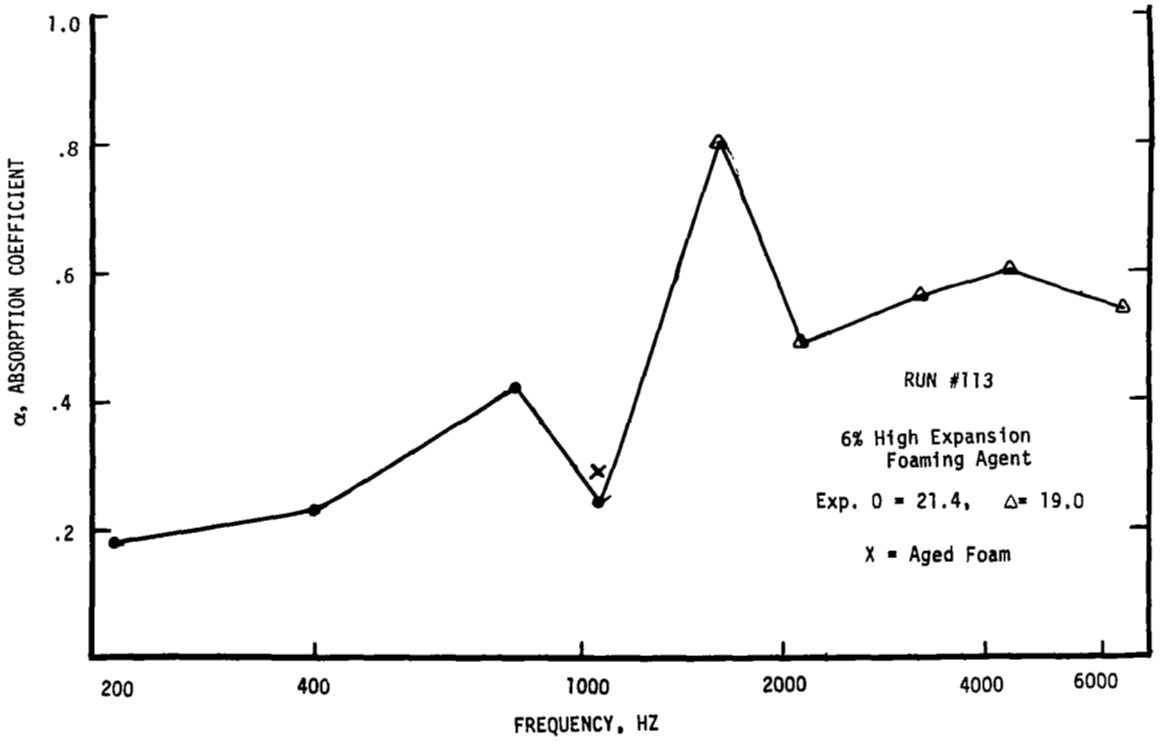

Figure 2-5. Absorption Coefficients, Standing Wave Tube Run 113

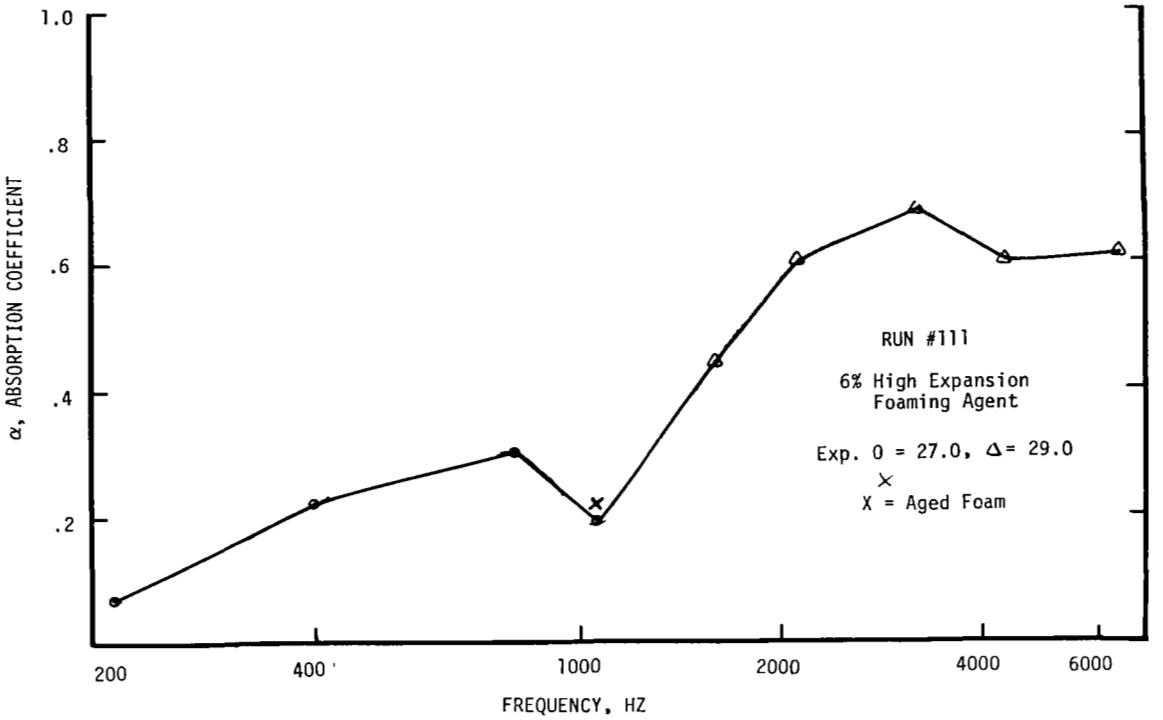

Figure 2-6. Absorption Coefficients, Standing Wave Tube Run 111

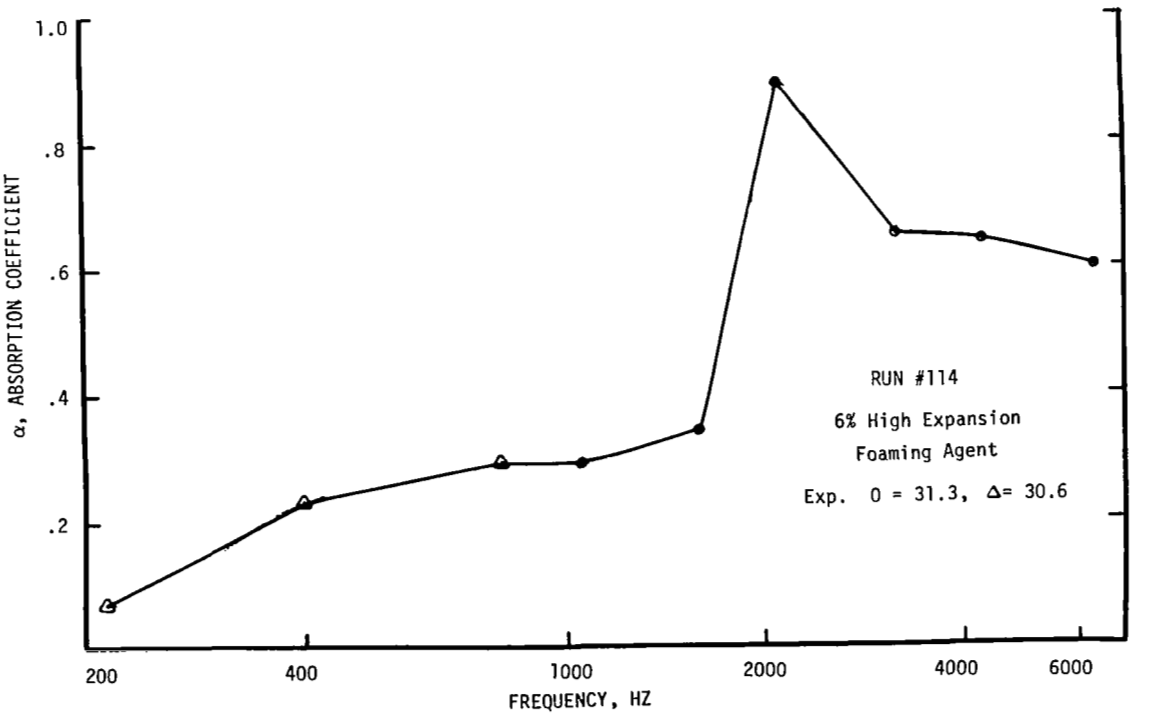

Figure 2-7. Absorption Coefficients, Standing Wave Tube Run 114

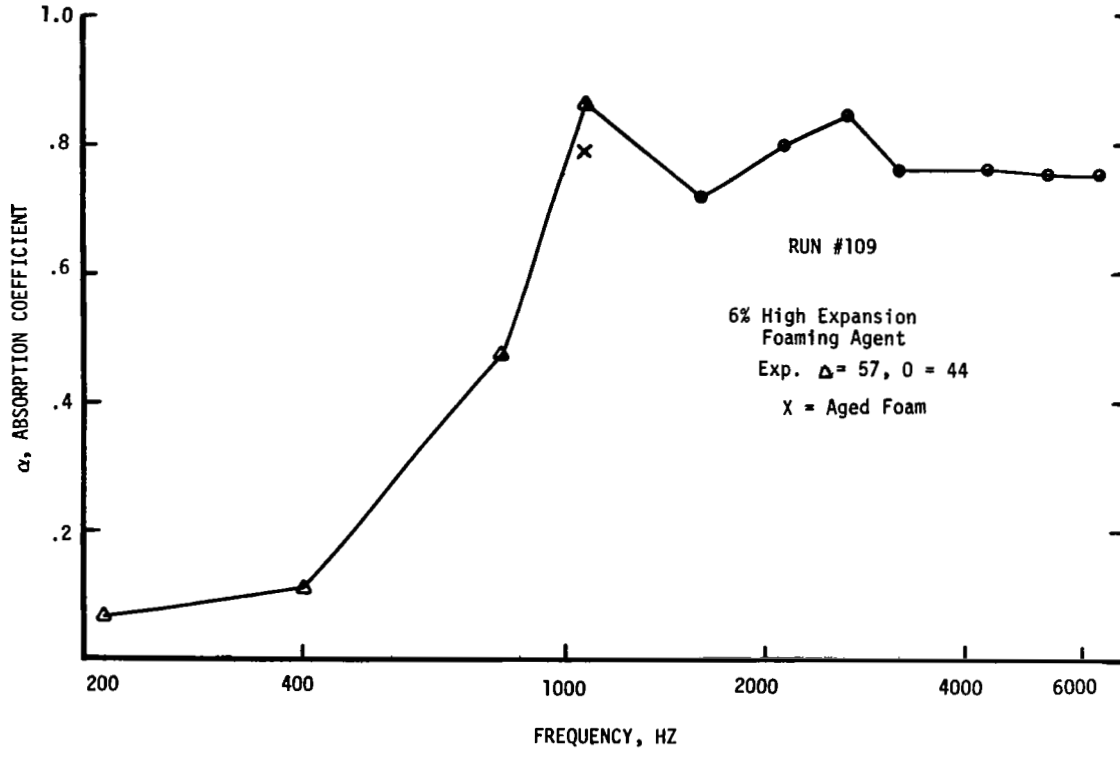

Figure 2-8. Absorption Coefficients, Standing Wave Tube Run 109

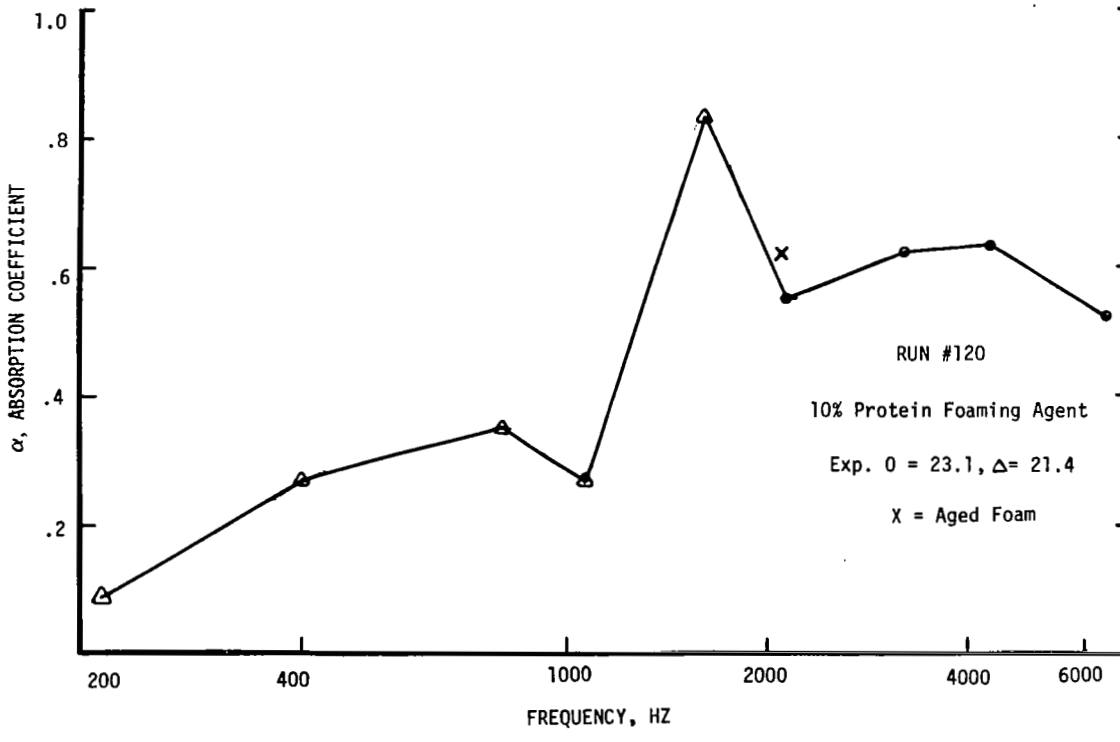

Figure 2-9. Absorption Coefficients, Standing Wave Tube Run 120

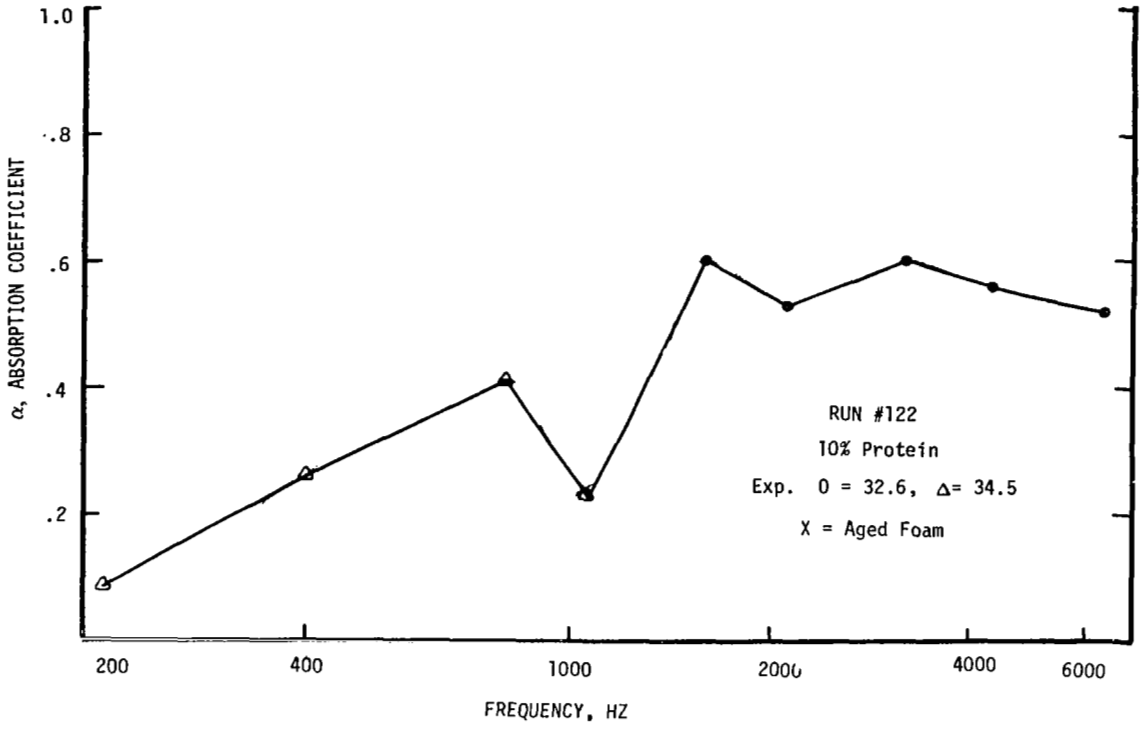

Figure 2-10. Absorption Coefficient, Standing Wave Tube Run 122

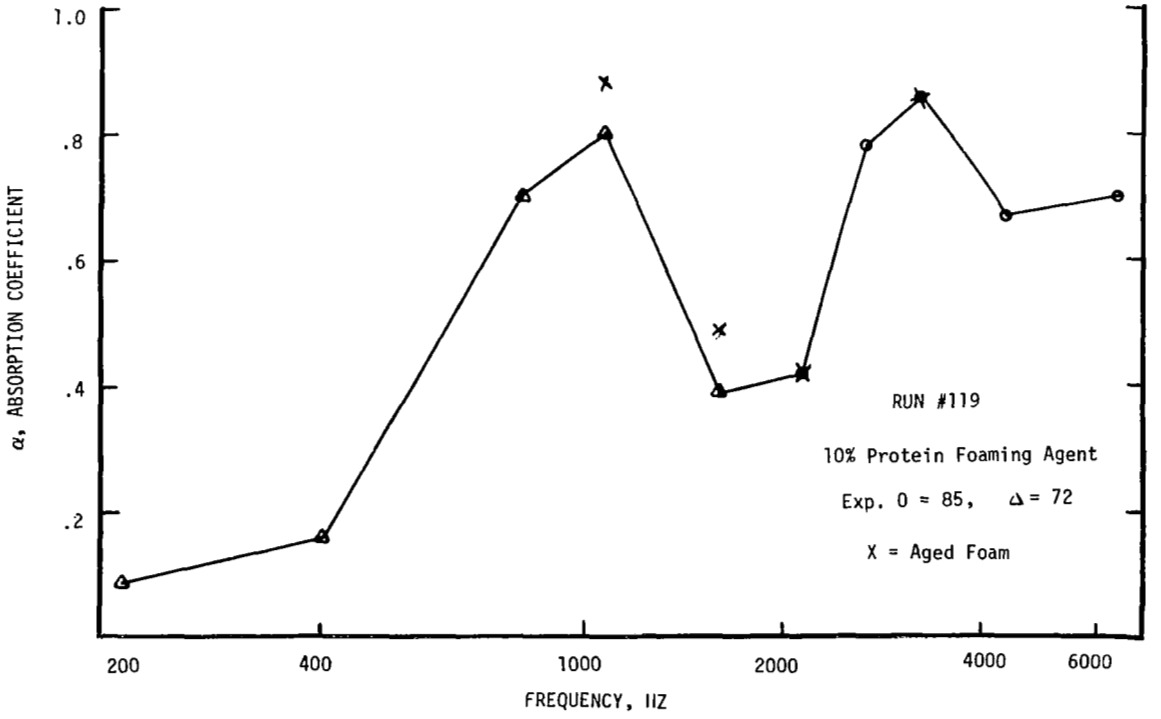

Figure 2-11. Absorption Coefficients, Standing Wave Tube Run 119

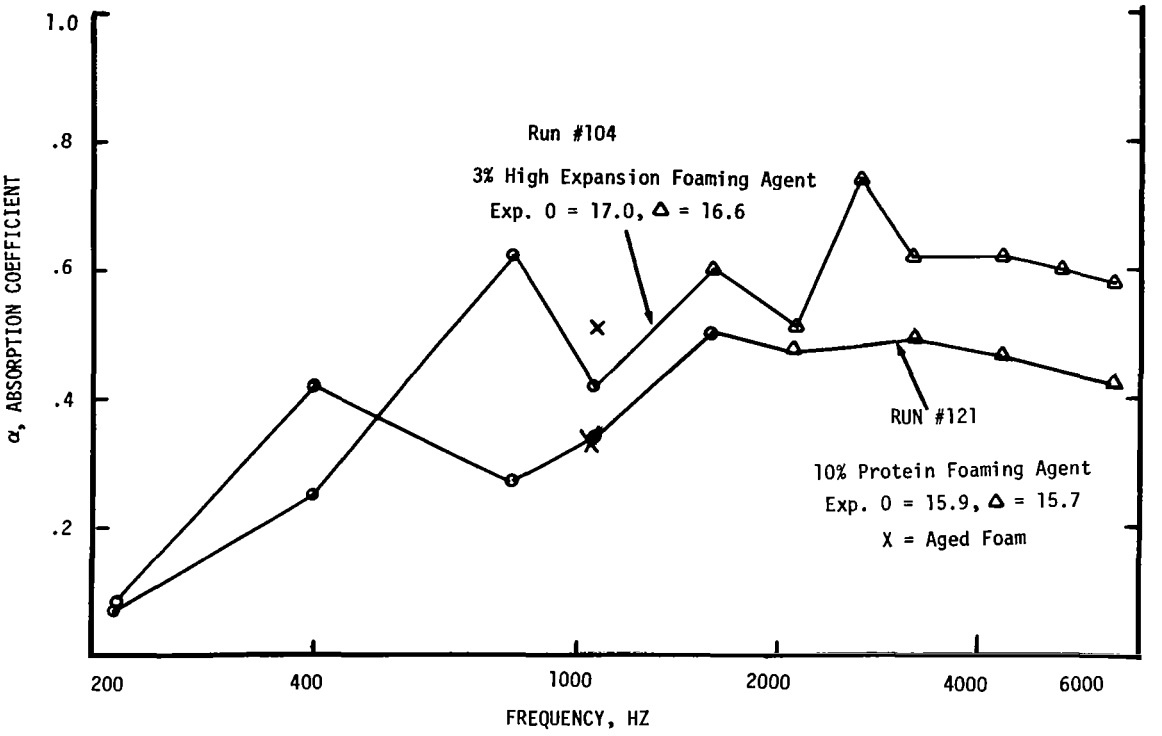

Figure 2-12. Absorption Coefficients for Two Foams with EXP ≃16, Runs 104 and 121

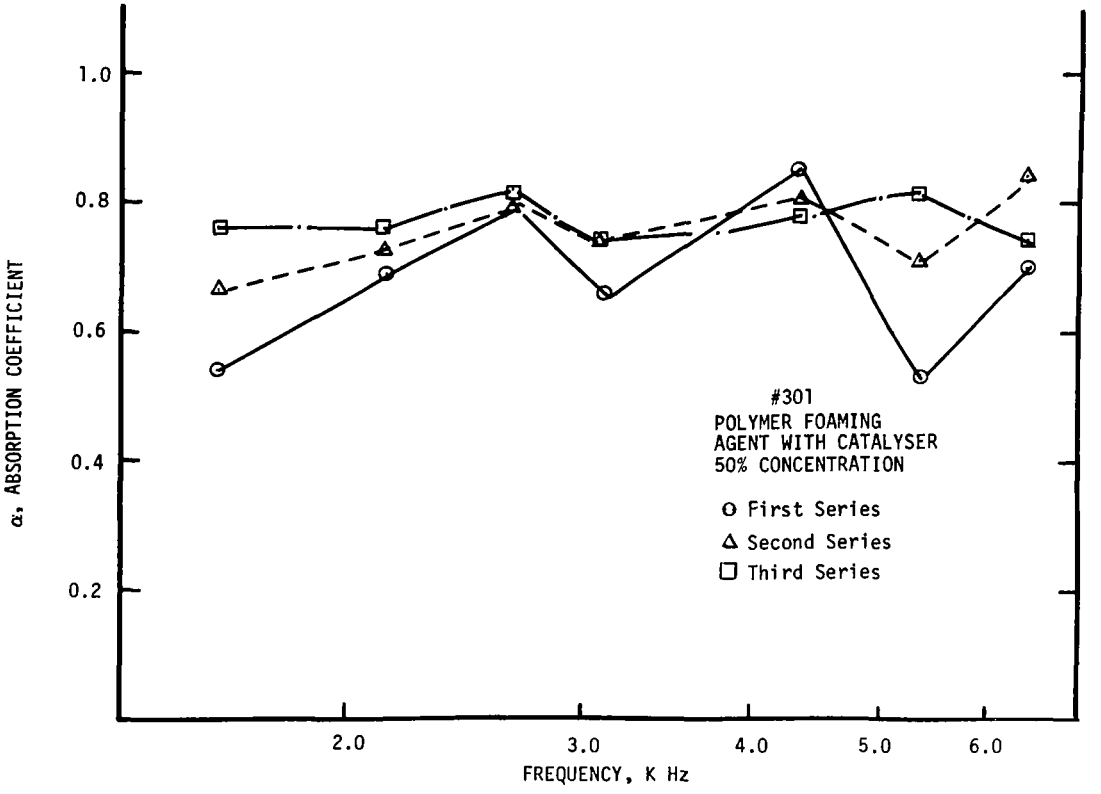

Figure 2-13. Aging of Foams, Run 301

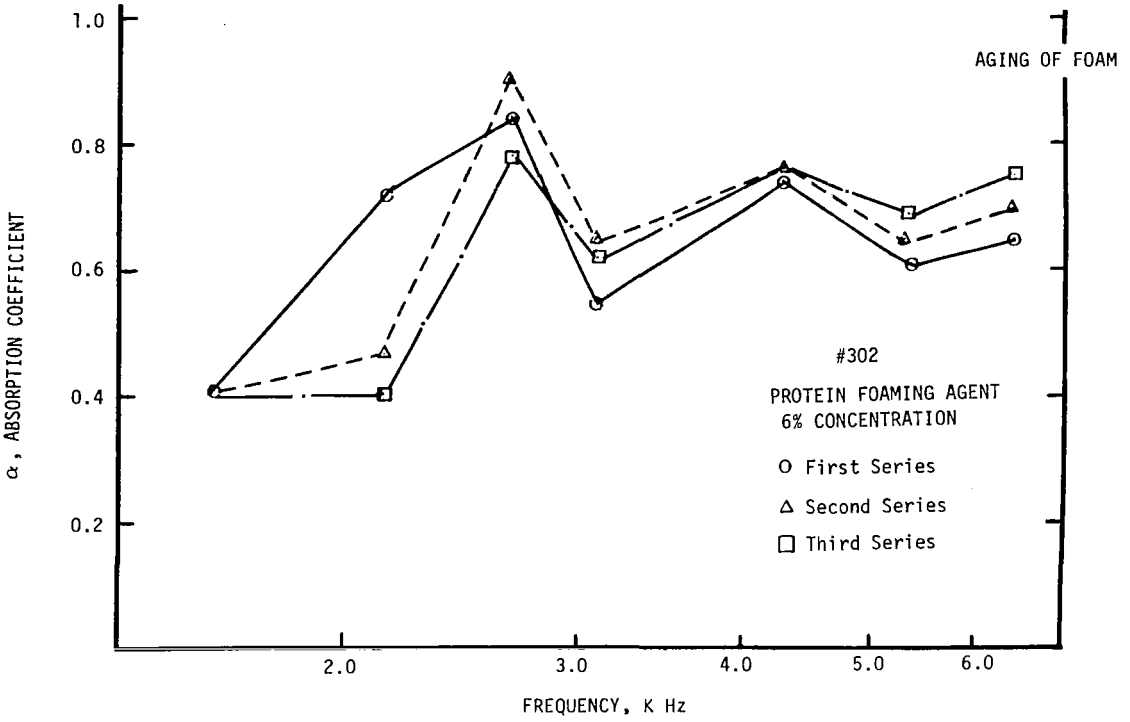

Figure 2-14. Aging of Foams, Run 302

1066 Hz, after a 3-minute interval. An appreciable change in the absorption coefficient, usually an increase, can be seen on most graphs. Figures 2-13 and 2-14 (runs #301 and 302) show three series of consecutively measured absorption coefficients; generally speaking, the absorption coefficient increases as the foam ages (i.e., the bubble size increases).

Despite the limited accuracy of the standing wave tube tests, a fairly successful attempt was made to obtain the characteristic impedance and the propagation constant of a foam. These properties are needed for modeling of sound absorption in foams.

In spite of the encountered difficulties discussed above, the results in general are quite favorable. Absorption was demonstrated and the higher frequencies exhibited higher absorption as expected. Also of interest is the fact that apparent resonance phenomena were observed.

2.1.3 Acoustic Impedance and Propagation Constant

2.1.3.1 Definition and Analytical Methods

The fundamental acoustic properties needed to build a mathematical model of the resonance dissipating phenomena in foamed liquids are the propagation constant (γ) and the foam characteristic impedance (Z_o). Both Z_o and γ are related to the real and imaginary parts of the mechanical

analogue of the responding foam. In order to obtain data for a model of the response of foam to sound waves, the standing wave tube approach was used to obtain an absorption coefficient, α, and a surface impedance, Z_1.

The normal plane wave absorption coefficient (α) measures the fraction of energy in the incident normal plane pressure wave which is not reflected off the test sample surface, i. e., the ratio of the energy that passes into the material to the normally incident energy

$$\alpha = 1 - |r|^2 \tag{13}$$

The normal specific impedance ratio (relative to free air) $(Z_1/\rho_o C)_{air}$ observing the test sample at the air/test sample interface, i. e., at the free surface of the sample, provides phase shift data. In general, this parameter has both magnitude and phase and is dependent on the boundary conditions imposed on the test sample

$$\frac{Z_1}{(\rho_o C)_{air}} = \frac{1 + r}{1 - r} \tag{14}$$

The propagation constant is in general a complex number ($\gamma = \alpha' + j\beta$). The real part of the propagation constant (α') corresponds to the attenuation constant of the material and it determines the decay in the pressure wave amplitude per unit length of traversed distance. Thus, it is a measure of the true internal energy dissipation characteristics of the acoustic material. The complex part of the propagation constant (β), called the phase constant, determines the change in phase per unit length for a given wavelength, i. e., $\beta = 2\pi/\lambda$, where λ = wavelength. Since the acoustic velocity of a plane wave can be expressed as

$$C = \lambda f$$

where f = frequency = $\omega/2\pi$ then

$$\beta = \frac{2\pi f}{C} = \frac{\omega}{C} \tag{15}$$

β is directly related to the acoustic velocity of the medium through which the plane wave is traveling. In general, C can vary with frequency, creating dispersion effects in the medium through which the plane wave is traveling, resulting in definite cut-off frequencies.

The characteristic impedance (Z_o) of the test sample material is the impedance for a free plane wave traveling in the unbounded test medium.

$$Z_o = \left.\frac{p}{v}\right|_{\text{free plane wave}}$$

where

p = sound pressure amplitude

v = particle velocity at any position in the infinitely long medium, i. e., in direction of wave motion

It is noted that for a low attenuation acoustic medium the characteristic impedance is a real number. For instance, in air $Z_{air} = (\rho_o C)_{air}$. However, in general, Z_o will be a complex number, i. e., have both magnitude and phase. Both the propagation constant and the characteristic impedance of a given medium completely define the acoustic reflection, attenuation, transmission, resonance, etc., characteristics for a given set of imposed boundary conditions.

In the standing wave tube configuration illustrated below the test sample "sees" essentially free air on one face and an essentially rigid wall on the other face.

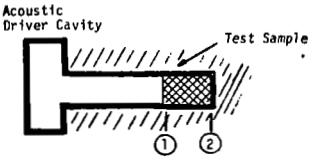

From transmission theory it can be shown that the impedance, Z_1, measured at station (1) on a test sample, with characteristic impedance Z_o looking into an impedance Z_2 (as shown below) can be expressed as

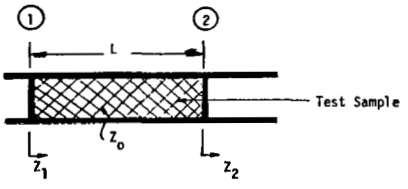

$$Z_1 = Z_o \frac{Z_2 + Z_o \tanh \gamma L}{Z_o + Z_2 \tanh \gamma L} \qquad (16)$$

where L = length of sample

For the standing wave tube $Z_2 \approx \infty$ (rigid wall) and thus

$$Z_1 = \frac{Z_o}{\tanh \gamma L} \tag{17}$$

Thus it is seen that the specific impedance ratio measured in the standing wave tube is actually

$$\frac{Z_1}{(\rho_o C)_{air}} = \frac{Z_o}{(\rho_o C)_{air}} \frac{1}{\tanh \gamma L} \tag{18}$$

and not the basic material property $Z_o/(\rho_o C)_{air}$, because of the imposed rigid end condition at station (2).

The propagation constant γ can be determined, in principle, by applying this result to measurements of the specific impedance ratio for two different sample thicknesses with

L_1 = length of first sample

L_2 = length of second sample

$$\frac{Z_{1\,1}}{(\rho_o C)_{air}} = \frac{Z_o/(\rho_o C)_{air}}{\tanh \gamma L_1} \tag{19}$$

$$\frac{Z_{1\,2}}{(\rho_o C)_{air}} = \frac{Z_o/(\rho_o C)_{air}}{\tanh \gamma L_2} \tag{20}$$

Thus

$$\frac{\left(Z_1/(\rho_o C)_{air}\right)_2}{\left(Z_1/(\rho_o C)_{air}\right)_1} = \frac{\tanh \gamma L_1}{\tanh \gamma L_2} = \frac{\tanh (\alpha' + j\beta) L_1}{\tanh (\alpha' + j\beta) L_2} \tag{21}$$

In general, the measured left side of this result is a complex number with real and imaginary parts. Thus, two equations can be obtained with two unknowns, α' and β, which can be solved for by trial and error since the resulting expressions are nonlinear. Once α' and β are found for a given frequency, then $Z_o/(\rho_o C)_{air}$ can be found from either equation (19) or (20). The resonant frequencies of the material can then be determined by inspection of α and of the phase versus frequency characteristics of $Z_1/(\rho_o C)_{air}$ since large amplitude changes and phase shifts will occur at internal resonant frequencies of the sample.

2.1.3.2 Experimental Determination of the Characteristic Impedance

The accuracy of measurements necessary to obtain reasonably accurate values for Z_o and γ by means of the two-thickness method is quite high. The two-thickness method for the determination of Z_o and γ has a serious drawback because it requires a high accuracy in the determination of the surface impedances Z_1 for the two sample depths. Good accuracy is hard to achieve (References 38 and 39), especially with foams. Moreover, the errors on Z_1 may be amplified when Z_o is calculated. The error ϵ_o on Z_o can be evaluated from the experimental errors ϵ_1, and ϵ_2 on the measurements of Z_1 for a depth L and depth 2L of the absorbing material:

$$\frac{\epsilon_o}{Z_o} = \frac{\tanh^2 \gamma L + 1}{(2\gamma L)(\tanh \gamma L)(1 - \tanh^2 \gamma L)} \left[\frac{\epsilon_1}{Z_{1,L}} + \frac{\epsilon_2}{Z_{1,2L}} \right] \qquad (22)$$

It was found that the experimental errors ϵ_1 and ϵ_2 are often greatly magnified in the calculation of the characteristic impedance.

A better approach would be to measure the characteristic impedance in a standing wave tube with a very deep foam sample ($Z_1 \rightarrow Z_o$ when $\gamma L \rightarrow \infty$) and to measure the propagation constant in a traveling wave tube, as was done by Scott on rock wool (Reference 40).

Since TRW did not possess a progressive wave apparatus, two-thickness measurements were made and the error amplification factor was evaluated. For frequencies at which the foams are highly absorbing, a foam depth of 2.75 inches (deepest sample holder of the B & K apparatus) may be sufficient to obtain Z_o directly ($Z_1 \rightarrow Z_o$ when $L \rightarrow \infty$). To obtain γ a second measurement with a much smaller foam depth was needed. Experimental errors, combined with the above discussed analytical error amplification, definitely limit the accuracy of Z_o and γ thus obtained.

Most of the standing wave tube measurements described in Section 2.1.2 were made for a foam depth of 1 inch (0.0254 m). To obtain the characteristic impedance and propagation constant of stable light foam (6% Protein foaming agent concentration EXP = 38) a preliminary run (#303, Figure 2-15) was made with a 1-inch deep foam sample. Only the absorption coefficient, α, was measured and a peak near 2200 Hz was found.

This was followed by three tests (#304 a, b and c) made at 1600, 2133 and 2666 Hz with samples of varying depths 1, 2, and 2.75 inches. The absorption coefficient curves are shown in Figure 2-16. The data of test #304 were reduced to yield the nine values of surface impedance and the three values of characteristic impedance at each frequency obtained by using two pairs of sample depths for each calculation. It was found that the experiments at 1600 Hz were in error and that the

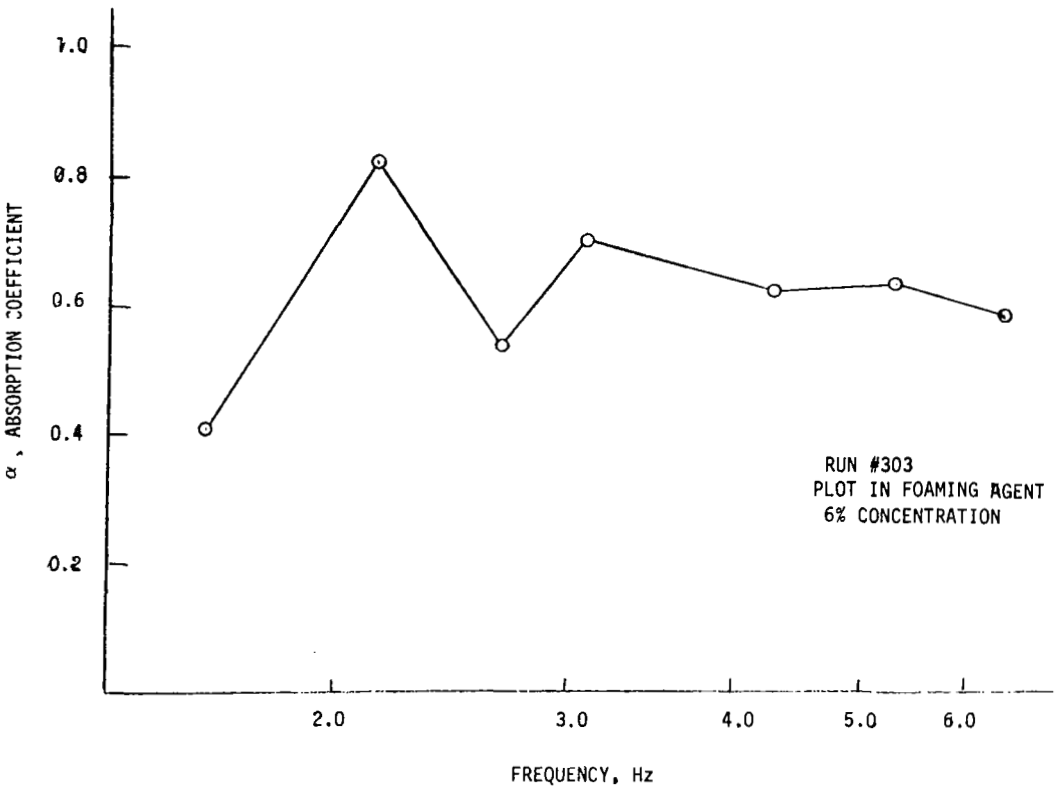

Figure 2-15. Resonance Determination, Preliminary Run 303

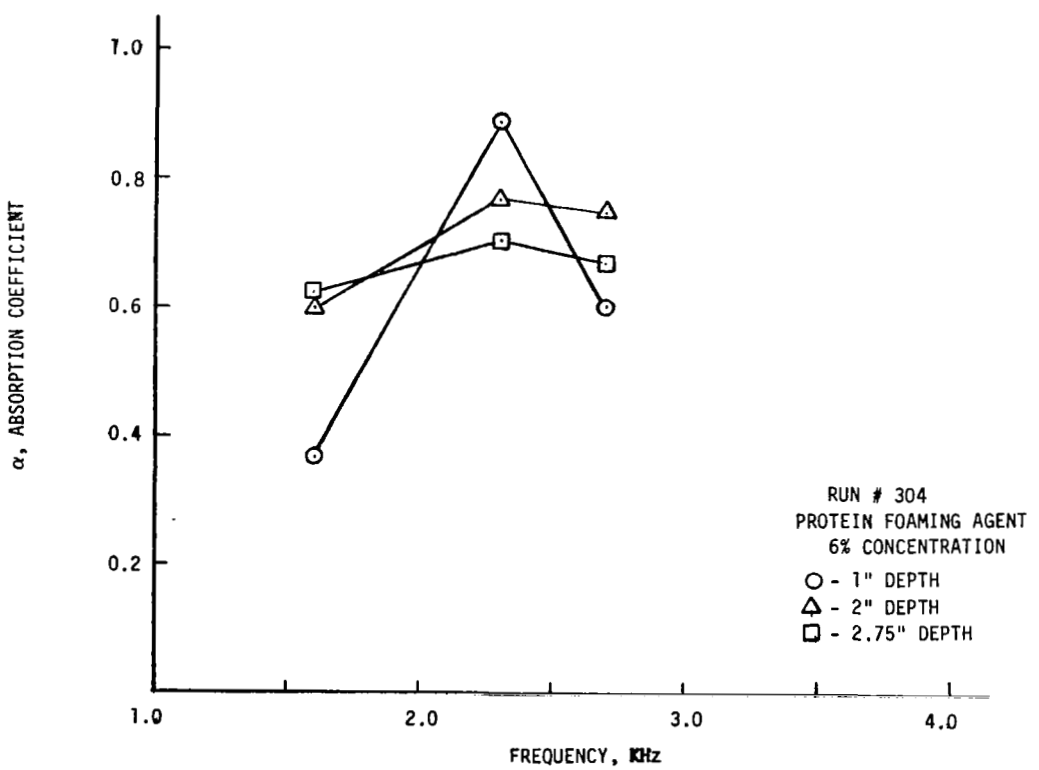

Figure 2-16. Absorption Coefficients for Three Depths of Foam, Run 304

depths of 2.0 and 2.75 inches were too close to each other to yield usable values of Z_o and γ at all three frequencies. The results for 2133 and 2666 Hz are shown in Table 2-2. Measurements on foam samples similar to those of tests #303 and #304 were made several weeks later using foam depths of 1, 2, 3, 4 and 5 inches for frequencies ranging from 1975 to 2860 Hz (tests #305 and #306). During these measurements, it became very clear that aging of the foam during the test had a large influence on the calculated values for Z_o and γ, and that aging was very pronounced in the first few minutes of foam life. The calculated values for Z_o and γ for test #305 are also shown in Table 2-2 while Figure 2-17 shows the data obtained in tests #305 and #306.

The error amplification factor (Reference 40) on the propagation constant was calculated for 2133 and 2666 Hz for the L = 1 inch and L = 2 inch depth combination for test #304. An error amplification by a factor of five was found for 2133 Hz, while at 2666 Hz the error was reduced by a factor of four relative to experimental errors. Several assumptions had to be made, such as equality of errors on all measurements (i.e., equal for both depths and equal for resistive and reactive components). This attempt at error calculation focuses our attention on the nonlinear response of calculated propagation constant values to experimental errors. Examination of data in #305 showed that experiments at 2133 Hz were in error and were therefore discarded. The error may be attributed to the possible inadvertent use of a foam sample that was not identical (or close) to the other samples. In #304 a single

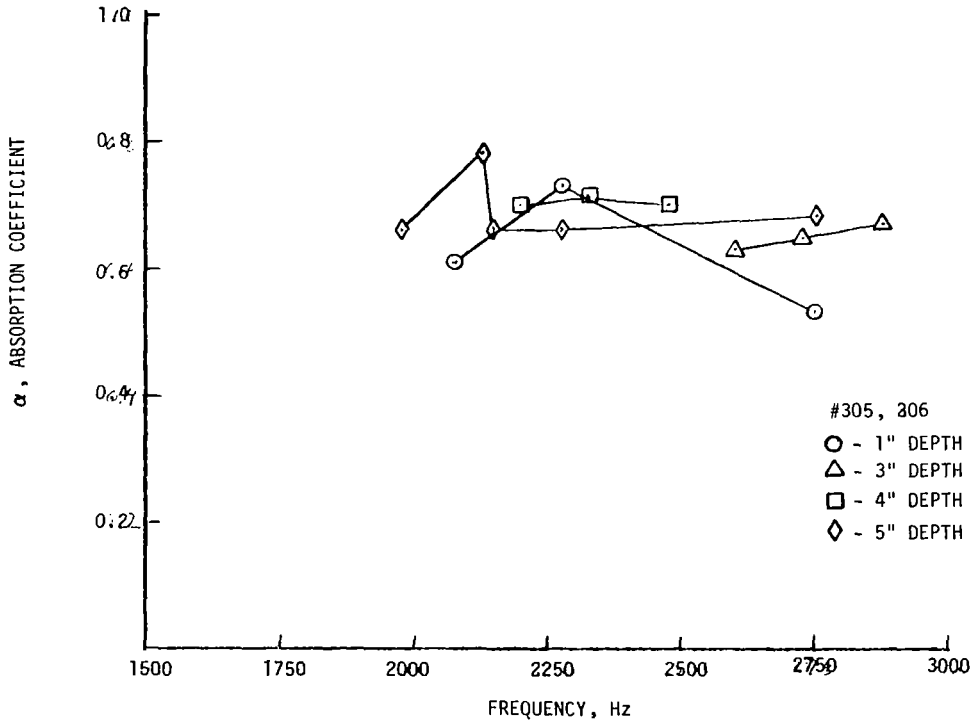

Figure 2-17. Absorption Coefficients for Four Depths of Foam, Runs 305 and 306

Table 2-2. Experimental Values of Characteristic Impedance and Propagation Constant of Foam

Run No.	L (in.)	α	Z_1	Z_o	γ (nep/inch)	c
f = 2133 Hz						
304	2	0.775	2.477 + j0.833	2.6 + j0.54	0.7 + j1.2	284 m/sec
304	1	0.895	1.906 - j0.272	3.1 + j0.59	0.6 + j1.3	263 m/sec
	2.75	0.705	3.316 + j0.431			
f = 2339 Hz						
305	1	0.725	2.356 + j1.318	3.1 + j1.31	1.05 + j1.8	206 m/sec
	5	0.675	3.114 + j1.235			
f = 2666 Hz						
304	2	0.755	2.835 + j0.56	3.2 + j0.56	0.7 + j2.4	178 m/sec
304	1	0.60	2.782 + j2.06	3.5 + j0.36	0.65 + j2.3	183 m/sec
	2.75	0.67	3.661 + j0.365			
f = 2729 Hz						
305	1	0.53	4.85 + j1.543	3.4 + j0.32	0.75 + j2.9	150 m/sec
	5	0.70	3.39 + j0.265			

sample was used for three frequencies at each foam depth. In #306 a fresh sample was taken for each frequency. Thus, the foam structure may have been different for one of the samples.

Variation of γ and Z_o with frequency was expected, but the cumulative errors incurred through the aging of foam and through the use of the two-thickness method do not permit conclusions on frequency dependence to be drawn from these tests. The frequencies for which measurements in test #305 were chosen coincide with predicted resonance for depths of 3, 4 and 5 inches. The predictions were based on an analysis discussed in Section 3. The calculations were based on values of Z_o and γ obtained in #304; it was assumed that these same values could be applied to other frequencies.

A final test, #306, showed that resonances did occur close to the predicted frequencies. This test is discussed in Section 3.

2.1.3.3 Resonance of Foam Samples in a Standing Wave Tube

The standing wave tube measurements of the surface impedance of foam samples confirm the contention that sound absorption in foams is characterized by resonance phenomena.

The surface impedance, Z_1, of a foam sample of depth L is a function of the characteristic impedance Z_o and of the propagation constant γ (see Section 2.1.3.2):

$$Z_1 = Z_o/\tanh \gamma L \tag{23}$$

Let

$$Z_o = R_o + j X_o \tag{24}$$

and

$$\tanh \gamma L = \tanh(\alpha' + j\beta) \equiv \sigma + j\tau$$

so that

$$\sigma = \frac{\tanh \alpha' L(1 + \tan^2 \beta L)}{1 + (\tanh \alpha' L \tan \beta L)^2} \tag{25}$$

$$\tau = \frac{(1 - \tanh^2 \alpha' L) \tan \beta L}{1 + (\tanh \alpha' L \tan \beta L)^2} \tag{26}$$

The magnitude $|Z_1|$ and phase angle ϕ_{Z_1} of the surface impedance are

$$|Z_1| = \left[\frac{R_o^2 + X_o^2}{\sigma^2 + \tau^2}\right]^{1/2} \tag{27}$$

$$\phi_{Z_1} = \arctan\frac{X_o\sigma - R_o\tau}{R_o\sigma - X_o\tau} \tag{28}$$

At resonance $L = n\lambda/4$ and $\beta L = n\pi/2$ ($n = 1, 3, 5$) since $\beta = 2\pi/\lambda$ and $\tan \beta L \to \infty$

$$\sigma \to \frac{1}{\tanh \alpha' L}$$

and

$$\tau \to 0$$

Hence

$$|Z_1| \to \left[\frac{R_o^2 + X_o^2}{\sigma^2}\right]^{1/2} \tag{29}$$

$$\phi_{Z_1} \to \arctan\frac{X_o}{R_o} \tag{30}$$

provided $\sigma \neq 0$. Thus the phase angle of Z_1 is equal to phase angle of $Z_o \pm n\pi$, and $|Z_1|$ becomes maximum when $\tau \to 0$.

The absorption coefficient α also goes through a maximum at resonance since

$$\alpha = 1 - |r|^2 \tag{31}$$

and

$$r = \frac{1 - Z_1/(\rho_o C)_{air}}{1 + Z_1/(\rho_o C)_{air}} \tag{32}$$

r is minimum when Z_1 = is maximum.

For the case of no-loss media ($R_o = 0$ and $\sigma = 0$), the surface impedance is

$$Z_1 = \frac{j X_o}{j\tau} = \frac{X_o}{\tau} \tag{33}$$

The phase angle of Z_1 tends to zero and its magnitude tends to ∞ at resonance. The experimentally determined characteristic impedances were predominantly resistive (see Table 2-2), X_o/R_o varying between 0.1 and 0.2; thus the phase angle of Z_1 at resonance will be small — less than 12 degrees. This phase angle increases continuously with frequency and is determined only by its tangent (i.e., lies in the fourth or first quadrant). Therefore, a change of sign of ϕ_{Z_1} from negative to positive indicates the approach to a resonant frequency.

Three of the experimentally determined curves of α and ϕ_{Z_1} are shown in Figures 2-18, 2-19, and 2-20. The data obtained did not include a sufficient number of points to permit correct detailed curves of α and ϕ_{Z_1} to be drawn. Often a peak in α was not detected where a change in the sign of ϕ_{Z_1} had occurred because of the sparseness of data points. The curves in Figures 2-18, 2-19 and 2-20 combine data points and analytical considerations and serve to illustrate phenomena. More refined experimental techniques are needed to conduct a quantitative investigation.

2.1.4 Foam Destruction by Sound Waves

The use of high intensity acoustic waves to destroy foams has often been proposed. Foam destruction has been attributed to resonance phenomena in the audible frequency range (Reference 34) and to radiation pressure forces in the high frequency range and for very high intensities (above 150 db, Reference 35). Foam buildup control by this means was not found practical for industrial applications.

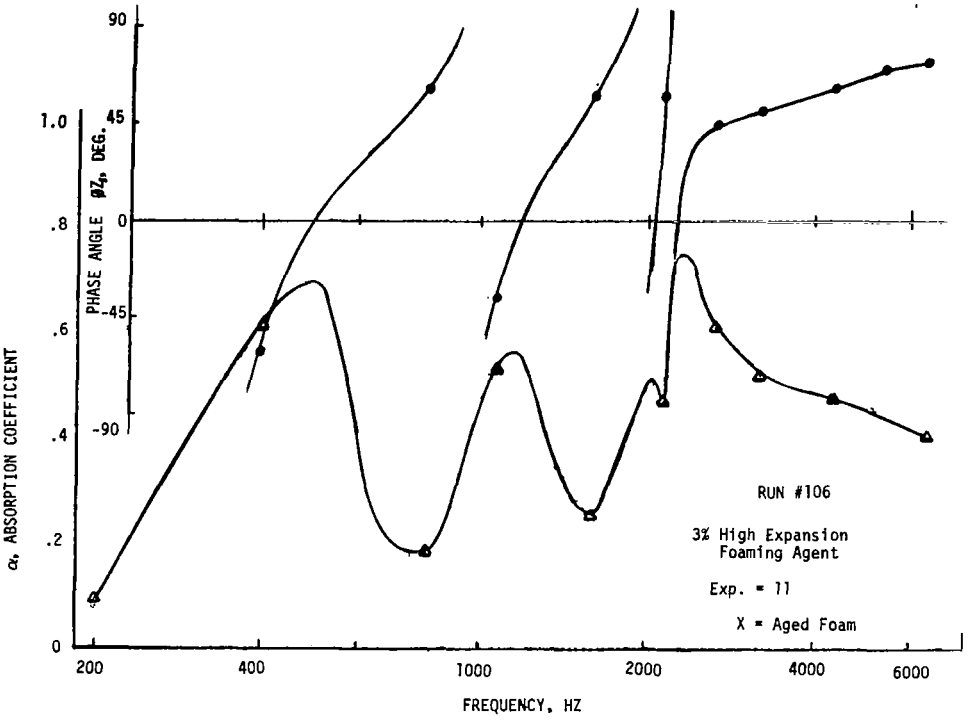

Figure 2-18. Absorption Coefficient and Phase Angle of the Surface Impedance of a Foam, Run 106

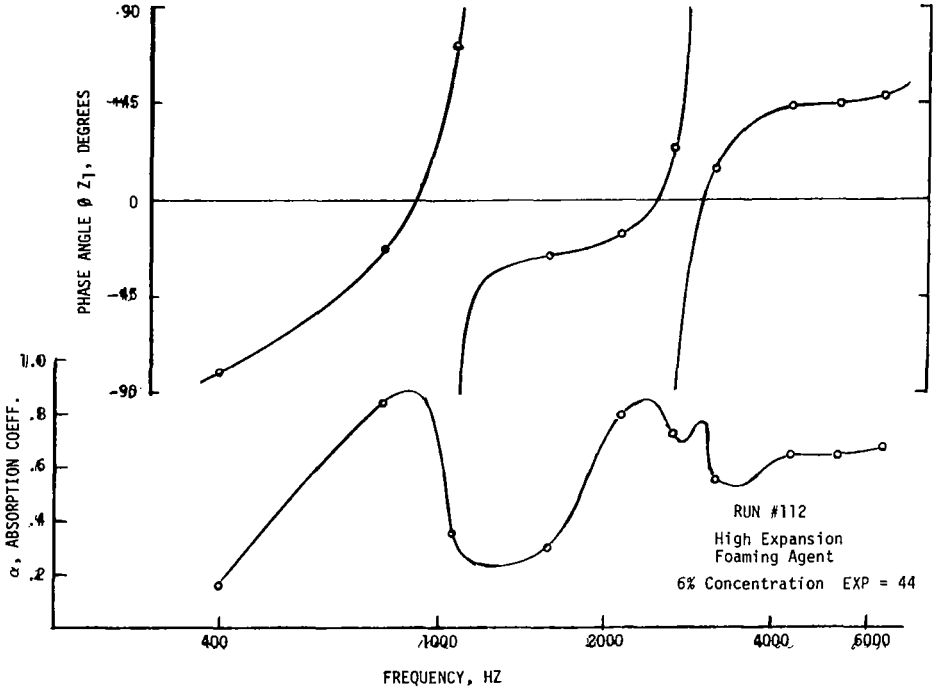

Figure 2-19. Absorption Coefficient and Phase Angle of the Surface Impedance of a Foam, Run 112

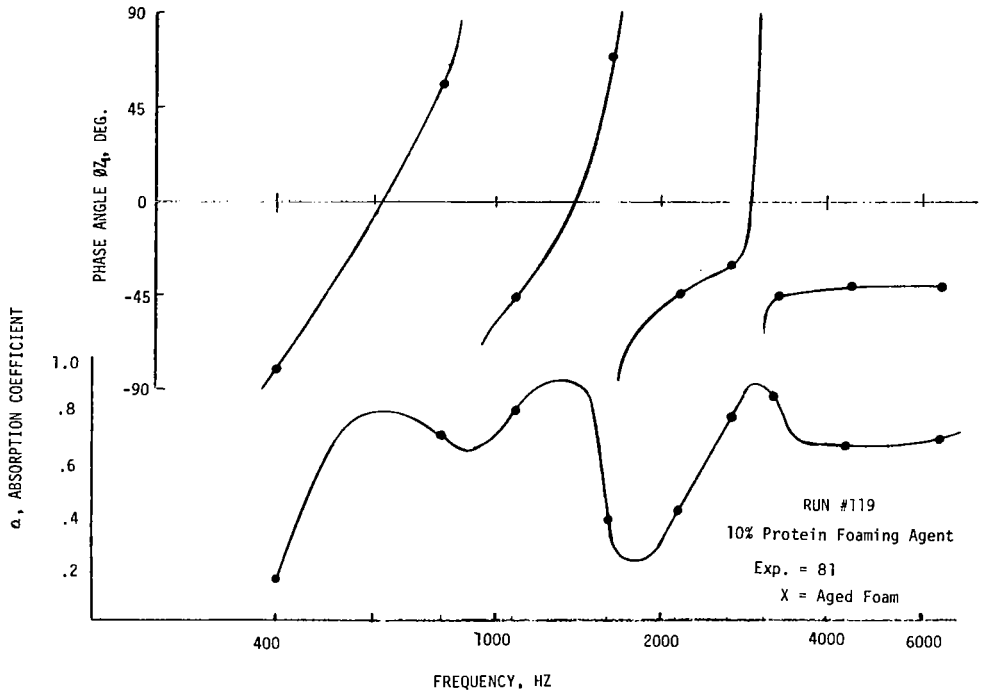

Figure 2-20. Absorption Coefficient and Phase Angle of the Surface Impedance of a Foam, Run 119

The high energy standing wave tube was used to observe foam destruction in tests 301 and 302. These tests began by three series of absorption coefficient measurements to observe foam aging (Figures 2-13 and 2-14) and took about 10 minutes. The sample was then removed, inspected, and photographed. The foam depth had not visibly changed in that time. The sample was then replaced in the tube and was subjected to a 5 minute exposure at 1600 Hz, 95 db sound waves. After that time both foams had been nearly completely destroyed. However the Aer-o-Foam 100 + Catalyst foam of #301 also showed considerable drainage in the large control sample (2.1 liters) not exposed to sound waves. The total volume had not changed during the period when the destruction test was made, but about 45 cc of liquid had drained so that the remaining foam had an expansion ratio of more than 80. The control sample of the protein foam not exposed to sound had not drained appreciably in the time when sound waves destroyed the 1-inch deep sample. The life of a foam, even a stable foam, is considerably shortened by exposure to sound waves. Foam destruction tests were not pursued any farther since the projected application for foams in jet noise reduction does not demand that foams survive for more than a fraction of a second.

2.1.5 Summary Test Result Observations

Several observations may be made from an examination of the absorption coefficient graphs.

- Generally high absorption coefficients (up to 0.9) have been measured in the 1 to 6.3 kHz range. In the 0.4 to 1 kHz range the values are usually below 0.5. Comparison was made with a styrofoam sample (Figure 2-21). Its absorption coefficient is below 0.1 in the low frequency range, averages about 0.2 in the higher frequencies, and reaches 0.48 at 6.3 kHz.

- Absorption coefficients generally increase with frequency but most of the graphs show several definite peaks at certain frequencies (Figures 2-4 through 2-12).

- No general trend or change of α with the foaming agent concentration (i.e., the surface tension on the gas-liquid interface) could be found. Somewhat higher absorption for low concentration foams may be attributable to faster draining.

- Light foams have higher absorption coefficients than heavier foams (Figures 2-4 through 2-8), but the change is by no means uniform or monotonic (Figures 2-9 through 2-11).

Foam density (or EXP) is not sufficient to determine the absorption coefficient. To illustrate this point the absorption coefficients of two foams of nearly equal density are shown in Figure 2-12. The role of bubble size and physical properties of foams is examined in Section 3 of this report.

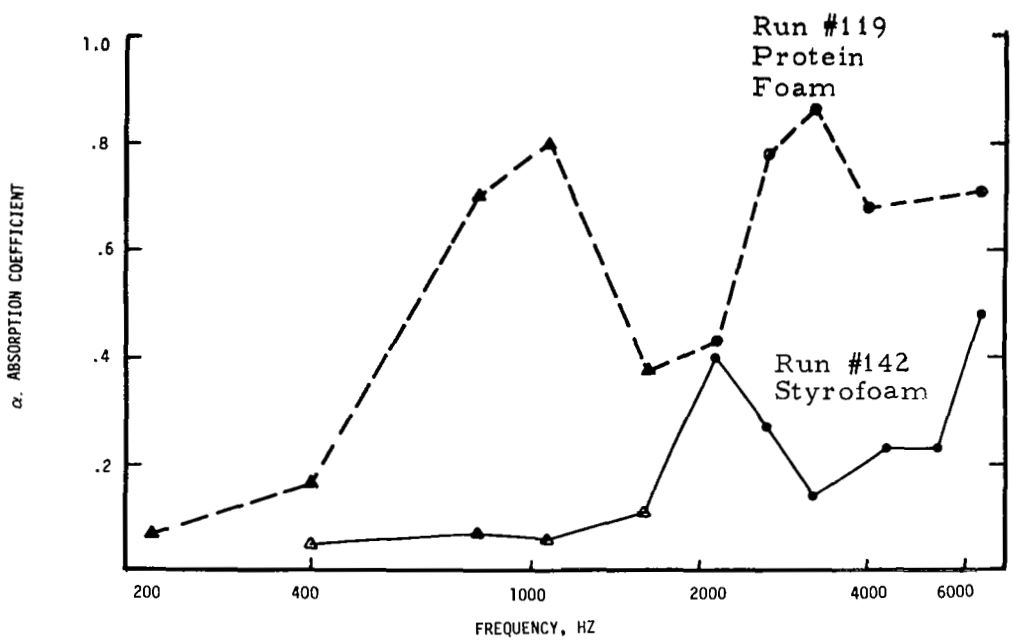

Figure 2-21. Absorption Coefficient of Styrofoam

2.2 REVERBERATION CHAMBER ABSORPTION COEFFICIENTS

2.2.1 Method, Test Facility, and Instrumentation

Absorption coefficients for completely diffuse wave motion obtained in highly reverberant rooms are widely used by architectural acousticians to characterize the sound absorbing properties of structural materials.

Reverberation chamber tests were conducted in the Western Electric Acoustic Laboratory's reverberation chamber. The reverberation chamber used for these measurements has dimensions of 28 x 17 x 12 feet and a volume of 5800 ft^3. Walls, ceilings and doors are of concrete construction, with nominal surface weight of 50 lbs/ft^2. The interior surfaces of the chamber have been specifically treated with an epoxy coating and the average value of wall acoustical absorption coefficients over the 125 Hz to 4 kHz frequency range vary from 0.01 to 0.02. Foam test specimens were placed in a wooden pan (treated to reduce water leakage) with dimensions 8 feet by 9 feet x 1.5 inches deep. The container was left in place during recording of empty chamber decays.

The instrumentation used for the measurements is shown in Figure 2-22. The wideband electrical noise source, power amplifier and loudspeaker are used to produce a wideband (80 Hz to 10 kHz) acoustical white noise in the reverberation chamber. Typical test signal overall level was 100 db sound pressure level (db re 0.0002 $dyne/cm^2$). The

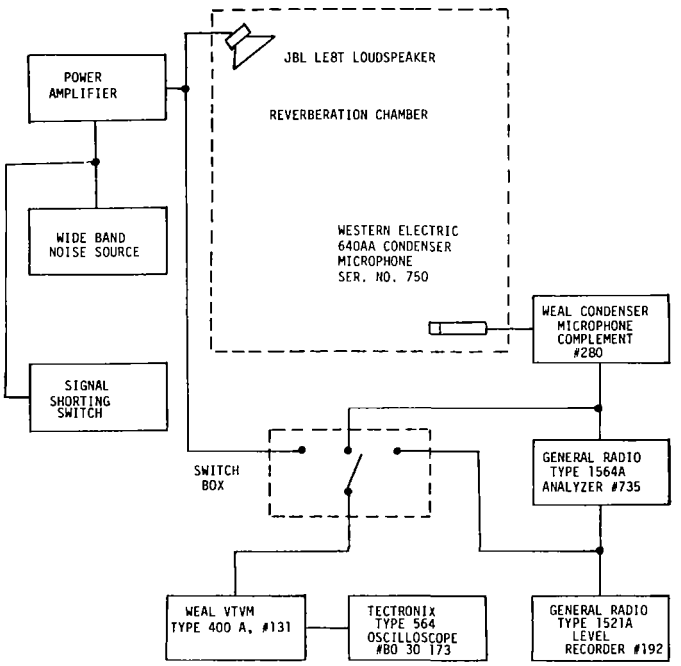

Figure 2-22. Block Diagram of Instrumentation Used to Measure Random Incidence Acoustical Absorption Coefficient

shorting switch allows instantaneous interruption of the signal to the loudspeaker which is located in one of the trihedral corners of the chamber.

The acoustical signal in the chamber is transduced to an electrical signal by the condenser microphone which is located in a trihedral corner of the chamber. This signal is then amplified and recorded on chart paper via the 1/3 octave analyzer shown in Figure 2-22. The switch box shown in the diagram allows monitoring of the signal amplitude and waveform by the vacuum tube voltmeter and oscilloscope at three locations in the circuit.

A typical measurement consists of recording on the level recorder chart paper the decaying sound in the chamber, in 1/3 octave bands. Five to seven decays were recorded in the 125, 250 and 500 Hz 1/3 octave bands and four decays were recorded for the 1000, 2000, 4000 and 6300 Hz 1/3 octave bands. The average of the several decays was used to obtain the reverberation time in each 1/3 octave band. The above measurement procedure was performed with the reverberation chamber empty and with the test specimen located in the chamber floor. Comparison of the two reverberation times at each of the 1/3 octave bands allows a determination of the average random incidence absorption coefficient for the test specimen.

The basic relationship used to obtain the random incidence acoustical absorption coefficient is the Sabine reverberation formula given by (Reference 42)

$$T = \frac{KV}{\bar{\alpha}S + 4mV}$$

where

T = reverberation time, seconds

K = 0.049 a constant for small changes in temperature

V = volume of the reverberation chamber, cubic feet

S = surface area of the chamber interior, square feet

m = energy attenuation coefficient, ft^{-1}

$\bar{\alpha}$ = average random incidence acoustical absorption coefficient

The $\bar{\alpha}S$ term is the total acoustical absorption in the chamber caused by surface absorption, while the 4mV term accounts for acoustical absorption in air. Using the above equation and subscripts "c" and "s" to designate the empty chamber and chamber with test specimen, respectively, the relationship for the average absorption coefficient is given by

$$\bar{\alpha} = \frac{KV}{S_s}\left[\frac{1}{T_s} - \frac{1}{T_c}\frac{(S_c - S_s)}{S_c}\right] + \frac{4V}{S_s}(m_c - m_s) - \frac{4m_c V}{S_c}$$

where

S_s = surface area of test specimen

S_c = surface area of reverberation chamber

m_c = energy attenuation constant during empty chamber measurement

m_s = energy attenuation constant during measurements with test specimen in the chamber

The derivation of the preceding equation assumes that the ambient temperature, and therefore velocity of sound in the chamber during the empty and occupied chamber runs, does not change appreciably. This was the case during all the measurements. The first term in the equation is the one normally used for this type of measurement. The $(S_c - S_s)/S_c$ term accounts for the fact that a small portion of the chamber surface area is covered by the test specimen. The second and third terms in the equation account for the absorption of sound in air. The third term is required since in general the empty chamber and occupied chamber data could not always be made under identical humidity conditions. However, generally, this term was found to be very small. The third term in the equation was also found to be small although not insignificant. In calculating these correction terms, the data published in Reference 43 have been used.

2.2.2 Test Procedures

The foam generator was located outside a door to the reverberation chamber, so that a long hose could be used to deposit the foam into the 8 foot x 9 foot x 1.5 inch deep pan placed on the floor of the reverberation chamber. Ten to 12 cubic feet of foam were necessary to sufficiently overfill the pan and permit scraping the foam to obtain a flat surface. Photographs 1 and 2 on Figure 2-23 show the filling and scraping of foam in the pan.

The liquid tank was filled with 14 liters of water and foaming agent, which yielded between 7.5 and 40 ft^3 of foam for the tested expansion ratio range of 15 to 80. For expansion ratios below 25, the liquid tank had to be refilled once. A liquid flow rate of about 50 cc/sec was selected for

1. Filling Pan with Foam. Run 32

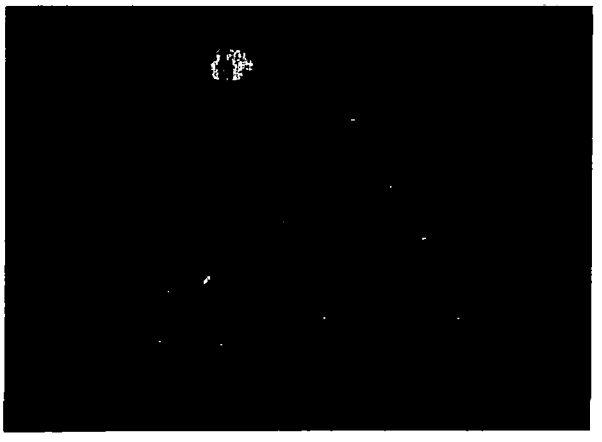

2. Scraping Foam to obtain a flat surface. Run 32

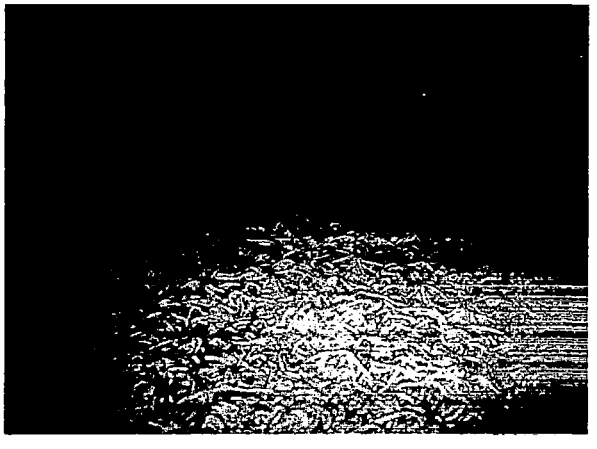

3. Shear Resistant Foam Run No. 18

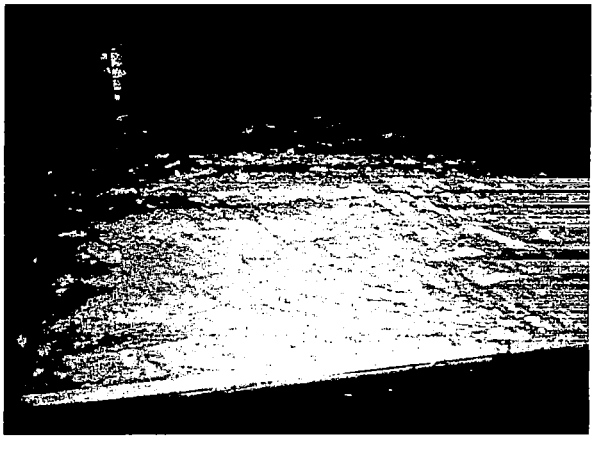

4. Shear Resistant Foam Surface After Scraping. Run No. 28

Fig. 2-23 Preparation of Foam-filled Pan for Acoustic Absorption Tests in a Reverberation Chamber

expansion ratios up to 40. For higher expansion ratios the liquid flow rate was reduced to 25 cc/sec in order to keep the foam flow rate reasonably low. The gas flow rate was adjusted to yield the desired expansion ratio which was measured by weighing a 3-liter sample obtained while the floor pan was being filled. Some of the high expansion foams obtained from high concentration solutions were extremely shear resistant. The cylindrical shape of the foam extruded through the hose persisted and could not be scraped flat (Photograph 3 and 4 on Figure 2-23). The influence of the surface irregularities on the absorption coefficient was probably minimal. To substantiate this assertion, tests were made on flat and grooved styrofoam panels.

Because of the relatively fast aging characteristics of the water-based foam specimens used for most of the measurements, it was desirable to record the

- Data in as short a time as possible after the manufacture of the foam
- Elapsed time for the measurements of sound decays

In an effort to record the effect of aging on the sound absorption coefficient of the test specimens, the 1000 Hz 1/3 octave band decays were repeated at the end of each run. That is, the sequence of recording 1/3 octave band sound decays was 125, 250, 500, 1000, 2000, 4000, 6300 and 1000 Hz. Total elapsed time for this series of recordings was about 8 minutes; the elapsed time between the two 1000 Hz set of decays was about 3 minutes.

The absorption coefficients for a frequency range of 125 to 6300 Hz were determined for 18 foams. A summary of the foam properties and flow conditions in the foam generator are given in Table 2-3.

Filling and scraping operations took about 15 minutes for high expansion foams and up to 25 minutes for the heavier foams because the liquid tank had to be refilled. The acoustic test lasted 6 to 8 minutes. Because of the length of time required, only very stable foams could be used in the reverberation chamber. The catalytic foam was not delivered on time and, hence, could not be tested. Runs #29 and #32 were made with the 100 percent concentrate without catalyst. Therefore, the foams obtained were very soft and drained rapidly; the highest expansion ratio obtainable without slugging was used for each concentration.

2.2.3 Summary Test Results

Absorption coefficients, whether measured in a reverberation chamber or in a standing wave tube are not a characteristic property of the material (Reference 44) because a material and its environment cannot be separated. The size of sample, the way it is mounted or contained, the nature of the sound field, the shape of the reverberation room, or the standing wave tube characteristics influence the measured value of the absorption coefficient.

Table 2-3. Characteristics of Foams Tested in a Reverberation Chamber

Run No.	Foaming Agent Type	Percent Foaming Agent	Expansion Ratio	Liquid Flow Rate Nominal (cc/sec)	Liquid Pressure (psig)	Tank Refill
2	High Expansion	6.0	35	50	105	No
3	High Expansion	6.0	21	50	85	Yes
6	High Expansion	4.5	33	50	95	No
7	High Expansion	4.5	15	50	75	Yes
10	High Expansion	4.5	16	50	75	Yes
11	High Expansion	4.5	48	25	80	No
14	High Expansion	3.0	17	50	88	Yes
15	3% Regular Protein	10	44	25	75	No
18	3% Regular Protein	10	80	25	125	No
19	3% Regular Protein	10	17	50	---	Yes
20	3% Regular Protein	10	32	50	---	No
22	3% Regular Protein	10	18	50	95	Yes
23	3% Regular Protein	6	17	50	100	Yes
26	3% Regular Protein	6	32	50	123	No
27	3% Regular Protein	6	47	50	137	No
28	3% Regular Protein	3	57	25	105	No
29	100% Concentrate Aerofoam no catalyst	6	29	25	100	No
32	100% Concentrate Aerofoam no catalyst	10	40	25	130	No

Note: Run numbers such as 1, 4, 5 etc. were assigned to "empty chamber" tests which preceded and followed each series of runs.

Moreover, foam absorption coefficients are time dependent since draining of the liquid by capillary forces and by gravity continuously change their structure.

For this reason a repeat point was taken on each foam sample at a nominal frequency of 1000 Hz. The difference between the absorption coefficient curve and the repeat points was on the order of 0.04 and is indicative of the drainage, bubble growth, and collapse occurring during the time necessary to complete the measurements from 1000 to 6300 Hz and return to 1000 Hz, i.e., 4 or 5 minutes. The foams used in the reverberation tests were among the most stable obtained in the previous experiments (except for runs 29 and 32, performed on a non-catalyzed agent), hence the repeat points are very close to the original curve.

Figures 2-24 through 2-27 show some typical absorption coefficient curves.

The reverberation chamber tests show that

- Absorption coefficients of foams generally increase with frequency from about 0.1 at 125 Hz, to 0.6 or 0.7 at 6300 Hz.
- No apparent systematic correlation exists between the foam expansion ratio and absorption.
- There are no steep absorption peaks, such as were found in the standing wave tube tests. As an example, corresponding runs in the reverberation chamber and in the standing wave tube are shown in Figures 2-24 to 2-27.

Absorption coefficients of solid and porous materials as measured in the standing wave tube apparatus are usually lower than those obtained for these materials in reverberation chambers (at least according to the Brüel and Kjaer instruction booklet for the 4002 apparatus used in our tests). The measurements on styrofoam showed this statement to be only partly true as can be seen in Figure 2-28. As stated before, a direct correspondence between standing wave tube and reverberation chamber measurements is not to be expected. The tests do show, however, that liquid foams absorb sound and that the absorption is higher for medium and high frequencies than in the lower frequency range. The absorption coefficients of liquid foams are considerably higher than those of styrofoam.

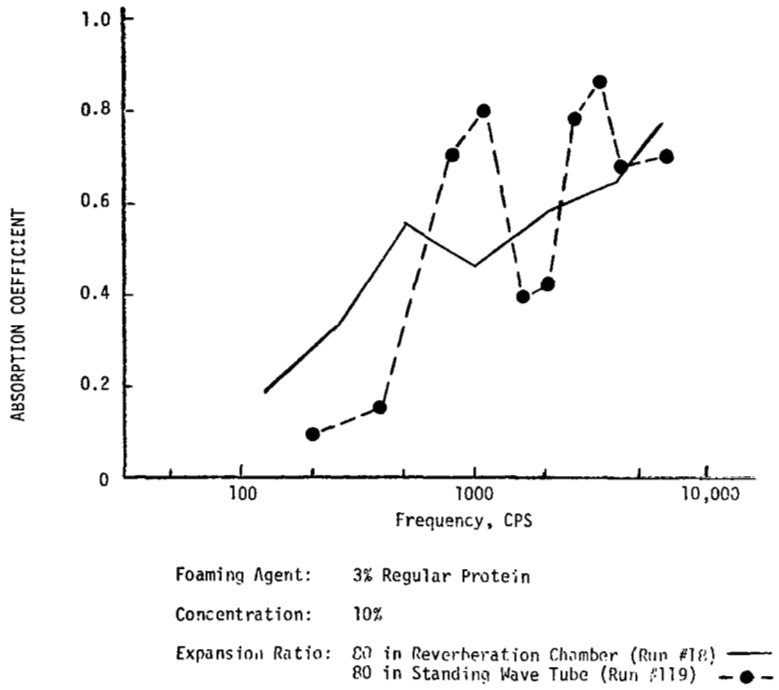

Figure 2-24. Absorption Coefficients of a Foam Measured in a Reverberation Chamber, Run 18, and in a Standing Wave Tube Apparatus, Run 119

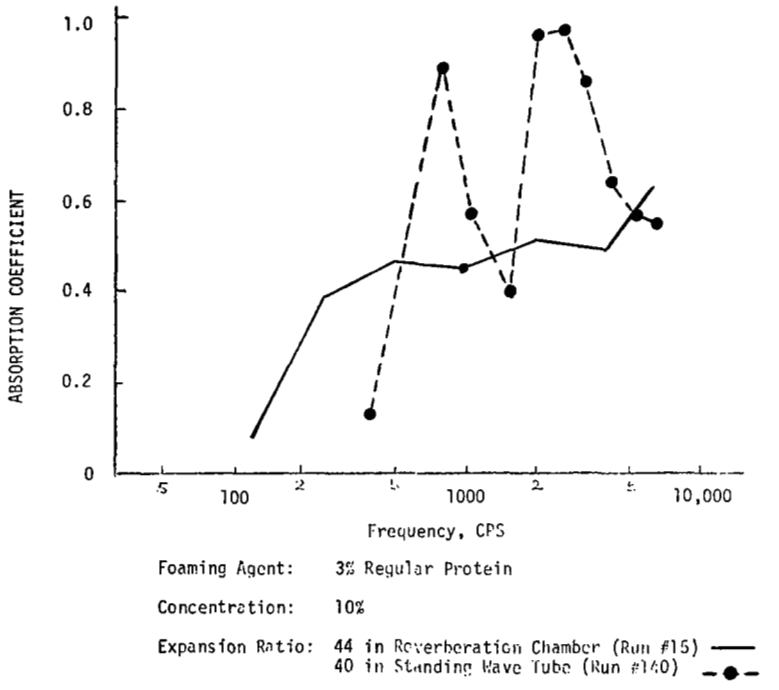

Figure 2-25. Absorption Coefficients of a Foam Measured in a Reverberation Chamber, Run 15, and in a Standing Wave Tube Apparatus, Run 140

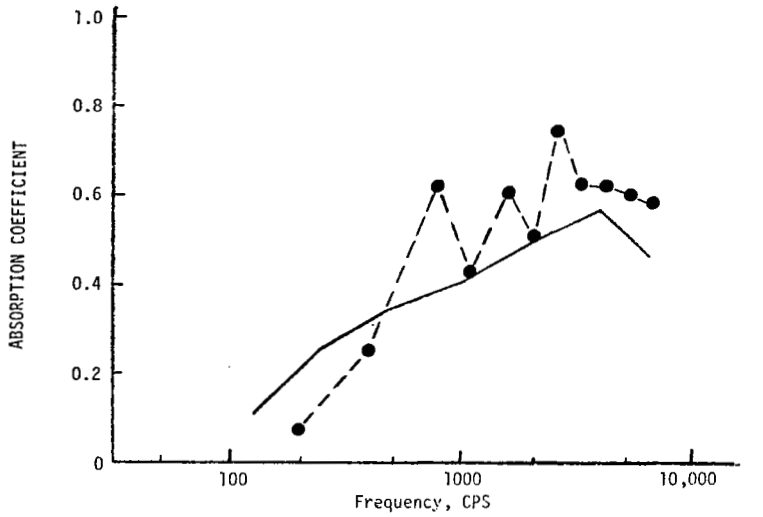

Foaming Agent: High Expansion

Concentration: 3%

Expansion Ratio: 17.5 in Reverberation Chamber (Run #14) ——
17 in Standing Wave Tube (Run #104) —●—

Figure 2-26. Absorption Coefficients of a Foam Measured in a Reverberation Chamber, Run 14, and in a Standing Wave Tube Apparatus, Run 104

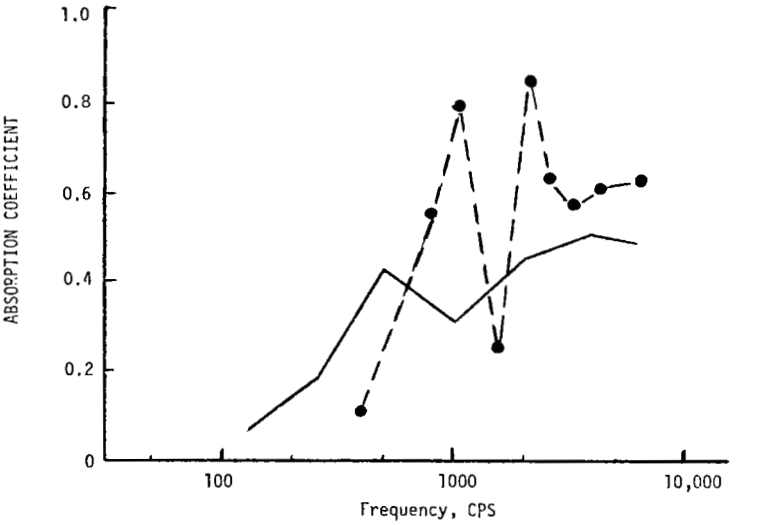

Foaming Agent: High Expansion

Concentration: 4.5%

Expansion Ratio: 47.6 in Reverberation Chamber (Run #11) ——
47 in Standing Wave Tube (Run #139) —●—

Figure 2-27. Absorption Coefficients of a Foam Measured in a Reverberation Chamber, Run 11, and in a Standing Wave Tube Apparatus, Run 139

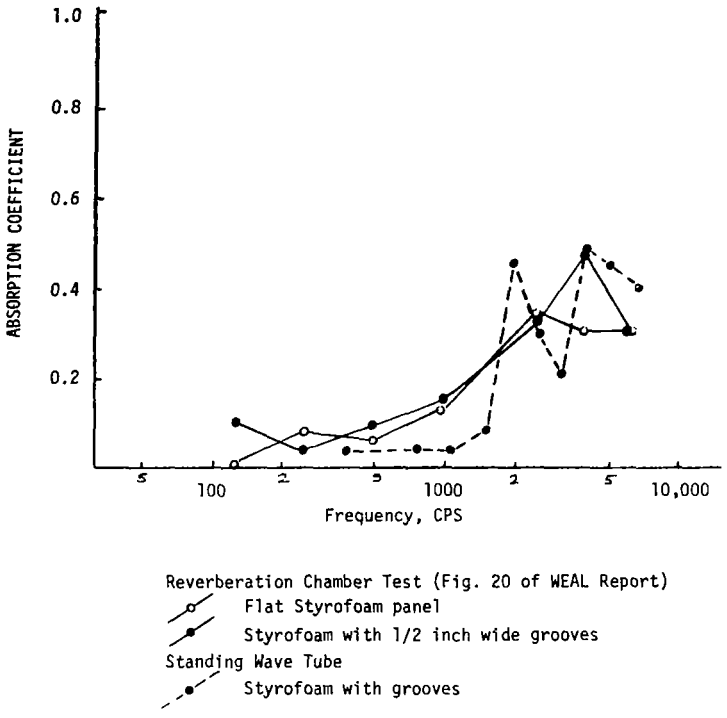

Figure 2-28. Absorption Coefficients of Styrofoam Measured in a Reverberation Chamber and in a Standing Wave Tube Apparatus

3. MODEL OF SOUND ABSORPTION MECHANISMS IN A FOAM

3.1 INTRODUCTION

The sound absorption properties of foams obtained by the standing wave tube method indicate that resonance phenomena may be responsible for the excellent sound absorptivity of foams. Resonance phenomena were hypothesised before the initiation of the present investigation, and a possible similarity between resonance in a foam and the behavior of gas bubbles in liquids under the action of pressure waves was postulated.

The approach chosen for examining the behavior of foams was to assume that every bubble of a set of bubbles with a given radius pulsated as if it were an isolated gas bubble in a liquid having the same density as the foam. A coupling between the motion of bubbles was also postulated. In this manner a distributed parameter mechanical model of the foam was formulated and an electrical analog of the mechanical system developed.

Numerical values for the equivalent mass and stiffness of a bubble were then used to obtain the absorption coefficient of the foam as a function of the driving frequency. The damping coefficients and coupling constants were variable parameters in this study, so that only an order of magnitude agreement could be expected from this simplified model. Such an agreement was obtained when the stiffness of the bubble was assumed to be one hundredth of the adiabatic stiffness of the gas; this indicates that the adiabatic compression and expansion of gas inside the bubble is not the only, or proper, energy storage and release mechanism present.

The analog model was also used in conjunction with acoustical characteristic impedances and propagation constants experimentally determined at two frequencies to obtain the mass, stiffness, and damping of the one bubble resonator plus the stiffness and damping of the coupling. The results were in excellent agreement for mass and damping constants and again indicated that the stiffness values were much lower than the adiabatic compression of gas and much lower than for isothermal compression.

3.1.1 Structure of Foams

Photographs of some of the foams tested in the standing wave tube are shown on Figure 3-1. The photograph magnification is about 4.5 to 1 (the graduated scale is in inches, 0.1 and 0.01 inch engraved divisions).

The following features detected on the photographs were important in the choice of a model for foam behavior. Gas bubbles of widely varying sizes were separated from adjacent bubbles by a liquid wall and usually a large bubble was surrounded by many smaller bubbles. Two foams of equal density may have widely different bubble size distributions and different sound absorption characteristics. For instance, the foams of

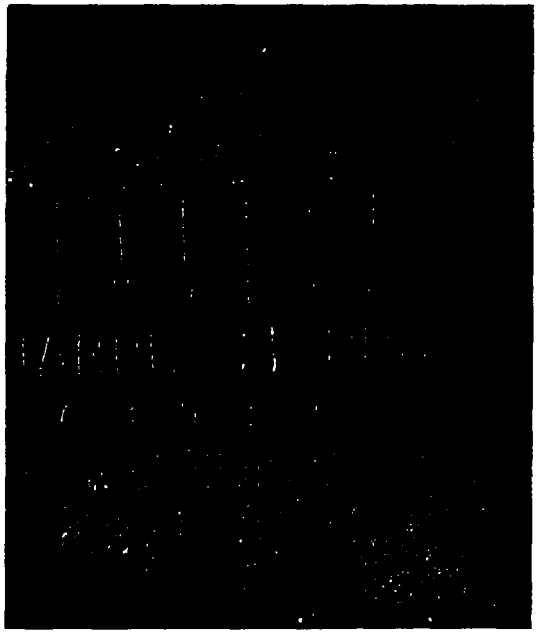

Run 104: High Expansion Foaming Agent, 3% Concentration EXP = 17

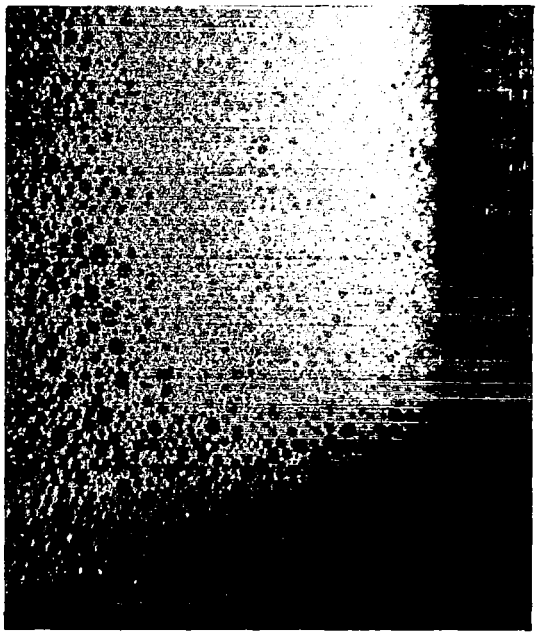

Run 131: Protein Foaming Agent 10% Concentration EXP = 16

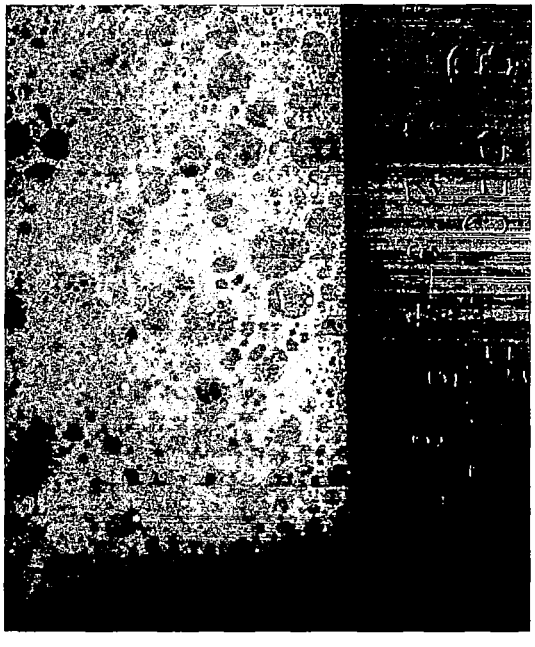

Run 108: High Expansion Foaming Agent, 3% Concentration EXP = 68

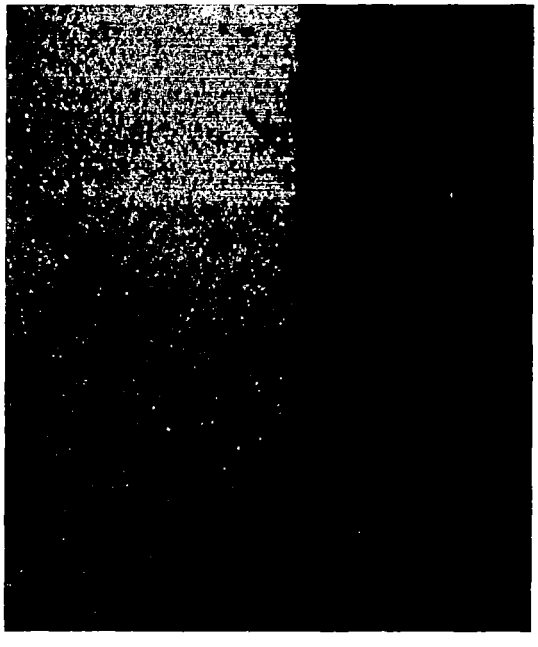

Run 119: Protein Foaming Agent, 10% Concentration EXP = 72

Figure 3-1. Photographs of Foam Surface

of tests #104 and 121 are of nearly equal density but the absorption coefficient curves are quite different. The #104 foam shows a wider range of bubble sizes; the largest was about 2.5 mm in diameter while the largest bubbles in foam #121 were only 0.85 mm in diameter. The smallest bubbles were so small as to be nearly invisible in both foams.

The surface of two very light foams are also shown at the bottom of Figure 3-1. Their structures were quite different. Large bubbles up to 4 mm in diameter were interspersed with smaller bubbles in the high expansion foam (#108), while only a narrow range of bubble sizes appeared in the protein foam (#119). Size, or mass, is usually a major factor in resonance phenomena; therefore, a bubble diameter distribution was obtained from the foam surface photograph of test #119. This was done by placing the photograph under a coordinate microscope with 5X magnification and measuring the mean diameter of all bubbles inside a 1/2-inch square. A computer program developed for droplet spray holography, was used to obtain the bubble size distribution by locking each bubble into a 2.5 micron wide band. The bubble diameter distribution and the corresponding volume distribution are shown in Figure 3-2. These distributions have not been incorporated into the model of foam behavior as yet. A need for this type of quantitative information is expected to arise when the analytical work has progressed further.

The bubble dynamics of a foam were obviously rather complex and there was little hope of arriving at a mathematical formulation without drastically simplifying the assumptions. Two models were considered: (1) an isolated bubble in a gas (balloon) with a coupling to other bubbles and (2) an isolated bubble in a liquid with the overall properties (density, viscosity, etc.) of the foam, coupled to other bubbles. In either case the coupling mechanism was difficult to define; the radiation of sound caused by bubble pulsation may be a possible explanation.

The second model has the advantage of known physical properties of the foam; therefore, a more straightforward examination of coupling is possible. Foam considered as an incompressible fluid is a valid assumption as long as no high velocity flows exist. In subsonic aerodynamics air is successfully assumed to be incompressible. If foam is assumed to be incompressible, analysis developed for the motion of bubbles in water can be applied to foam without further modifications. Actually there is little difference between the two models. Mainly the mass in motion is three times lower for the balloon bubble than the equivalent mass of the bubble in liquid.

3.1.2 Dynamics of a Bubble in a Foam

Several authors, including Rayleigh (Reference 45) and Minnaert (Reference 46), have mathematically described the pulsation of a bubble under the action of periodic pressure waves (References 47, 48 and 49). Rayleigh formulated the nonlinear differential equation of the radial

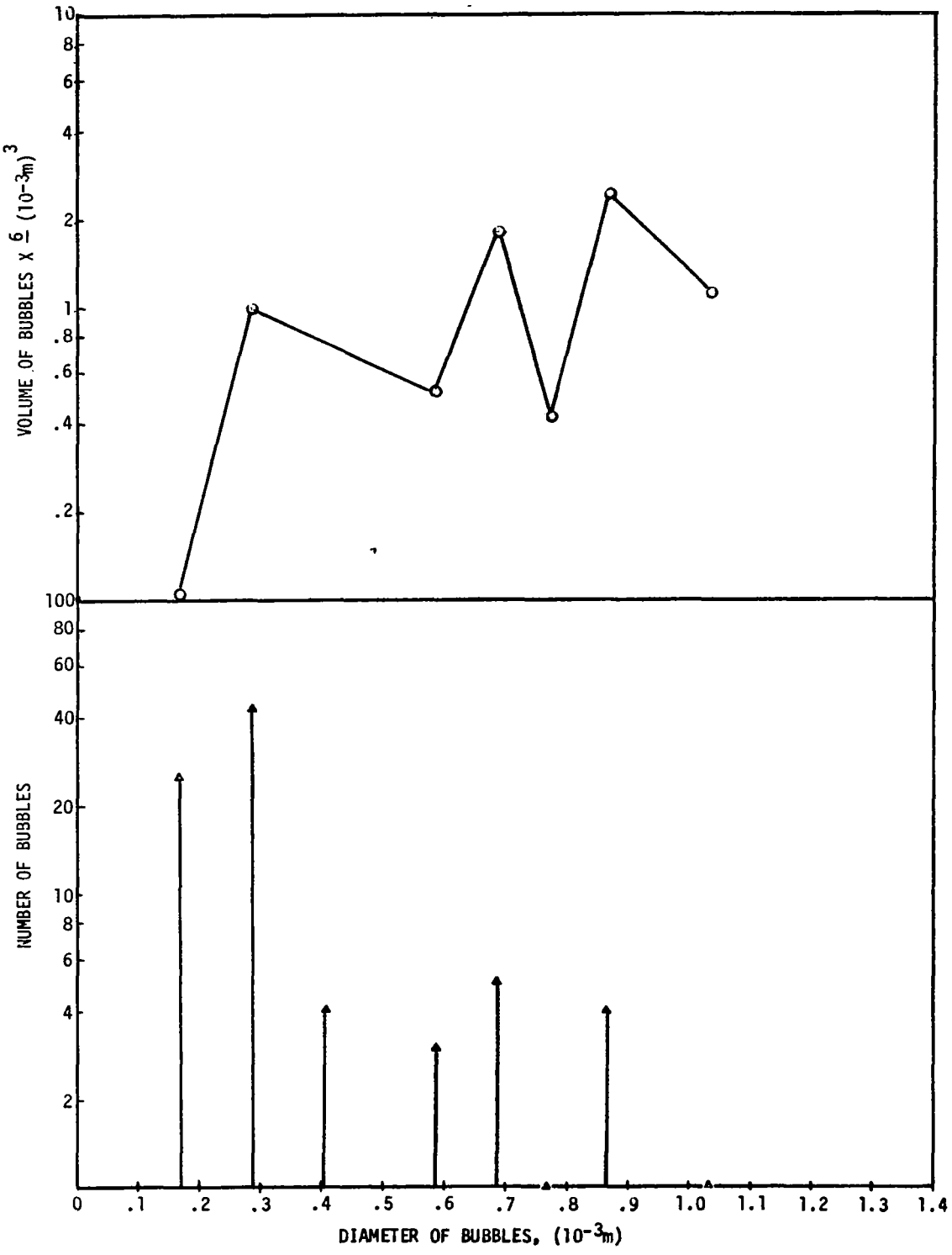

Figure 3-2. Bubble and Volume Distribution

motion of a spherical cavity, i.e., the most general and most complex case; Minnaert obtained the resonant frequency of the bubble by a simple energy balance while neglecting the influence of damping or of nonlinearities

$$f_M = \frac{\sqrt{3\gamma P_o/\rho}}{2\pi R_o}$$

Devin (Reference 47) also neglects the contribution of surface tension but introduces damping into the linearized differential equation and evaluates the magnitude of dissipation caused by thermal conduction, viscosity, and sound radiation at resonance. He assumes that damping does not affect the resonant frequency. Houghton (Reference 50) however includes viscous dissipation and surface tension forces in his equations and finds the resonant frequency to be

$$f = \frac{1}{2\pi R_o}\left\{\frac{3\gamma P_o}{\rho}\left[1 + \left(1 - \frac{1}{3\gamma}\right)\frac{2\sigma}{P_o R_o}\right] - \frac{4\nu^2}{R_o^2}\right\}^{1/2}$$

Numerical evaluation of the surface tension and viscous terms in the above expression showed that the surface tension term was important only for bubbles of very small diameter (less than 100 microns). The resonant frequencies of these small bubbles are too high (100 kHz) to be of interest here. Similiarly, viscous damping does not affect the resonant frequency for bubbles larger than 10 microns.

Hence Minnaert's resonant frequency evaluation is accurate enough for our purpose, and Devin's differential equation and evaluation of the damping constant are applicable provided that total damping does not far exceed viscous damping. The resonant frequency, as a function of bubble size, is shown in Figure 3-3. Devin derives the differential equation of radial motion of the bubble by means of Lagranges equation in the absence of a forcing function

$$\frac{d}{dt}\left(\frac{\partial L}{\partial \dot{v}}\right) - \frac{\partial L}{\partial v} = 0$$

where the Lagrangian L is the difference of the kinetic energy and the potential energy of the system {bubble-liquid} and v is an elementary change in the bubble volume. Dissipation is introduced in terms of

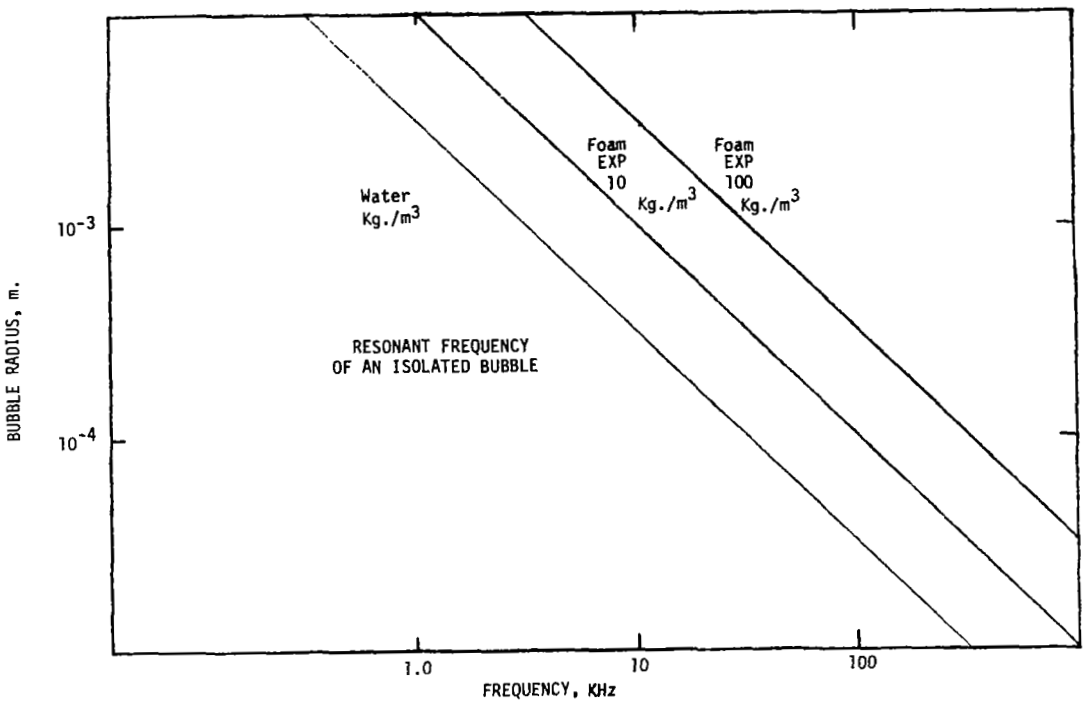

Figure 3-3. Resonant Frequency of a Bubble

Rayleigh's dissipation function B (Reference 51) under the assumption that the dissipation pressure is proportional to the bubble volume velocity $\dot{v}$

$$B \equiv b\dot{v}^2/2$$

where b is the dissipation coefficient.

The full generalized equation of motion is

$$\frac{d}{dt}\left(\frac{\partial L}{\partial \dot{v}}\right) + \frac{\partial B}{\partial \dot{v}} - \frac{\partial L}{\partial v} = - P \exp(j\,\omega t)$$

where P exp(j ωt) is the driving function for the motion.

The potential energy of the system is obtained by assuming that the gas in the bubble is compressed and expanded adiabatically during volume pulsations of the bubble, so that

$$P V^{\gamma} = P_o V_o^{\gamma}$$

For small amplitude pulsations

$$\delta P = - (\gamma P_o / V_o)\, \delta V = - (\gamma P_o / V_o) v$$

The potential energy of the system is

$$P E = - \int_0^v (\delta P)\, dv = (\gamma P_o / V_o) v^2 / 2$$

The kinetic energy of the system is obtained by noting that the flow of liquid near a radially pulsating bubble is irrotational and that the velocity potential Ω of the flow is caused by a simple source at the center of the bubble:

$$\Omega = -\dot{v}/4\pi R$$

The velocity of a liquid particle at a distance R from the bubble center is

$$\dot{R} = -\nabla\Omega = \dot{v}/4\pi R^2$$

The kinetic energy of the liquid of density ρ surrounding the bubble is

$$K E = \tfrac{1}{2}\rho \int_{R_o}^{\infty} (\dot{R})^2 (4\pi R^2)\, dR = (\rho / 8\pi R_o)\dot{v}^2$$

Hence the Lagrangian is

$$L = (\rho / 8\pi R_o)\dot{v}^2 - (\gamma P_o / V_o)(v^2 / 2)$$

The equation of motion is therefore

$$(\rho/4\pi R_o)\ddot{v} + b(\dot{v})\dot{v} + \left(3\gamma P_o/4\pi R_o^3\right)v = - P \exp(j\,\omega t)$$

$\rho/4\pi R_o$ is the equivalent mass of the liquid set in motion by the bubble, while $(3\gamma P_o/4\pi R_o^3)$ is the stiffness (or spring constant) of the system. The general form of the equation is that of a damped spring-mass system:

$$m\ddot{x} + b\,\dot{x} + k\,\Delta x = F$$

with a resonant frequency

$$f_r = \frac{1}{2\pi}\left[\frac{k}{m} - \frac{b^2}{2m}\right]^{1/2}$$

The dissipation function $b(\dot{v})$ must include the influence of all damping mechanisms present. The function $b(\dot{v})$ is not known explicitly even for water. If the damping is moderate its influence on the resonant frequency will be small, hence the resonant frequency

$$f_r = \frac{1}{2\pi}\left[\frac{3\gamma P_o/4\pi R_o^3}{\rho/4\pi R_o}\right]^{1/2} = \frac{1}{2\pi R_o}\left[\frac{3\gamma\, P_o}{\rho}\right]^{1/2}$$

is the Minnaert frequency (Figure 3-3).

We have shown that the influence of viscous dissipation on the resonant frequency is indeed small. If energy dissipation by radiation and thermal conduction is of the same order of magnitude as that of viscous dissipation, the influence on the resonant frequency will also be minimal.

3.1.3 Damping Mechanisms in Foams

Devin defines a total damping coefficient as the sum of damping coefficients for sound radiation, thermal conduction damping and viscous damping as

$$\delta = \delta_{rad} + \delta_{th} + \delta_{vis} = 1/Q$$

where the Q of the bubble system at the resonant frequency f_r is

$$Q = 2\pi f_r \, m/b$$

Viscous damping cannot be obtained from the Navier-Stokes equation of motion because it can be shown that there are no net viscous forces acting on any volume element in the liquid. Only viscous forces acting on the surface of the bubble give rise to viscous strains. The equation of motion, including viscous forces, is derived by Devin (Reference 47) and is given as

$$(\rho_f/4\pi R)\ddot{v} + \left(\mu/\pi R_o^3\right)\dot{v} + \left(3\gamma P_o/4\pi R_o^3\right)v = - P \exp(j\,\omega t)$$

$$\delta_{vis} = b_{vis}\,[\omega\rho_f/4\pi R]^{-1} = (\mu/\rho_f)\left(4/\omega R_o^2\right) = \frac{4\mu}{\rho_f}\,\frac{1}{2\pi f R_o^2}$$

At resonance, δ_{vis} can be written as

$$\delta_{vis} = 4\mu/\left(R_o\sqrt{3\gamma P_o \rho_f}\right)$$

The viscosity, μ, is the surface viscosity of the liquid (not the overall viscosity of the foam) because only viscous forces on the surface of the bubble cause viscous damping. Surface viscosity, rather than bulk viscosity, is applicable to these calculations since viscous damping is a surface phenomenon. Surface viscosity is usually greater than bulk viscosity (Reference 4, p. 158). Quantitative information on surface viscosity of the foaming agent solutions was not available. The bulk viscosity of water (μ = 1 centipoise = 10^{-3} N-sec/m) was used in the calculations.

Sound radiation damping can be evaluated by replacing the pressure field created by a pulsating bubble by an equivalent field created by a point source at the center of the bubble. Devin (Reference 47) obtains an approximate expression for the equation of motion

$$(\rho/4\pi R_o)\ddot{v} + (\rho\omega^2/4\pi c)\dot{v} + k'v = - P \exp(j\,\omega t)$$

where k' is the change of pressure on the bubble surface.

The damping constant in the above equation is

$$\delta_{rad} = b/m\omega = 2\pi f R_o/c$$

where c is the velocity of sound propagation in the liquid and ω is the angular frequency of pulsations. The velocity of sound propagation in foams was measured for a typical foam with moderate accuracy (see Section 2.1.3). The measured velocity was 290 m/sec at 2133 Hz and 180 m/sec at 2666 Hz for a light protein foam (EXP = 38). Not surprisingly the sound propagation velocity is frequency dependent. Assuming an average value 250 m/sec the dissipation coefficient at resonance is

$$\delta_{rad} = \frac{1}{c}\left[\frac{3\gamma P_o}{\rho}\right]^{1/2}$$

yielding

$$\delta_{rad} = 0.26 \text{ for } \rho = 100 \text{ kg/m}^3 \text{ (EXP = 10)}$$

and

$$\delta_{rad} = 0.80 \text{ for } \rho = 10 \text{ kg/m}^3 \text{ (EXP = 100)}$$

Thermal damping of bubble pulsations is caused by a phase lag between pressure and volume changes of the bubble (Reference 52) which result in a net heat flow from bubble to liquid. In Devin's derivation of the thermal damping constant it is assumed that the liquid is isothermal because of its large heat capacity and conductivity. This assumption is also valid for foams because the heat capacity of the thin liquid bubble wall is at least two orders of magnitude higher than that of the gas inside the bubble. The final correlation is

$$\delta_{th} = 2\left[\frac{\left(\frac{16}{9(\gamma-1)^2}\frac{Fg}{f_o} - 3\right)^{1/2} - \frac{3\gamma-1}{3(\gamma-1)}}{\frac{16}{9(\gamma-1)^2}\frac{Fg}{f_o} - 4}\right]$$

where

$$g = 1 + \frac{2\sigma}{P_o R_o}\left(1 - \frac{1}{3\gamma}\right)$$

is the surface tension correction of the adiabatic bubble stiffness. This correction is small (Section 3.2.2). Thus

$$g \cong 1$$

The function F in the expression for δ_{th} is

$$F \equiv 3\gamma P_o/(4\pi\rho_f D)$$

where D is the thermal diffusivity of the gas. For air or nitrogen at 25°C D = 1.6 10^{-5} m^2/sec. Hence

$$F \cong (2/\rho_f)10^9 \quad (sec)^{-1}$$

A simplified relation for δ_{th} applies within one percent for frequencies below 10,000 Hz

$$\delta_{th} = \left[9(\gamma - 1)^2/4F\right]^{1/2} f^{1/2}$$

and for air

$$\delta_{th} = 1.34 \ 10^{-5} \sqrt{\rho_f f}$$

At resonance

$$\delta_{th} = 1.35 \ 10^{-4} \ \rho_f^{1/4} \ R^{-1/2}$$

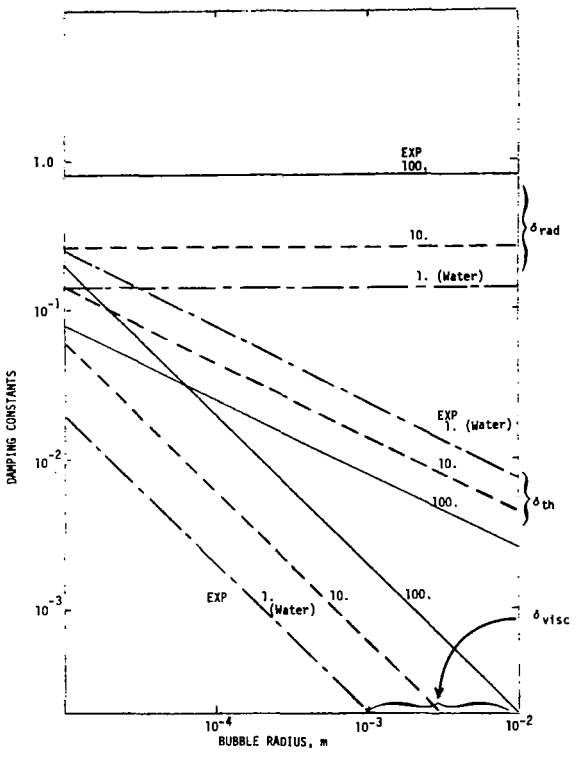

Figure 3-4. Damping Constants at Resonance

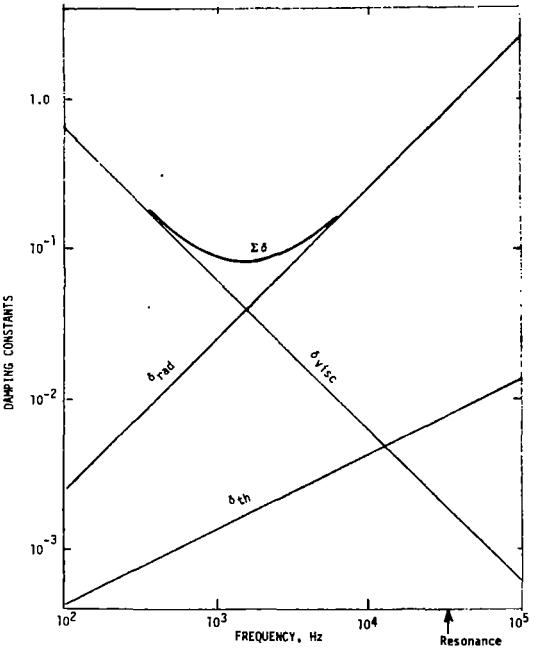

Figure 3-5. Damping Constants for a Bubble Radius R = 10^{-3} inches in a Foam of 10 Kg/m^3 Density (EXP = 100)

The three damping constants at resonance are shown in Figure 3-4. For large bubbles (radii > 10^{-4}) radiation damping is dominant. Radiation damping is two orders of magnitude larger than viscous damping and may well be large enough to appreciably decrease the resonant frequency of the larger bubbles. At frequencies lower than the resonant frequency, viscous damping may become dominant. For example Figure 3-5 shows damping constant variation with frequency for a large bubble (radius = 10^{-3} m) in a light foam (EXP = 100). The resonant frequency here is 33,000 Hz. For frequencies below 1,000 Hz viscous damping is dominant, while above 5,000 Hz radiation damping is most important.

Similarly viscous damping is dominant below 10,000 Hz and radiation damping is dominant above 50,000 Hz for the smaller bubbles (radius $\approx 10^{-4}$ m) in a heavier foam (Figure 3-6). Thermal damping will be important for small bubbles in a dense medium (water) exposed to high frequency, >10,000 Hz. This is the case partially because radiation damping is inversely proportional to sound velocity, which is high in water, and partially because thermal damping increases with frequency for a given bubble size.

Devin's theoretical results are substantiated by experimental results of Meyer and Tamm (Reference 53) who, working at resonance with air, hydrogen, and oxygen bubbles in water and in glycerin, found that the damping decrement was composed of two parts - the constant radiation damping component and a frequency-proportional component. They attributed the weak influence of liquid viscosity on damping

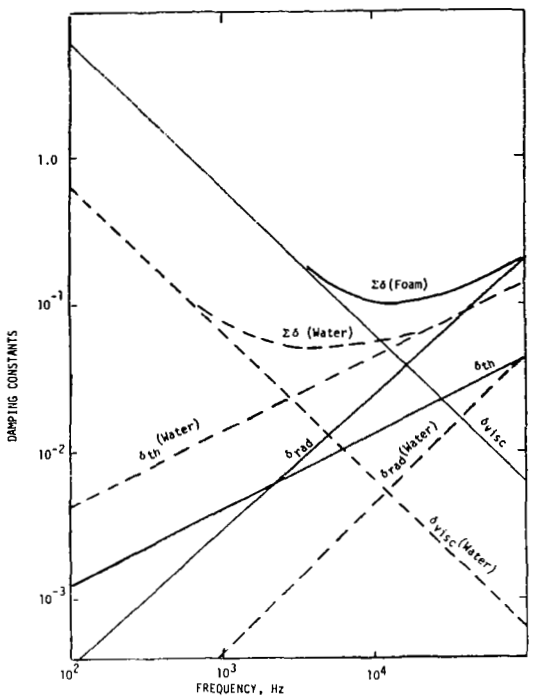

Figure 3-6. Damping Constants for a Bubble of Radius R = 10^{-4} inches in a Foam of 100 Kg/m^3 Density (EXP = 10) and in Water

to the fact that viscosity only affects volumetric change.

Examination of the behavior of an isolated bubble must now be followed by an overall mechanical model comprised of isolated bubble resonators coupled to neighboring bubbles. At the present time we have no rationale for the coupling mechanism. Hence, it can only be postulated that the coupling can be represented by a damped spring and a parametric approach to further study can be taken. In the following section, a mechanical analog for the behavior of foams will be postulated and an electric analog will be developed.

3.2 OVERALL MODELING

One of the simplest schematic representations of the behavior of foams under the action of a pressure wave is obtained by considering one of the elements in a series of adjacent slices of foams. Such an element is composed of one pulsating bubble and its coupling to the next bubble of similar size, is shown below

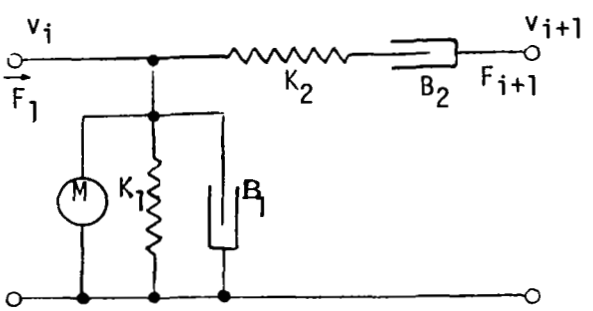

The {mass M, spring K_1, friction B_1} system represents an elementary system — a bubble of mass M. The spring K_1 represents the compressibility of the enclosed gas. B_1 takes into account all of the dissipation mechanisms — heat conduction, viscous dissipation and radiation as described in Section 3.2.3. The system {K_2 - B_2} represents the coupling of each element to its neighbors. A one-dimensional schematic may be sufficient if plane wave propagation is considered.

The electric analog of the above mechanical system may be constructed from the force and velocity balance equations

$$F_i - F_{i+1} = M \frac{d\, v_i}{dt} + B_1 v_i + K_1 \int v_i \, dt$$

$$v_i - v_{i+1} = \frac{1}{K_2} \frac{d\, F_{i+1}}{dt} + \frac{F_{i+1}}{B_2}$$

The electrical analog is obtained by setting

$$F \equiv V, \quad v \equiv I$$

and

$$L \equiv M \qquad K \equiv C^{-1} \qquad B \equiv R$$

The circuit corresponding to the analog equations

$$V_i - V_{i+1} = L \frac{d\, I_i}{dt} + R_1 I_i + \frac{1}{C_1} \int I_i \, dt$$

$$I_i - I_{i+1} = C_2 \frac{d\, V_{i+1}}{dt} + R_2^{-1} V_{i+1}$$

is shown as:

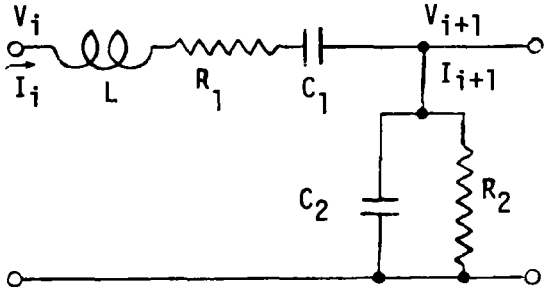

The impedance of the elementary system in the mechanical and electric notation is

$$Z_m = B_1 + j\omega M + \frac{K_1}{j} \rightarrow Z_e = R_1 + j\omega L_1 + \frac{1}{j\omega C_i}$$

$$Y_m = \frac{1}{B_2} + \frac{1}{j\omega K_2} \rightarrow Y_e = R_2 + j\omega C_2$$

where

$$Z_m = F/v \qquad \text{and} \qquad Z_e = V/I$$

$$Y_m = v/F \qquad\qquad Y_e = I/V$$

The characteristic impedance of the material, Z_o, is

$$Z_o = \sqrt{Z/Y} \tag{34}$$

while the propagation constant, γ, is given by

$$\gamma = \sqrt{Z \cdot Y} \quad \text{(Reference 53)} \tag{35}$$

Thus, when Z_o and γ are obtained from standing wave tube measurements, Z and Y become available. Now some assumptions can be made for the values of a foam element; for instance, an average bubble size (obtained from the photograph) and the expansion ratio will yield mass (i.e., inductance). The spring constant can be evaluated by neglecting the surface tension contribution and using the perfect gas law and adiabatic compression. An order of magnitude of dissipation was obtained from isolated bubble studies.

Thus, Z_o and γ are considered to be the fundamental building blocks for the development of a mathematical model for the acoustic behavior of foams. These two properties were obtained from standing wave tube measurements as discussed in Section 2.1.3. Before these data became available, a parametric study, based on chosen values for the mechanical model parameters, was conducted. Afterwards, when experimental values for Z_o and γ had been obtained, some calculations of the corresponding mechanical properties were made and surprisingly good agreement between the two sets of numbers was shown.

3.3 PARAMETRIC STUDIES ON A FOAM STRUCTURE MODEL

3.3.1 A Distributed Parameter Model of the Acoustic Behavior of Foam

A distributed parameter model of the foam was evolved from the lumped parameter model described in Section 3.3. The transition was achieved by evaluating mass, spring constants, and damping coefficients on a per-unit length basis.

Using the notation of L. L. Beranek (Reference 42, p. 52-54) as shown in Figure 3-7.

$$Z_m = R'_{m_i} + j\left(\omega M'_m - \frac{K'_{m_i}}{\omega}\right) \tag{36}$$

$$Y_m = r'_{m_2} + j\omega C'_{m_2} \tag{37}$$

where the notation used as compared to the notation in Section 3.3 is:

K'_m = mechanical spring constant per unit length $\equiv K/L$

C'_m = mechanical compliance per unit length $\equiv \frac{1}{K}/L$

r'_m = mechanical responsiveness per unit length $\equiv \frac{1}{B}/L$

R'_m = mechanical resistance per unit length $\equiv B/L$

M'_m = mass per unit length $\equiv m/L$

ω = angular velocity $\equiv 2\pi f$

Z_o and γ are described as follows:

$$Z_o = R_o + jX_o \tag{38}$$

$$\gamma = \alpha' + j\beta \tag{39}$$

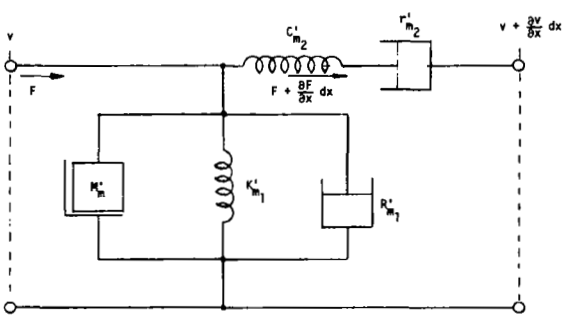

Figure 3-7
Steady-State AC Distributed-Parameter Mechanical Model

where

R_o = real or resistive part of Z_o

X_o = imaginary or reactive part of Z_o

α' = attenuation constant

β = phase constant

If the values of the model parameters M'_m, K'_{m_1}, R'_{m_1}, C'_{m_2} and r'_{m_2} are known or selected, it is possible to determine α', β, R_o and X_o i.e., the complex values of γ and Z_o.

Having obtained Z_o and γ from the mechanical properties of foam, the response of that foam to plane sound pressure waves in a standing wave tube can be predicted as follows. The surface impedance Z_1 of a foam sample of depth L was obtained in Section 2.1.3 because

$$Z_1 = Z_o/\tanh \gamma L \tag{40}$$

Not that the surface impedance Z_1 was obtained from the measured reflection coefficient r; hence Z_1 is only known in terms of its ratio to the characteristic impedance of air. Since the mechanical model of the behavior of foam is based on a damped mass-spring model of a bubble, it will be convenient to express the impedances such as Z_1 and Z_o in terms of a free air impedance

$$Z_{air} = (\rho_o C)_{air} \times (\text{area})$$

where the area is the surface area of the bubble $4\pi R^2$. Thus the complex reflection coefficient r at the interface of air and foam in the standing wave tube apparatus is written as a modification of Equation (14)

$$r = \frac{Z_1/Z_{air} - 1}{Z_1/Z_{air} + 1} \tag{41}$$

For a typical bubble of radius $R = 10^{-3}$ m

$$Z_{air} = 5.2\ 10^{-3}\ (\text{N-sec})/\text{m}\ (2.96 \times 10^{-5}\ (\text{lb-sec})/\text{in})$$

The corresponding measured absorption coefficient (α) of the foam in the standing wave tube apparatus is given by Equation (13).

$$\alpha = 1 - |r|^2 \tag{42}$$

Thus, starting from a set of mechanical parameters, the surface impedance and absorption coefficient of the corresponding foam in a standing wave tube was obtained.

3.3.2 Parametric Study of Foam Behavior

A short study was carried out to determine what effect parameter changes, e.g., R'_m or r'_m, would have on the resonance and frequency response characteristics of the proposed foam model. In order to do this (since γ is a complex number) let

$$\tanh \gamma L = \sigma + j\tau \tag{43}$$

Using a hyperbolic expansion formula

$$\tanh \gamma L = \tanh (\alpha' + j\beta)L = \frac{\tanh \alpha' L + j \tan \beta L}{1 + j \tanh \alpha' L \tan \beta L} \tag{44}$$

Further algebraic manipulation of the right-hand side of Equation (44) to separate it into its real and imaginary parts leads to

$$\sigma = \frac{1}{2} \frac{\sinh 2 \alpha' L}{\epsilon} \tag{45}$$

and

$$\tau = \frac{1}{2} \frac{\sin 2\beta L}{\epsilon} \tag{46}$$

where

$$\epsilon = \text{Cosh}^2 \alpha' L \, \text{Cos}^2 \beta L + \sinh^2 \alpha' L \, \sin^2 \beta L \tag{47}$$

The values of α', β, R_o and X_o have to be determined in terms of the input parameters selected for the mechanical model of the foam structure in order to determine R_o, X_o, σ, and τ which are needed to obtain the input impedance Z_1. To determine α' and β let

$$Z_m = R_Z + jI_Z \tag{48}$$

$$Y_m = R_Y + jI_Y \tag{49}$$

where by inspection of Equations (36) and (37)

$$R_Z = R'_{m_1} \tag{50}$$

$$I_Z = \omega M'_m - \frac{K'_{m_1}}{\omega} \tag{51}$$

$$R_Y = r'_{m_2} \tag{52}$$

$$I_Y = C'_{m_2}\omega \tag{53}$$

From Equations (35), (48), and (49)

$$\gamma^2 = Z_m Y_m$$

or

$$(\alpha' + j\beta)^2 = (R_Z + jI_Z)(R_Y + jI_Y)$$

$$\alpha'^2 - \beta^2 + j2\alpha'\beta = (R_Z R_Y - I_Z I_Y) + j(R_Z I_Y + I_Z R_Y) \tag{54}$$

Let

$$U = R_Z R_Y - I_Z I_Y \tag{55}$$

$$V = R_Z I_Y + I_Z R_Y \tag{56}$$

then Equation (54) reduces to

$$\alpha'^2 - \beta^2 + j2\alpha'\beta = U + jV \tag{57}$$

and by comparison of the real and imaginary parts it is seen that

$$\alpha'^2 - \beta^2 = U \tag{58}$$

$$2\alpha'\beta = V \tag{59}$$

Solving Equations (58) and (59) simultaneously for α' in terms of U and V, by eliminating β, we get

$$\alpha' = \sqrt{\frac{U}{2} + \frac{1}{2}\sqrt{U^2 + V^2}} \tag{60}$$

and then from Equation (58) β can be determined as follows

$$\beta = \alpha'^2 - U \tag{61}$$

It should be noted that signs on all the square roots have been selected to insure that both α' and β are positive real numbers in order to be physically meaningful. Equations (50) through (53), (55), (56), (60), and (61) can now be used to determine the values of α' and β as a function of frequency, for a given set of mechanical model parameters. A similar approach based on Equation 40 could be used to determine the value of R_o and X_o, however, in this case there would be a question as to what sign to take for the square root when determining X_o; i.e., X_o has to be real but not necessarily positive. To avoid this problem the previously determined values of α' and β are used to determine R_o and X_o as follows: from Equations (34), (35), (38), (39), and (48)

$$Z_o\gamma = \sqrt{\frac{Z_m}{Y_m}}\sqrt{Z_m Y_m} = Z_m \tag{62}$$

$$(R_o + jX_o)(\alpha' + j\beta) = R_Z + jI_Z \tag{63}$$

Expanding and comparing real and imaginary parts we get

$$\alpha' R_o - \beta X_o = R_Z \tag{64}$$

$$\beta R_o + \alpha' X_o = I_Z \tag{65}$$

which can be solved for R_o and X_o in terms of α', β, R_Z, I_Z to give

$$R_o = \frac{\alpha' R_Z + \beta I_Z}{\alpha'^2 + \beta^2} \tag{66}$$

$$X_o = \frac{\alpha' I_Z - \beta R_Z}{\alpha'^2 + \beta^2} \tag{67}$$

We can now find the input impedance measured in the standing wave tube on foam from Equations (38), (45) and (46) since the values of α', β, R_o and X_o have all been found. Thus

$$Z_1 = \frac{Z_o}{\tanh \gamma L} = \frac{R_o + jX_o}{\sigma + j\tau} = |Z_1|_e\, j\phi_{Z_1} \tag{68}$$

where

$|Z_1|$ = magnitude of Z_1

ϕ_{Z_1} = phase angle of Z_1.

The value of the absorption coefficient, α, can also be determined through Equations (41) and (42). A summarized list of the equations programmed on the on-line computer used to calculate the absorption coefficient of foam and the other parameters in this analysis is given in Table 3-1.

Table 3-1. Summary of Programmed Equations Used to Determine Absorption Coefficient of Foam and Other Parameters (Based on a Simple Mechanical Structure Model for Foam)

$$\omega = 2\pi f \qquad I_Z = \omega M'_m - \frac{K'_{m_1}}{\omega}$$

$$R_Z = R'_{m_1} \qquad I_Y = \omega C'_{m_2}$$

$$U = R_Z R_Y - I_Z I_Y \qquad V = R_Z I_Y + I_Z R_Y$$

$$\alpha' = \sqrt{\frac{U}{2} + \frac{1}{2}\sqrt{U^2 + V^2}} \qquad \beta = \sqrt{\alpha'^2 - U}$$

$$R_o = \frac{\alpha' R_Z + \beta I_Z}{\alpha'^2 + \beta^2} \qquad X_o = \frac{\alpha' I_Z - \beta R_Z}{\alpha'^2 + \beta^2}$$

$$\epsilon = (\cosh \alpha' L \cos \beta L)^2 + (\sinh \alpha' L \sin \beta L)^2$$

$$\sigma = \frac{1}{2}\frac{\sin h\, 2\alpha' L}{\epsilon} \qquad \tau = \frac{1}{2}\frac{\sin 2\beta L}{\epsilon}$$

$$Z_1(\omega) = \frac{R_o + jX_o}{\sigma + j\tau} = |Z_1(\omega)|\, e^{j\phi_{Z_1}}$$

$$|Z_1(\omega)| = \sqrt{\frac{R_o^2 + X_o^2}{\sigma^2 + \tau^2}}$$

$$\phi_{Z_1} = \arctan\left(\frac{X_o}{R_o}\right) - \arctan\left(\frac{\tau}{\sigma}\right)$$

$$r = \frac{Z_1/Z_{air} - 1}{Z_1/Z_{air} + 1} \qquad \alpha = 1 - |r|^2$$

Input: f, R'_{m_1}, M'_m, K'_{m_1}, r'_{m_2}, and C'_{m_2}

Output: α, $|Z_1|$, ϕ_{Z_1}, α', β

Having established and programmed the equations needed to calculate the absorption coefficient, α, and the surface impedance, Z_1, a foam was selected and the mechanical model for that foam was established. The parameters needed are mass, spring constant and damping coefficient of the pulsating bubble, and the spring constant and damping for the coupling between bubbles.

Calculations of resonant frequencies of pulsating bubbles (Section 3.2.2) showed that bubble resonance frequencies in the audible range correspond to the large bubbles, 1 millimeter or larger in diameter. The bubble size distribution (Figure 3-2) obtained for a light protein foam showed bubble diameters up to 1 millimeter. Larger bubbles can be seen in Figure 3-1. A bubble radius of 10^{-3} m was selected for the mechanical model. The equivalent mass of the foam can be obtained from the equation of motion from Section 3.2.2.

$$\frac{\rho_f}{4\pi R}\ddot{v} + b(\dot{v})\dot{v} + \frac{3\gamma P_o}{4\pi R^3}\Delta v = -P \exp(\gamma\omega t)$$

The mechanical model was based on a driving force, while the pressure P in the equation of bubble motion acted on the surface $4\pi R^2$ of the bubble:

$$F = 4\pi R^2 P$$

$$\rho_f R\ddot{v} + 4\pi R^2 b\dot{v} + (3\gamma P_o/R)\,\Delta v = -F \exp(\gamma\omega t)$$

In the equation of motion Δv is the volume increment of the bubble while the mechanical model is based on a linear increment Δx:

$$\Delta v = 4\pi R^2 \Delta R \rightarrow 4\pi R^2 \Delta x$$

and

$$\rho_f 4\pi R^3 \ddot{x} + \left(4\pi R^2\right)^2 b\dot{x} + 12\pi\gamma P_o R\,\Delta x = -F \exp(j\omega t)$$

To obtain the equivalent mass, stiffness, and damping on a per unit length basis, the coefficients of the differential equation are divided by 2R

$$M'_m = 2\pi R^2 \rho_f$$

$$K'_m = 6\pi\gamma P_o$$

$$R'_m = 8\pi^2 R^3 b$$

For $R = 10^{-3}$ m, the equivalent mass per unit length will vary from 6×10^{-5} kg/m (or N-sec^2/m^2) (0.87×10^{-8} lbf-sec^2/in^2) for a light foam ($\rho_f = 10$ kg/m^3, EXP = 100), to 6×10^{-4} kg/m ($8.7\ 10^{-8}$ lbf-sec^2/in^2) for a heavy foam ($\rho_f = 100$ kg/m^3, EXP = 10).

The adiabatic stiffness K'_{m_1} is on the order of 2.6×10^6 N/m^2 (380 lb-sec^2/in.^{2}). The corresponding isothermal stiffness is 1.89×10^6 N/m^2 (270 lb-sec^2/in.^{2}). The damping constant $\delta = (4\pi R^2)^2 b / (2\pi f)(4\pi R^3)\rho_f$ varies between 0.08 and 0.25 (Figure 3-5 in the frequency range of interest; i.e., 350 to 10,000 Hz.

$$\delta = \frac{2bR}{f\rho_f} \cong 0.15$$

$$R'_m = 8\pi^2 R^3 b = 0.6\pi^2 R^2 (\rho_f \times f)$$

for $R = 10^{-3}$ m

$$R'_m \cong 6 \times 10^{-6} (\rho_f \times f)$$

$$0.02 < R'_m < 6 \quad (\text{N - sec/m}^2)$$

The values chosen to conduct a numerical study in which the damping parameter was varied from 0.007 to 7.0 N-sec/m^2, (10^{-6} to 10^{-3} lb-sec/in^2) were:

$M'_m = 0.26\ 10^{-4}$ N-sec^2/m^2 ($0.3751\ 10^{-8}$ lb-sec^2/in.^{2})

$K'_m = 1.89\ 10^4$ N/m^2 (2.7338 lb/in.^{2})

$r'_{m_2} = 0$

$C'_{m_2} = K'_m{}^{-1}$ $\qquad Z_{air} = 1.3\ 10^{-3}$

The mass and area chosen correspond to a 1.0^{-3}m bubble diameter and the stiffness is about 100 times lower than the isothermal stiffness of air. (Preliminary calculations showed that resonant frequencies were at least an order of magnitude too high when these adiabatic or isothermal stiffnes values were used.) The object of the parametric study was to verify resonant behavior of foam and to point to changes in the mechanical model necessary to obtain a more realistic representation. One of the changes needed is a different approach to the compressibility of foams.

Figure 3-8 shows that the absorption coefficient has a resonance at about 5500 Hz for relatively low resistance. This appears as a dip (minimum value) in the magnitude of the Z_1 curve of Figure 3-9. That this is a true resonance condition is further substantiated by the zero crossover for the phase of Z_1, at the same frequency as shown in Figure 3-10. This same figure shows that there is an antiresonant condition at about 8000 Hz. Again this is substantiated by the peaking out of the Z_1 magnitude at the same frequency. It is seen that a resonance situation corresponds to a minimum in the magnitude of the input impedance measured in the standing wave tube and that the phase of the input impedance goes through zero (from negative to positive). These results are in agreement with a simple one-degree of freedom R, L, C series electrical circuit where the ac input impedance can be expressed as

$$Z_{in} = R + j(\omega L - 1/\omega C)$$

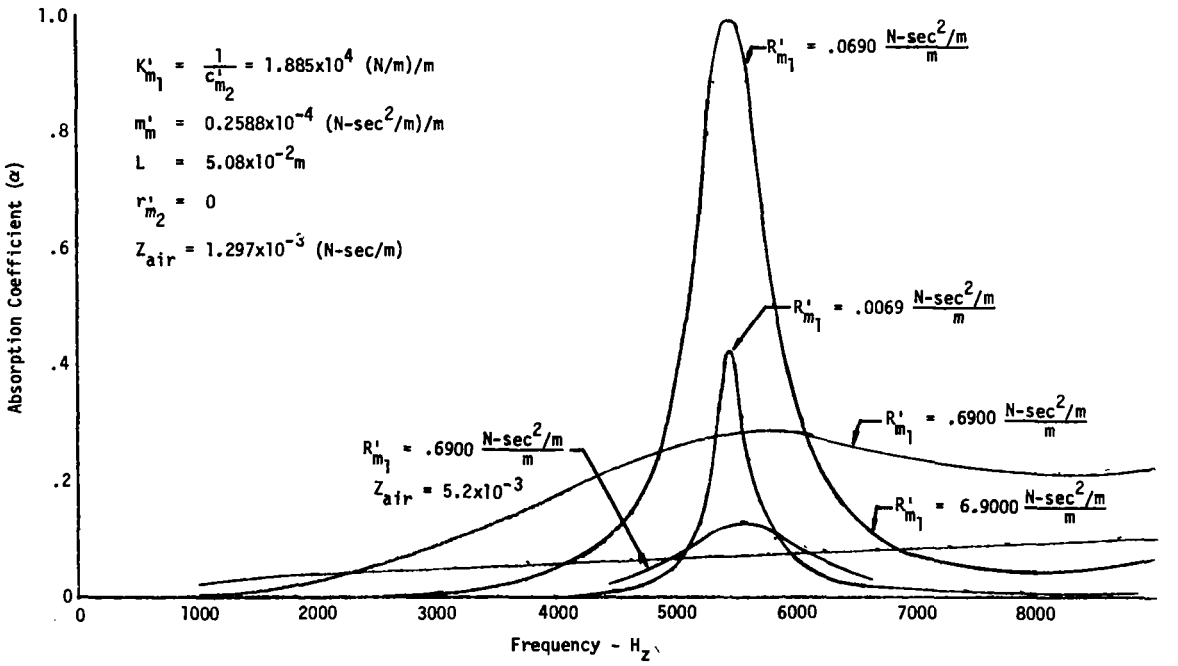

Figure 3-8. Absorption Coefficient vs. Frequency

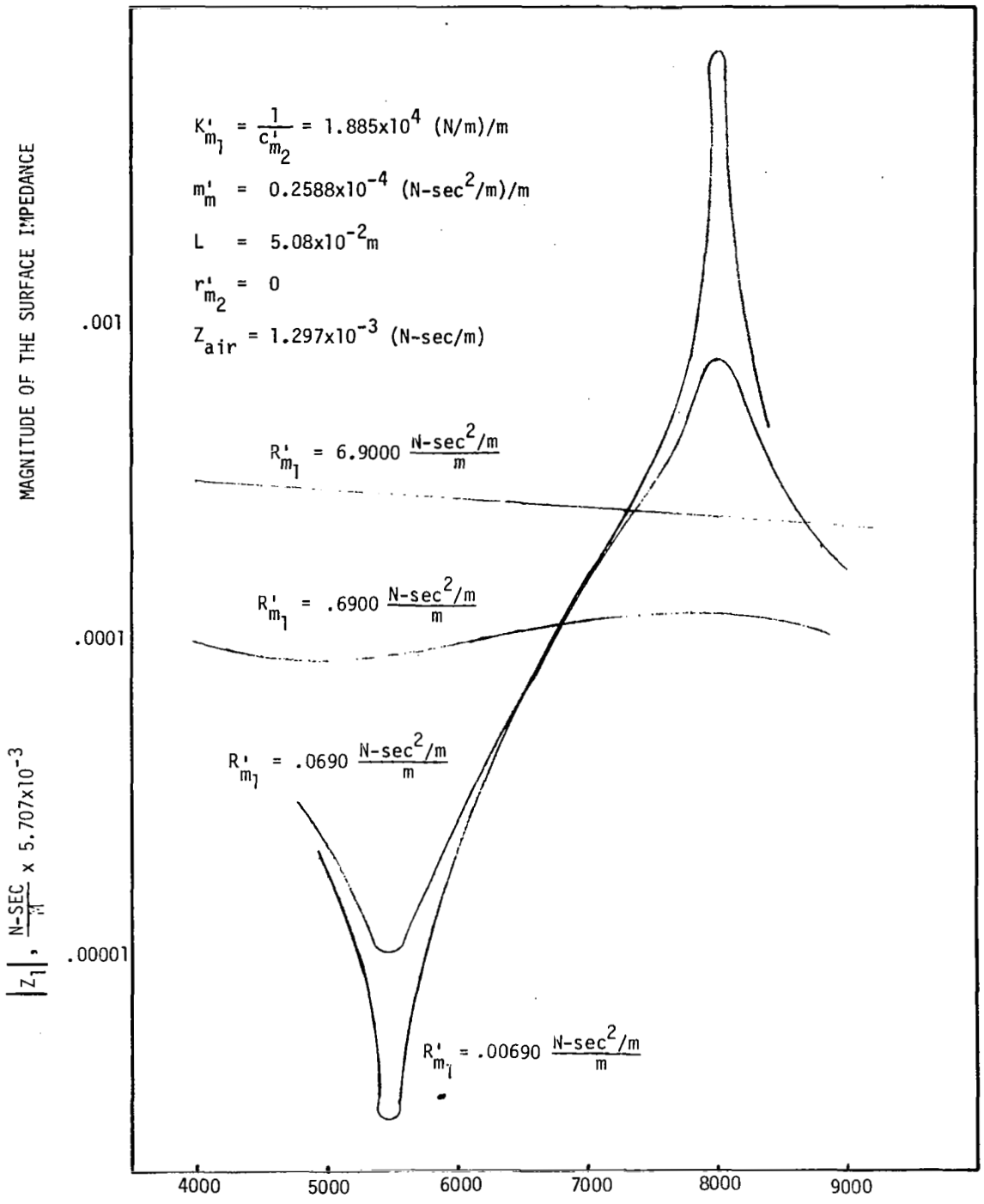

Figure 3-9. Magnitude of Surface Impedance vs. Frequency

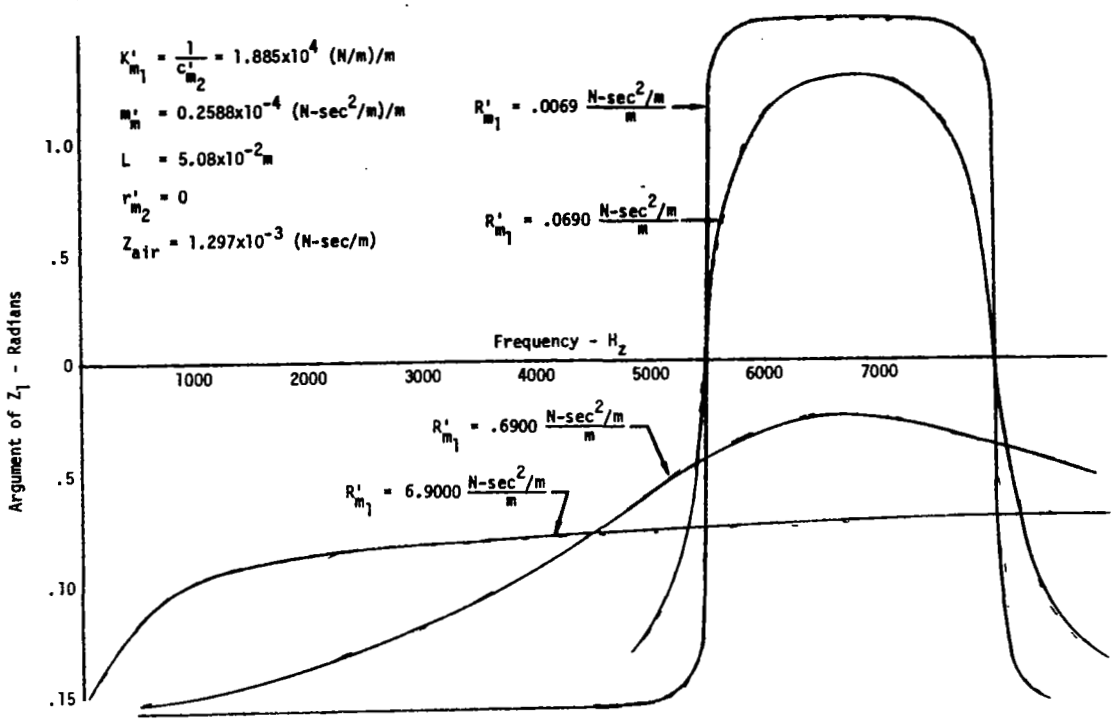

Figure 3-10. Phase of Z_1 vs. Frequency

For relatively low R', at resonance, $\omega = \omega_o$

$$\omega_o L = 1/\omega_o C \rightarrow f_o = \frac{1}{2\pi} \sqrt{\frac{1}{LC}}$$

and

$$|Z_1| = Z_{min}$$

$$\phi_{Z_1} = 0^o$$

For

$$\omega < \omega_o: \phi_{Z_1} < 0^o$$

$$\omega > \omega_o: \phi_{Z_1} > 0^o$$

Figure 3-11 shows how the attenuation coefficient (α') varies with frequency for the various values of resistance. At a given frequency the attentuation coefficient increases with increased resistance as should be expected. It should be noted that for low resistance or dissipation, α' increases with frequency while for very low resistance, α' decreases with increased

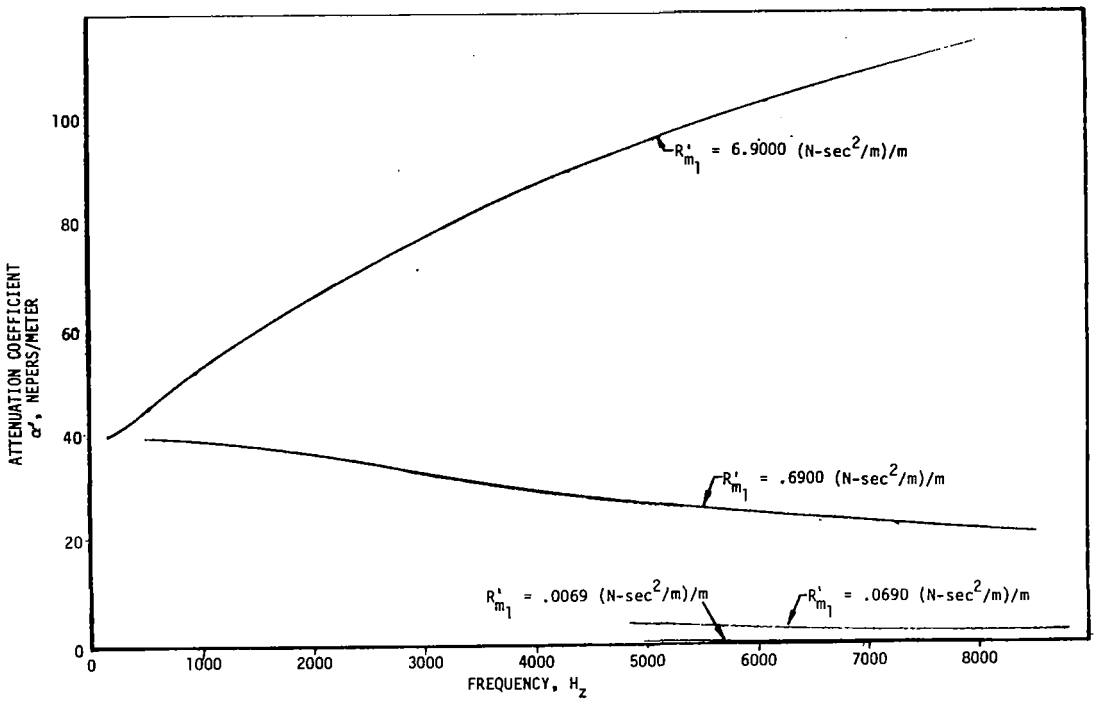

Figure 3-11. Attenuation Constant vs. Frequency

frequency. There appears to be some critical value of R'_{m1} (possibly corresponding to critical damping) which separates these two regions. The phase constant, β, which determines the phase or acoustic velocity in the hypothesized structural model, is shown in Figure 3-12 as a function of frequency for various values of resistance. In general β increases with increased frequency for a fixed value R'_{m1}. For a given frequency, β increases with increased dissipation. The first resonance condition (corresponding to $L = \lambda/4$ for a closed-end tube) corresponds to a $\beta = 0.785$ (for L = 2 inches) which results in a frequency corresponding to low dissipation ($\approx$5500 Hz) which is in agreement with the previous discussion. The same is true for the antiresonant case corresponding to a $\beta = 1.57$ (frequency = 8000 Hz). It is seen that, as the dissipation increases, the first resonant frequency decreases.

3.3.3 No Loss Distributed Parameter Model Resonance Calculations

In order to verify the previous results, the undamped resonant frequencies of the selected distributed parameter model shown in Figure 3-7 were determined by setting R'_{m1} and r'_{m2} to zero. Then

$$Z_m = j\left(\omega M'_m - \frac{K'_{m_1}}{\omega}\right) \tag{69}$$

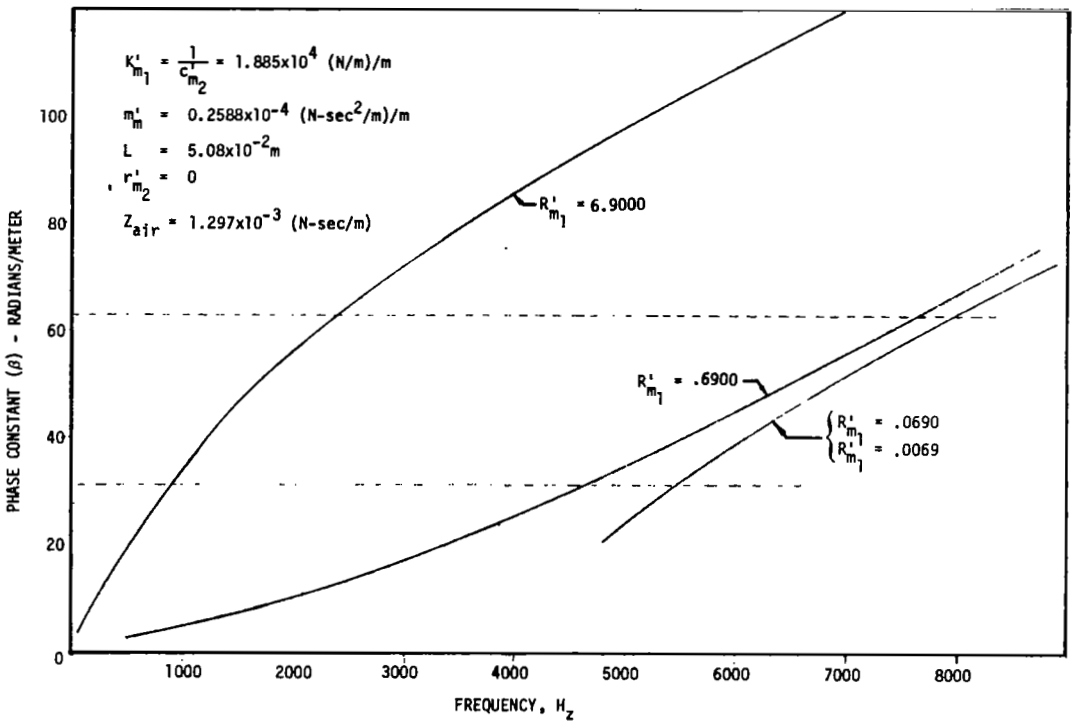

Figure 3-12. Phase Constant vs. Frequency

and

$$Y_m = \omega j\, C'_{m_2} \tag{70}$$

From Equation (35)

$$\gamma = \sqrt{j\left(\omega M'_m - \frac{K'_{m_1}}{\omega}\right)\left(j\, C'_{m_2}\right)} = j\sqrt{\omega C'_{m_2}\left(\omega M'_m - \frac{K'_{m_1}}{\omega}\right)} \tag{71}$$

By comparison of Equations (35) and (71) it is seen that

$$\alpha' = 0 \text{(i. e., no dissipation)}$$

and

$$\beta = \sqrt{\omega C'_{m_2}\left(\omega M'_m - \frac{K'_{m_1}}{\omega}\right)} \tag{72}$$

For sample resonance in the capped-end standing-wave tube the sample depth is given by

$$L = n\lambda/4 \qquad n = 1, 3, 5 \tag{73}$$

thus as resonance

$$\beta = \frac{2\pi}{\lambda} = \frac{n\pi}{2L} \tag{74}$$

For an L = 2 inches

$$\beta = \frac{n\pi}{4} \tag{75}$$

Substituting Equation (68) in (72) and solving for the undamped resonant frequencies, we get

$$f_n = \frac{1}{2\pi}\sqrt{\frac{K'_{m_1}}{M'_m}\left[1 + \left(\frac{n\pi}{4}\right)^2 \frac{1}{K'_{m_1} C'_{m_2}}\right]} \tag{76}$$

Using the parameters selected in the previously discussed studies we get the first resonant frequency for n = 1

$$f_1 = 5464 \text{ Hz}$$

which checks the results of Figures 3-8, 3-9 and 3-10.

For n = 2, which corresponds to an antiresonance situation, f_2 calculates out to 8000 Hz, which also checks.

For the second resonant frequency f_3 = 11,000 Hz, etc.

From Equations (17) and (74) it is seen that since βL is a multiple of $\pi/2$ then at the undamped resonant frequencies $|Z_1| = 0$ and at the undamped antiresonant frequencies $|Z_1| = \infty$ which checks with the results shown in Figure 3-9.

3.3.4 Results of the Distributed Parameter Model

The results obtained in this study are essentially in agreement with results reported in Section 2 in regards to the phase characteristics of Z_1 and the peaking characteristic of α observed under resonance or high energy absorption conditions. This qualitative agreement points out the basic validity of the hypothesized distributed parameter foam structure model.

3.4 CALCULATION OF DISTRIBUTED PARAMETERS IN THE MECHANICAL MODEL FROM MEASURED ACOUSTIC PROPERTIES OF FOAM

The experimentally determined values for the characteristic impedance and propagation constants (Section 2.1.3.2) can be used to calculate the mechanical parameters in the foam structure analogue.

3.4.1 Analysis

The propagation constant and characteristic impedance of the sample are, combining Equations (34) and (35) and defining R_Z and I_Z as follows

$$Z_o\gamma = \sqrt{Z_m Y_m} \times \sqrt{\frac{Z_m}{Y_m}} \equiv Z_m = R_Z + jI_Z \tag{77}$$

$$\frac{\gamma}{Z_o} = \frac{\sqrt{Z_m Y_m}}{\sqrt{Z_m / Y_m}} \equiv Y_m = R_Y + jI_Y \tag{78}$$

The values of α', β, R_o and X_o are experimentally determined using the techniques described in Section 2.1.3.1, then values of R_Z, I_Z, R_Y and I_Y, which characterize the structure of the test sample, can be determined as follows:

The experimental values of Z_o, i.e., of R_o and X_o were obtained in $(\rho C)_{air}$ units, i.e., $R_o/(\rho C)_{air}$ and $X_o/(\rho C)_{air}$, while the propagation constant is calculated on a per unit length basis. Moreover, calculations of Z_o and γ are defined in systems in which the driving function is a pressure while the analog used here has a driving force. The two systems are conciliated by normalizing R_o and X_o to the previously defined air impedance

$$Z_{air} = (\rho C)_{air} \times \text{area}$$

$$\frac{Z_o}{Z_{air}}\gamma = \frac{R_z}{Z_{air}} + j\frac{I_z}{Z_{air}}$$

where R_Z and I_Z are per unit length values because γ has not been normalized.

Combining Equations (38), (39) and (77)

$$\left(\frac{R_o}{Z_{air}} + j\frac{X_o}{Z_{air}}\right)(\alpha' + j\beta) = \frac{R_Z}{Z_{air}} + j\frac{I_Z}{Z_{air}} \tag{79}$$

Equating real and imaginary parts in Equation (79) we get

$$\frac{R_Z}{Z_{air}} = \alpha'\left(\frac{R_o}{Z_{air}}\right) - \beta\left(\frac{X_o}{Z_{air}}\right) \tag{80}$$

$$\frac{I_Z}{Z_{air}} = \alpha'\left(\frac{X_o}{Z_{air}}\right) + \beta\left(\frac{R_o}{Z_{air}}\right) \tag{81}$$

From Equation (78)

$$\frac{\gamma}{Z_o/Z_{air}} = R_Y Z_{air} + j\, I_Y Z_{air} \tag{82}$$

and from Equations (38) and (39) this becomes

$$\frac{\alpha' + j\beta}{\frac{R_o}{Z_{air}} + j\frac{X_o}{Z_{air}}} = R_Y Z_{air} + j\, I_Y Z_{air} \tag{83}$$

Algebraically expanding the left-hand side of Equation (83) and matching the real and imaginary components on the left- and right-hand sides, we get

$$R_Y Z_{air} = \frac{\alpha'\left(\frac{R_o}{Z_{air}}\right) + \beta\left(\frac{X_o}{Z_{air}}\right)}{\left|\frac{Z_o}{Z_{air}}\right|^2} \tag{84}$$

$$I_Y Z_{air} = \frac{\beta\left(\frac{R_o}{Z_{air}}\right) - \alpha'\left(\frac{X_o}{Z_{air}}\right)}{\left|\frac{Z_o}{Z_{air}}\right|^2} \tag{85}$$

$$\left|\frac{Z_o}{Z_{air}}\right| = \sqrt{\left(\frac{R_o}{Z_{air}}\right)^2 + \left(\frac{X_o}{Z_{air}}\right)^2} \qquad (86)$$

Equations (80), (81), (84), (85) and (86) can be used to calculate the normalized values of R_Z, I_Z, R_Y and I_Y from known values of α', β, R_o/Z_{air} and X_o/Z_{air} at a given frequency. Knowing Z_{air}, the unnormalized values of these parameters can be obtained. The desired equivalent mechanical parameters

$$M'_m,\ R'_{m_1},\ K'_{m_1},\ r'_{m_2},\ \text{and}\ C'_{m_2}$$

can then be calculated provided that data from two or more test frequencies are available.

3.4.2 Experimental Results

Standing wave tube measurements taken at two driving frequencies on 6 percent concentration Protein foam, carried out in Run No. 304 (Section 2.1.3.2) for the different sample thicknesses, resulted in the average propagation values (within experimental errors) listed in Table 3-1, as determined by the method outlined in Section 2.1.3.2 and given in Table 2-2.

Table 3-1. Experimentally Determined Acoustic Propagation Constants for Foam Sample

Frequency, Hz	2133	2666	2133	2666	Hz
α, nepers/meter	23.6	25.6	0.60	0.65	α, nepers/inch
β, radians/meter	51.2	90.6	1.30	2.30	β, radians/inch
c, (acoustic velocity), meters/sec	262	185	859	607	c, feet/sec
R_o/Z_{air}, dimensionless	3.13	3.46	---	---	---
X_o/Z_{air}, dimensionless	0.59	0.36	---	---	---

The values of R_Z/Z_{air}, I_Z/Z_{air}, $R_Y \cdot Z_{air}$, $I_Y \cdot Z_{air}$ determined using Table 3-1 data in Equations (80), (81), (84), and (85) are presented in Table 3-2.

Table 3-2. Normalized Components of Distributed Impedance and Admittance Parameters

Frequency, Hz	2133	2666	2133	2666	Hz
R_Z/Z_{air}, per meter	43.7	55.9	1.11	1.42	per inch
I_Z/Z_{air}, per meter	174.1	322.7	4.42	8.19	per inch
$R_Y \cdot Z_{air}$, per meter	10.2	9.9	0.26	0.25	per inch
$I_Y \cdot Z_{air}$, per meter	14.6	25.2	0.37	0.64	per inch

Using the value 5.2×10^{-3} N - sec/m (2.96×10^{-5} lb-sec/in) obtained in Section 3.4.1 for a nominal air bubble radius of 10^{-3}m, the basic structural parameters are derived from Table 3-2 data using the following equations

$$R'_{m_1} = R_Z = Z_{air}(R_z/Z_{air}) \tag{87}$$

$$\omega M'_m - \frac{K'_{m_1}}{\omega} = I_Z = Z_{air}(I_Z/Z_{air}) \tag{88}$$

$$r'_{m_2} = R_Y = (R_Y \cdot Z_{air})/Z_{air} \tag{89}$$

$$\omega C'_{m_2} = I_Y = (I_Y \cdot Z_{air})/Z_{air} \tag{90}$$

It can be seen from Equation (88) that values of M'_m and K'_{m1} are indeterminate unless data from at least two frequencies are available.

The results presented in Table 3-3 combined the I_Z values for the two frequencies to separate out M'_m and K'_{m1}, assuming that these values are frequency insensitive. This latter assumption is acceptable, in view of the experimental procedures, since the other foam structural parameters are relatively insensitive to frequency over the range tested. This further indicates that the assumed model is also relatively applicable. If test data at more than two frequencies were obtained, then the selection of the foam structural parameters M'_m, K'_{m1}, and C'_{m2} could be determined using optimizing curve fitting techniques to obtain a good overall match of $I_Z(Z_{air})$ and $I_Y(Z_{air})$ to the test data.

Table 3-3. Experimentally Determined Distributed Foam Structural Parameters

Frequency, H_Z	2,133	2,666	2,133	2,666	Frequency, H_Z
ω, radians/sec	13,402	16,751	13,402	16,751	ω, radians/sec
R'_{m_1}, (N-sec/meter)/meter	0.23	0.29	3.3×10^{-5}	4.2×10^{-5}	R'_{m_1}, (lb-sec/in)/in
r'_{m_2}, (meter/N-sec)/meter	2,000	1,900	8,800	8,400	r'_{m_2}, (in/lb-sec/in
C'_{m_2}, (meter/N)/meter	0.21	0.29	0.92	1.29	C'_{m_2}, (in/lb)/in
M'_m, (N-sec^2/meter)/meter	1.6×10^{-4}		2.35×10^{-8}		M'_m, (lb-sec^2/in)/in
K'_{m_1}, (N/meter)/meter	1.64×10^{4}		2.36		K'_{m_1}, (lb/in)/in

Additional testing was carried out at a later date to further determine the reproducibility of the experimental technique and the validity of the proposed foam structural model parameters. The results obtained from Run No. 305 test data are presented in Tables 3-4 and 3-5 for comparison with results in Tables 3-3 and 3-6.

Table 3-4. Reviewed Foam Structural Parameters Based on Run 305 Test Data

Frequency, H_Z	2,339	2,729	2,339	2,729	Frequency, H_Z
ω, radians/sec	14,696	17,147	14,696	17,147	ω, radians/sec
R'_{m_1}, (N-sec/meter)/meter	0.18	0.33	2.64×10^{-5}	4.84×10^{-5}	R'_{m_1}, (lb-sec/in)/in
r'_{m_2}, (meter/N-sec)/meter	3,800	2,200	16,800	10,000	r'_{m_2}, (in/lb-sec)/in
C'_{m_2}, (meter/N)/meter	0.18	0.37	0.85	1.62	C'_{m_2}, (in/lb)/in
M'_m, (N-sec^2/meter)/meter	1.8×10^{-4}		2.72×10^{-8}		M'_m, (lb-sec^2/in)/in
K'_{m_1}, (N/meter)/meter	1.88×10^{4}		2.84		K'_{m_1}, (lb/in)/in

Table 3-5. Calculated Undamped First Three Resonant Frequencies Based on Table 3-4 (Run 305)

L, sample depth, inches	1	2	3	4	5
Resonant frequencies Hz					
First	2122	1763	1689	1662	1649
Second	4400	2612	2122	1921	1820
Third	7005	3775	2793	2355	2122

Table 3-6. Calculated Undamped First Resonant Frequency (Based on Table 3-3 Data)

L, sample depth, inches	1	2	2.75
f_1, calculated undamped first resonant frequency, Hz	2259	1800	1717

$$f_1 = \frac{1}{2\pi}\sqrt{\frac{K'_{m_1}}{M'_m}\left[\frac{(\pi/2L)^2}{C'_{m_2}K'_{m_1}} + 1\right]}$$

It is seen that the first resonant frequencies from the two independent tests match within engineering accuracy for the 1- and 2-inch sample depths.

Experimental measurements of α as a function of frequency for three different depths tested (Run No. 305) are shown in Figure 3-13. It is seen that the calculated third resonant frequencies are in relatively good agreement with the peaks of these curves. Again this indicates good agreement between the proposed foam structural model and test data.

3.4.3 Summary of Analytical Model Results

The order of magnitudes and trends exhibited in Table 3-3 are generally in good agreement with the physical situation.

- The proposed mechanical analog for the behavior of foams and the results of transmission line theory applied to the corresponding distributed parameter electric analog show a good agreement with the behavior of foams observed in the standing wave tube apparatus. The orders of magnitude and trends of physical properties shown in Table 3-3 are generally in good agreement with the calculated values.

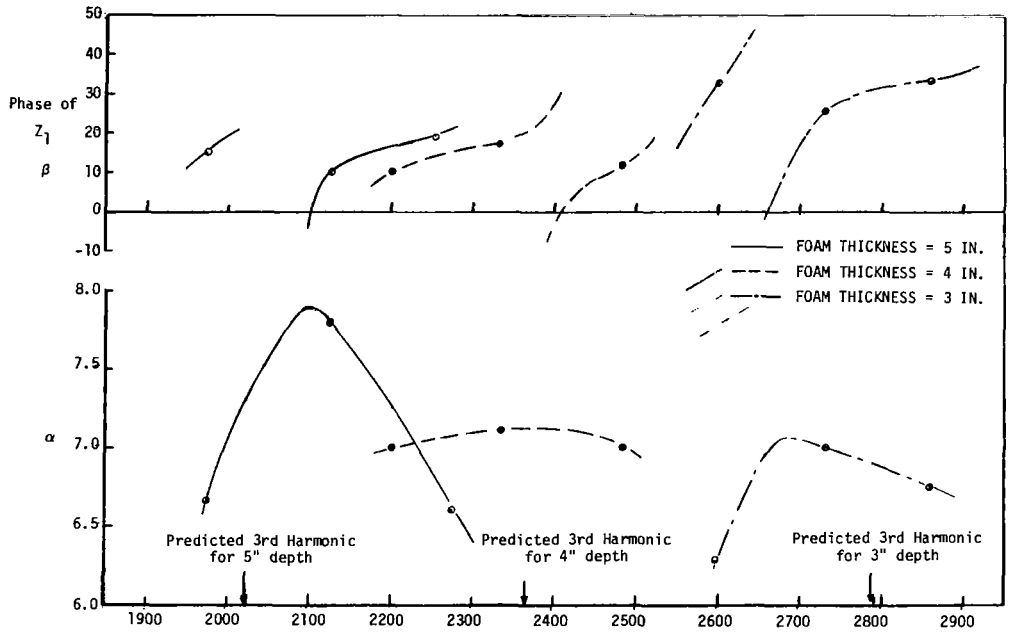

Figure 3-13. Experimental Results (Run No. 305)

- The effective bubble mass per unit length, calculated assuming an isolated bubble surrounded by foam, leads to a value on the order of

$$10^{-4} \frac{N - sec^2}{m^2} \quad (10^{-8}(lb\text{-}sec^2/in)/in)$$

The results in Table 3-3 are in very good agreement considering the experimental measurement errors involved in determing this value.

- The average acoustic velocity, C, in the foam is on the order of 250 m/sec (800 ft/sec). This is higher than the normal (gas-bubble-liquid) equilibrium thermodynamic theory would indicate (see Figure 1-3).

- The mechanical spring constant of the bubble calculated on the basis of gas compressibility is about 100 times larger than the value determined on the basis of measured acoustical properties.

- The undamped third frequency for 3, 4 and 5 inch deep samples, calculated from Equation (76) using the results given in Table 3-4 correspond to measured maxima in the absorption coefficient (Figure 3-13).

- It can definitely be stated that the experimentally observed acoustic absorption of foam is a resonance phenomenon.

4. JET NOISE REDUCTION EXPERIMENTS

The model jet noise reduction experiments were conducted at the TRW Malibu Facility. The Malibu Facility, located in the Santa Monica mountains, offers the advantage of a low background noise environment and the absence of sound reflecting surfaces near the test stand. All of the equipment used was portable.

The choice of a small 1-inch (0.0254 m) diameter cold jet was made on the basis of test convenience. True scale model jet tests would necessitate reproducing many parameters; the most important ones are jet density, velocity and Mach number (Reference 54). Since the low temperature of the cold nitrogen jet affects density and Mach number, any attempt to translate directly the results of this study into airplane jet noise prediction would be negated.

Foam flow requirements on the small scale nozzle may be expected to be much larger than on the corresponding engine exhaust jet since foam presumably acts on the peripheral area (~diameter) jet, while the jet flow rate is proportional to the cross sectional area (~diameter squared). Hence, comparisons of foam flow rate to gas flow rate ratio cannot be made, except that a reduction of the flow rate ratio is proportional to the geometric scaling factor when all other variables are unchanged.

Much of the basic work on jet noise has been conducted on small jets and yielded results applicable to engine jets. Thus, there is reason to expect that the significant noise reduction effected by foam injection and measured on the small cold jet will also be obtained in engine jets.

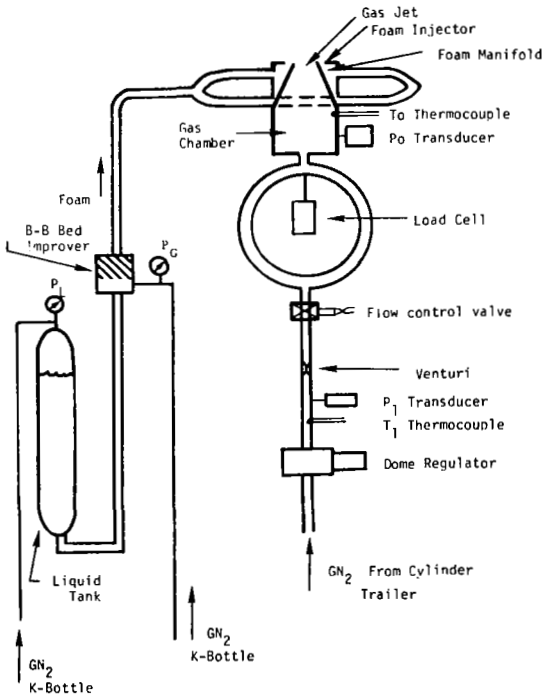

Figure 4-1

Flow Schematic for Model Jet Noise Attenuation Tests

4.1 TEST APPARATUS AND PROCEDURES

4.1.1 Model Jet and Foam Injector

Figure 4-1 schematically shows the model jet and associated foam injection apparatus. The model jet (detail shown in Figure 4-2) consists of a 0.304-m long by 0.152-m diameter (12 inch by 6 inch diameter) chamber and nozzle holder with interchangeable convergent and convergent-divergent nozzles (Figures 4-3 and 4-4). The nozzle holder also incorporates an annular foam manifold with three readily selectable diameters and gaps for the injection of foam. A 3.1 inch by 5 inch pipe duct was also attached for some tests, (Figures 4-5, 4-6 and 4-7). Figure 4-6 shows the model jet assembly

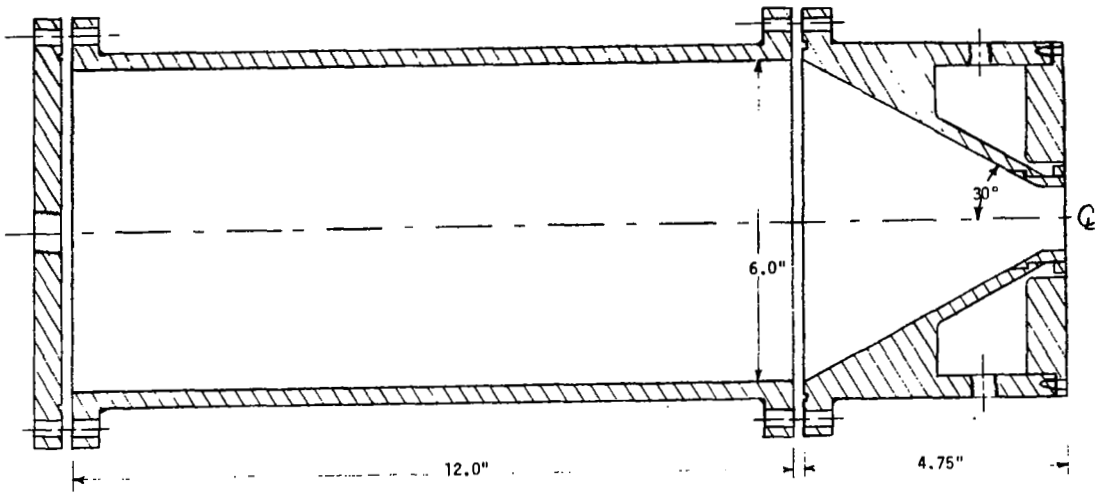

Figure 4-2. The Model Jet (For Nozzle Diameters and Configurations see Figures 4-3 and 4-4)

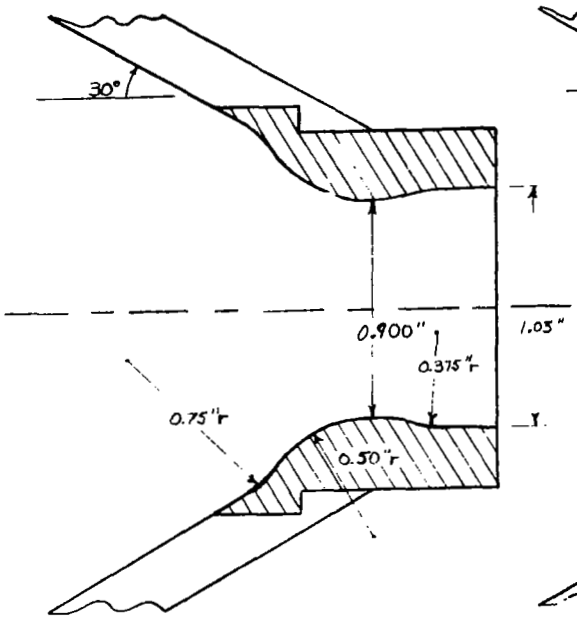

Figure 4-3. Convergent-Divergent Nozzle

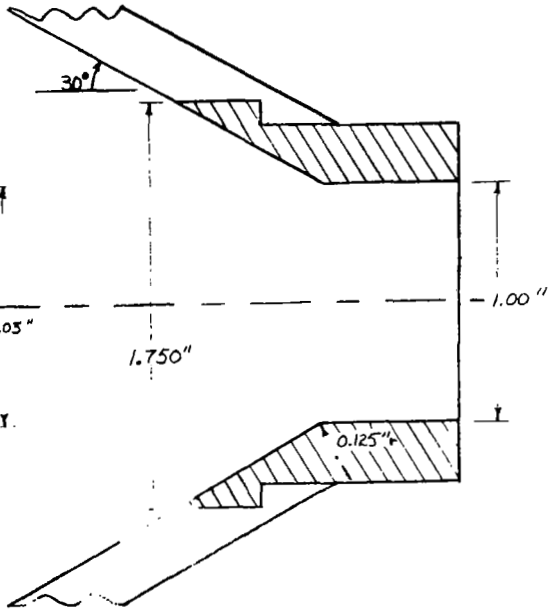

Figure 4-4. Convergent Nozzle

supported on a rigid stand by four flextures to provide longitudinal translation for thrust measurement. A 0-445 Newton (0 to 100 lbf) transducer is shown mounted to a rigid plate at the rear of the jet. Thrust errors created by unbalanced loads and constricting hoses were minimized by forming the GN_2 supply flex lines into a large diameter hoop, and using flex hose to supply the foam.

(a)

3.1-Inch Foam Injector

(b)

2.25-Inch Foam Injector

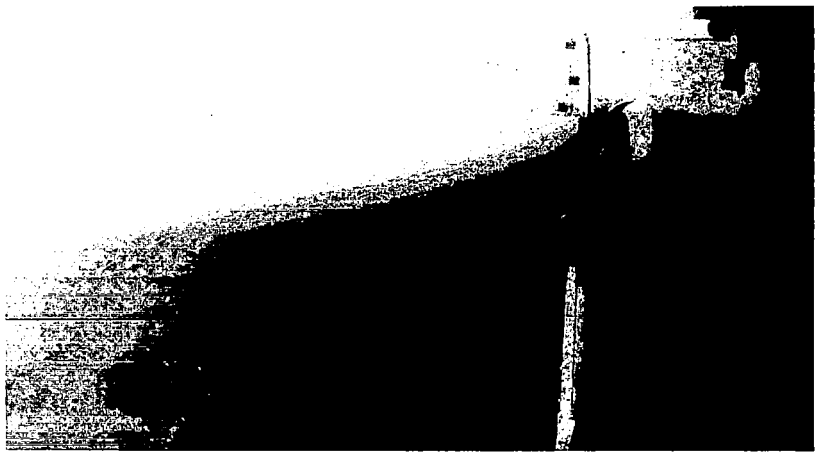

(c)

3.1-Inch ID Pipe Duct

Figure 4-5. Gas and Foam Jets (Note Ingestion Patterns)

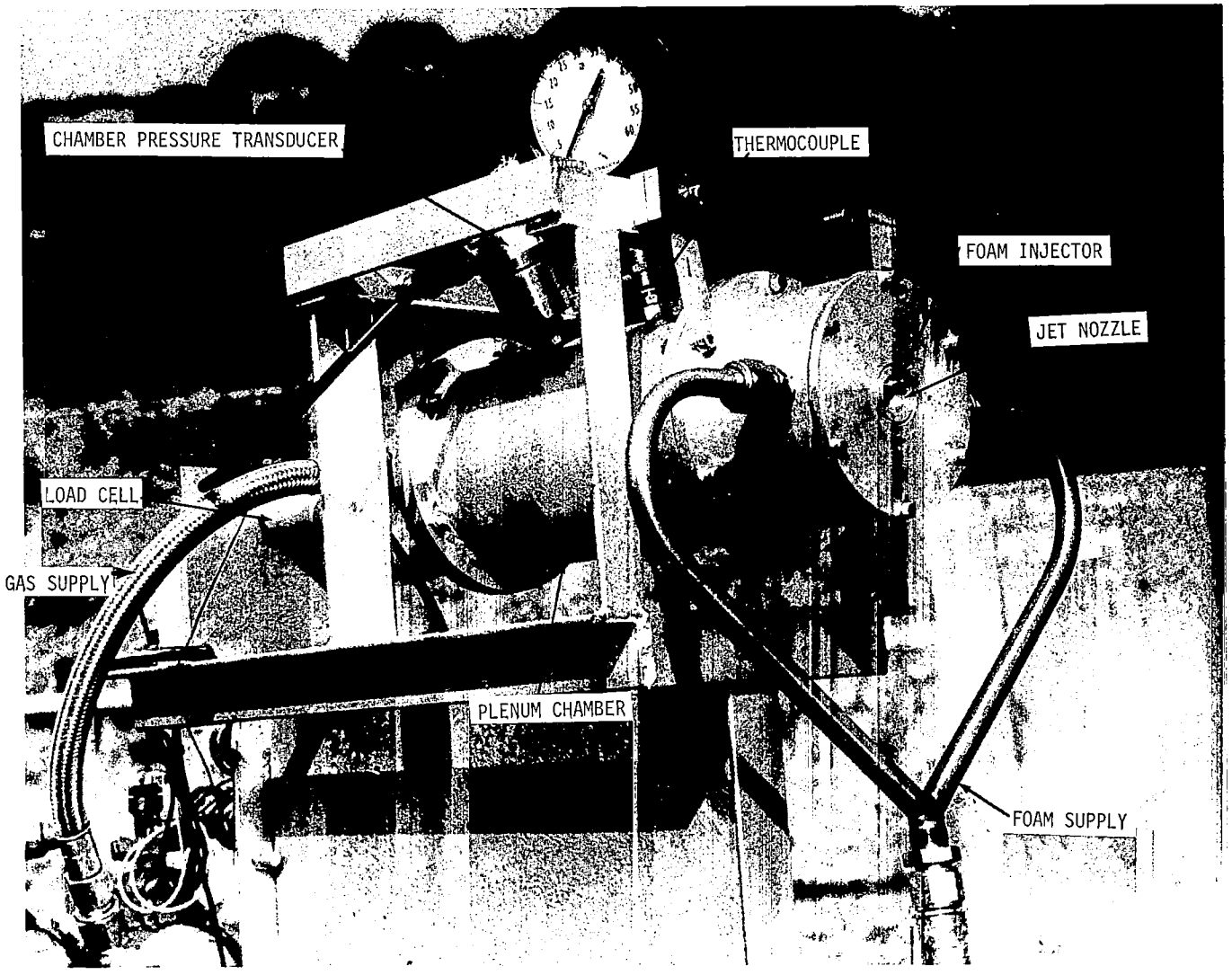

Figure 4-6. The Model Jet and Foam Injector

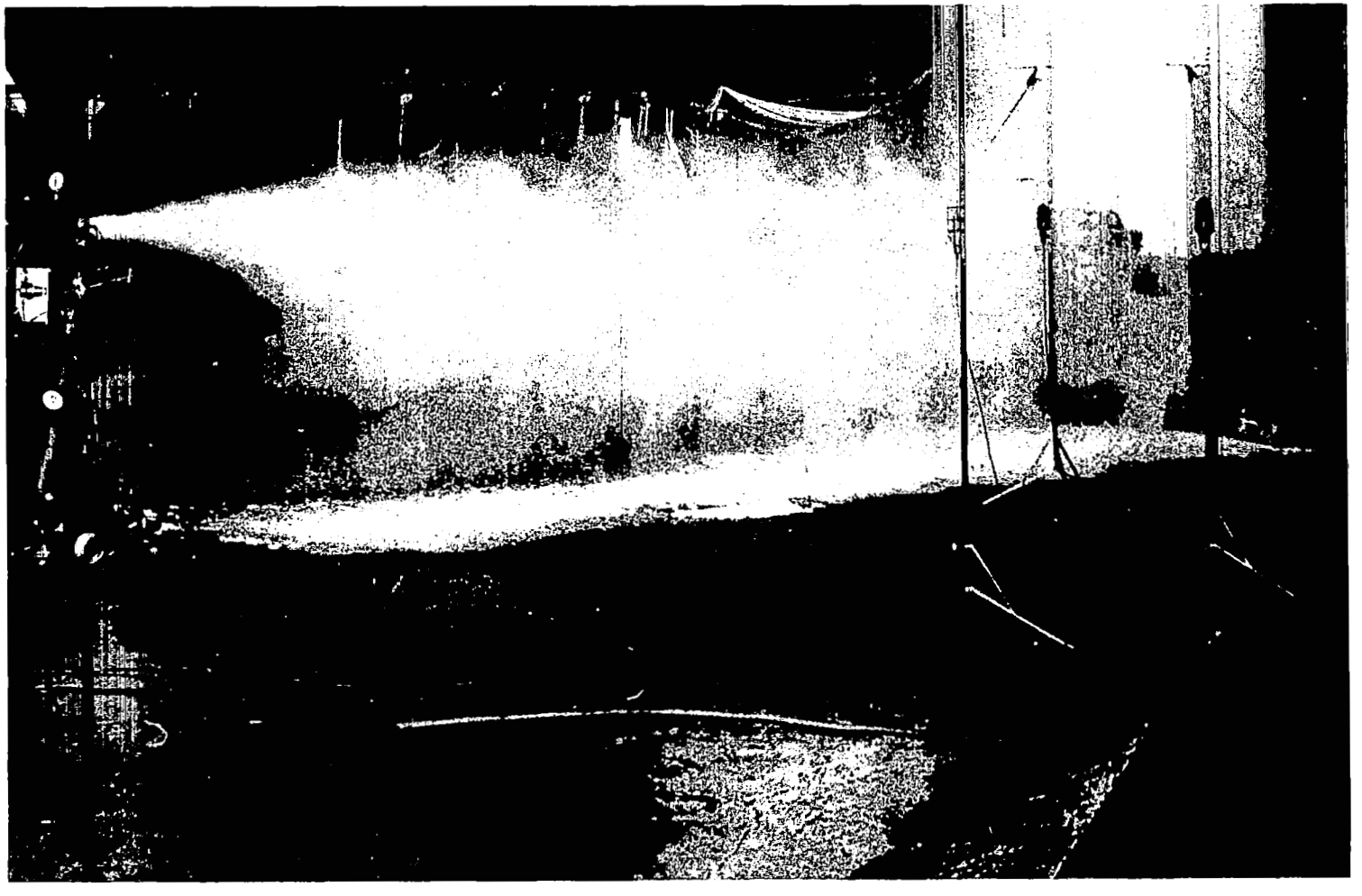

Figure 4-7. Gas Jet with Foam Injection

Gaseous nitrogen for the jet was taken from a cylinder trailer via 40 feet of 0.75 inch ID tube. Pressure control was accomplished by a dome regulator. The regulator downstream pressure and temperature were monitored by means of transducers located upstream from a calibrated 0.009525 m (0.375 inch) venturi.

This venturi was placed in a 0.304 m (12 inch) length of 0.0381 m (1.5 inch) ID tube (the only section of flow path not 0.01905 m (0.75 inch) ID tube). A solenoid actuated ball valve was used to initiate and terminate the jet flow.

The foam system, also plumbed exclusively with 0.01905 m (0.75 inch) ID tubing, consisted of a 14 liter foam solution tank pressurized with GN_2 and B-B bed improver; a 2.13 m (7 foot) flex hose connected the improver with the foam manifold. The pressurized foam solution, consisting of foam concentrate and water, was mixed with pressurized GN_2 from a separate K-bottle within the improver. The foam developed its characteristic expansion ratio and bubble size within the 2.13 meters (7 feet) of flex line before entering the foam manifold. Indication of liquid and gas flow rate in the foam system was obtained from pressure gauges located on the test apparatus.

Figure 4-7 shows the model jet in operation with foam injection.

4.1.2 Test Site Layout and Position of Measurement Microphones

Figure 4-8 is a plan view of the measurement site. The test site was ideally suited for noise measurements because the background noise level was very low. In addition, atmospheric conditions during the field survey were ideal. All measurements were made under near zero wind conditions. The nearest large reflecting surface was a building located about 40 meters (130 feet) from the model jet and about an equivalent distance from the nearest measurement microphone. The location of the measurement microphones relative to this building was not considered ideal; however, the choice was dictated by the limited area of flat terrain available. It is believed, however, that this building did not affect measurements appreciably. This statement is supported by the following reasoning.

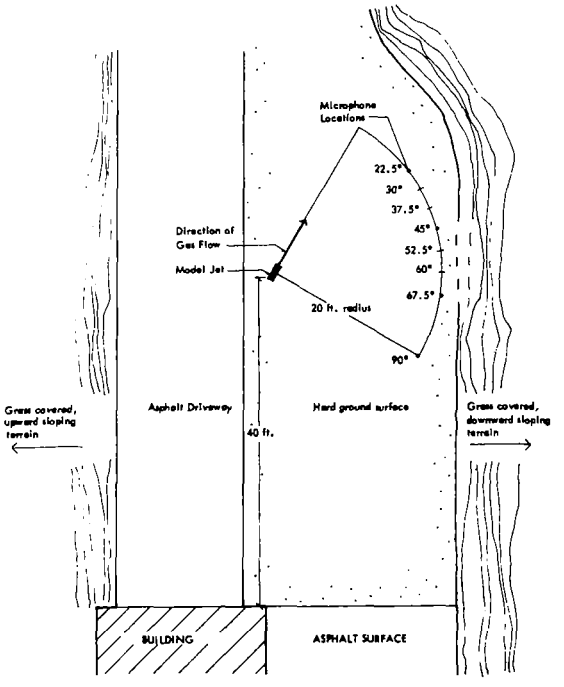

Figure 4-8
Plan View of Measurement Site

Four microphone locations were used for all measurements. Standard microphones, located at 22.5, 45, 67.5 and 90 degrees, are designated as dots in Figure 4-8. The remaining locations at 30, 37.5,

52.5 and 60 degrees were used for a small number of test runs. The four standard microphone locations were chosen in order to determine noise output and noise reduction in the areas where maximum noise is radiated. All microphone heights were placed in a horizontal plane which included the model jet noise source. The heights, which varied slightly to accommodate small terrain elevation variations, were approximately 66 inches above ground level.

4.1.3 Instrumentation and Data Collection

The jet flow instrumentation is presented in Figure 4-9. The pressure transducers and load cell were conditioned by Endevco Model 4470 universal signal conditioning modules with complimentary strain gauge bridge cards. Calibration was maintained through bidaily use of R-cal values provided by TRW Metrology. Copper-Constantan thermocouples were employed in both the line and chamber temperature positions. These thermocouples were referenced to an external voltage source which was corrected three times during the testing day. All transducer and thermocouple outputs were recorded on a six point Leeds and Northrup type W recorder. The interval between consecutive data points was about 5 seconds. The scales were calibrated to read directly, in lbf, psia and °C.

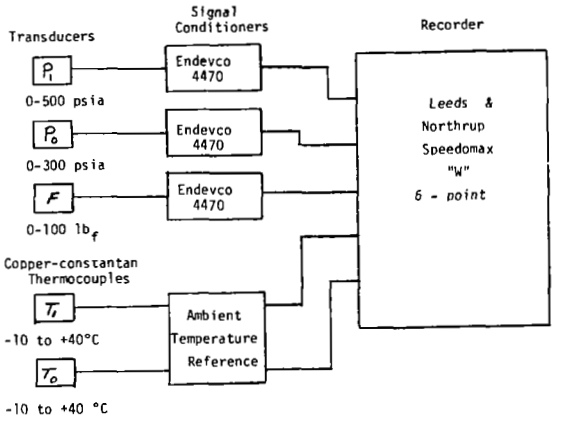

Figure 4-9

Model Jet Instrumentation

The acoustical recording instrumentation is shown in Figure 4-10. The noise levels at the four microphone locations were recorded on magnetic tape using a four channel Ampex Model AG-440B recorder. The microphones used were of the 1 inch condenser type. The VTVM, octave filter set and oscilloscope shown were used for direct monitoring of the noise levels during a run. Channel four of the system was used to insert voice information between test runs, as well as to indicate by voice the onset or end of foam injection into the jet stream. The measurement system was calibrated prior to each series of test runs by use of an acoustical calibrator with known sound pressure level. A 1000-Hz, 90-db sound pressure level signal was recorded on each of the four channels. This information, along with recorded data on amplifier and tape recorder gain settings, allowed the determination of the absolute sound levels during later tape analysis.

Coordination of both jet and acoustical instrumentation was achieved through the operator's visual observation of signal lights. These signals were connected to jet control and foam signal switching located on the test stand.

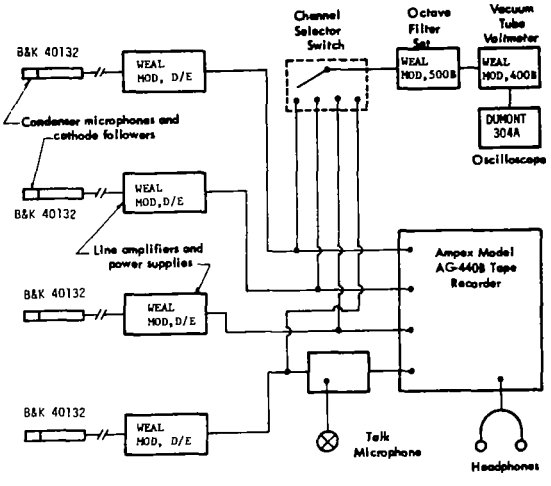

Figure 4-10

Block Diagram of Recording Instrumentation

4.1.3.1 Jet and Foam Flow Parameter Measurements

The flow rate on nitrogen was measured by recording the pressure and temperature at the entrance to a venturi operated under choked flow conditions. The venturi was calibrated against a flowmeter between 6.89×10^5 to 27.6×10^5 N/m^2 (100 psia and 400 psia) and a contraction coefficient K = 0.924 was obtained. The accuracy of the flow measurements is approximately ±1 percent.

The temperatures measured in the plenum chamber were close to 0°C. The temperature drop between the gas storage cylinders and the plenum chamber reflects the deviation of high pressure nitrogen from a perfect gas law. [Note that a pressure drop at constant enthalpy from 160 atm (2360 psia) and 300°K (27°C) to 3 atm (44 psia) results in a temperature drop to 275°K (+2°C) (Reference 55).]

Thrust measurements were checked against thrust values calculated from flow rate and calculated jet velocity (Reference 56)

$$F = \dot{w} V_{jet} + (P_o - P_{atm}) A_{jet}$$

For low thrust levels, the measured values were too low by as much as 2 lbf (8.9 N) at 30 lbf (133.5 N) but were correct for thrust levels on the order of 43 lbf (191 N) or more. Heavy gas and foam supply lines probably caused this error. Uncorrected measured values are given in Table 4-1*, (Section 4.2) because the increase in thrust caused by foam injection is of more interest in these tests than the thrust itself. This thrust increase reflects the momentum of the injected foam, verifying the concept as a no-loss system.

Foam flow rates were not measured during the tests. The liquid flow rates indicated in Table 4-1 were obtained by recording the liquid supply pressure and establishing a liquid flow rate versus pressure curve in a separate run.

*Table 4-1 is at the end of Section 4. All figures containing test results are located immediately before the table and the figure numbers are given in the table.

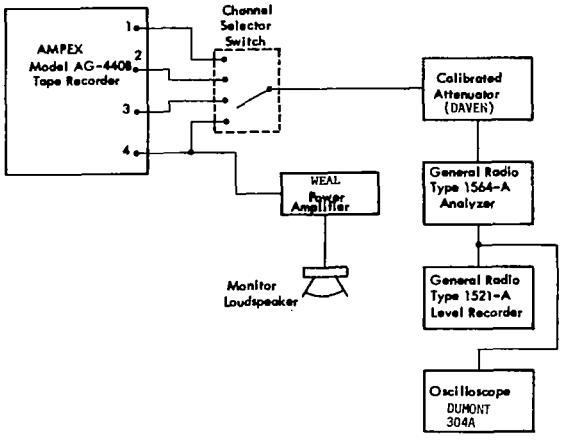

Figure 4-11

Block Diagram of Data Analysis Instrumentation

4.1.3.2 Acoustical Measurements

Sound pressure levels at the four microphones were recorded on tape. The tape analysis system is shown in Figure 4-11. The recorded runs were analyzed in 1/3 octave bands ranging from 400 Hz to 10 kHz. The calibrated attenuator shown is used to insert system frequency response corrections during analysis. The 1/3 octave frequency information for each of the test runs was recorded on a graphic level recorder with sound pressure levels and noise reductions read directly and tabulated. All noise levels were read from the charts during the stable portion of the test run. Typically, the pure jet and the jet with foam required 5 to 10 seconds to stabilize to a relatively constant level. For a few runs the stabilization was not ideal and a best judgment of the levels was made.

The perceived noise level for the complex sound as defined in Reference 57, was then determined by the following formula (Reference 58):

$$N_T = 0.85\, N_{max} + 0.15 \sum N$$

where

N_T = total noisiness in Noys,

N_{max} = number of Noys in the noisiest band

$\sum N$ = sum of the noisiness in all the bands

Upon the determination of N_T, for each run with and without foam, the computer consulted the Noy tables at 1000 Hz and printed out the corresponding PNdB levels.

4.2 TEST MATRIX

A total of 65 tests were made. The data from some of these were not reduced for various reasons: some were duplicate runs to check out good functioning of instruments: one test was spoiled by airplane noise interference; and there were a few runs with faulty test sequence. The data for 51 tests were reduced; 40 of these were chosen for presentation in this report as shown in Table 4.1. The data for all of the tests are submitted separately.

4.3 CHOICE OF TEST CONDITIONS

The test program was exploratory rather than exhaustive. Test conditions were chosen to clarify under what flow conditions foam injection was effective in reducing sound emission levels, to see if the choice of foaming agent and concentration was important or just the flow rate, to see if the foaming injector geometry had a large influence, etc. The large number of variables having a possible influence on sound reduction and the fact that accurate noise reduction measurements were not available during the test, combined with limitations in time and compressed nitrogen gas supply, made a more systematic approach impractical.

In retrospect, many variations on the tests were possible. However, the tests performed did show the relative importance of the main parameters.

4.4 TEST RESULTS

4.4.1 Noise Generation in Gas Jets

The sound generated by the jet issuing from the convergent nozzle was quite reproducible in the narrow range of plenum pressures tested (Table 4-1 and Figures 4-12 through 4-32). The perceived noise was 123 ±1 PNdB. At this level of sound only limited reduction could be achieved through foam injection; hence only a few tests were conducted, all of them with sonic flow at nozzle exit.

The sound generated by the convergent-divergent nozzle jets varied considerably with plenum chamber pressures (112 to 129 PNdB). The design Mach number of the nozzle was 1.67 (throat-to-exit area ratio 0.763), corresponding to a plenum pressure $P_o = 4.8 \times 10^5$ N/m^2 (69.5 psia). For low chamber pressures ($P_o = 1.85 \times 10^5$ to 2.14 N/m^2 or 27-31 psia) a normal shock wave formed inside the nozzle so that the jet back pressure was equal to atmospheric pressure and the sound level was low (about 112 PNdB). For high plenum pressures (4.1 to 4.8×10^5 N/m^2 or 60-69 psia) exit pressure again nearly matched the back pressure (runs #20, 28 and 16); the sound emission level was 125 to 126 PNdB. For intermediate flow regimes, for which the exit pressure was much lower than atmospheric, the sound emission was more intense and less reproducible. The erratic appearance of a high intensity, high frequency tone can be detected for plenum pressures between 2.97×10^5 and 3.72×10^5 N/m^2 (43 and 54 psia). Tests #59 and #60 (runs #59 and 60 and Figures 4-19 and 4-20) were made under conditions as identical as possible. Neverless, there is a difference of 4.5 db at 6.3 kHz on the 45 degree microphone. (The PNdB rating was the same because the differences compensated each other). Comparison with #43 (run #43, Figure 4-18) with identical flow rate shows a lower sound intensity throughout the frequency range. Similar lack of sound-reproducibility may be noted for plenum pressures of 3.38×10^5 and 3.72×10^5 N/m^2 (49 and 54 psia). The erratic nature of some of the high

frequency emissions is probably caused by the sound source, i.e., an overexpanded jet with a shock wave structure at the exit of the nozzle. Shock wave configurations are generally not very reproducible; small changes in flow rate or the manner in which a stable flow rate was reached may result in significant changes in flow patterns.

The PNdB noise level scale amplifies the importance of the noise emission at the frequency of maximum noise level (as does the human ear), thus exaggerating the influence of the erratic pure tone contribution. An illustration of the erratic nature of pure tone generation can be found in runs #32 and #33 (Figures 4-24 and 4-25). Jet and foam flow conditions are the same in both runs, although a 108 db peak at 5000 Hz appears on the jet without foam in run #33, the maximum emission on #32 is 106 db. The sound level curves on both runs are nearly identical and the noise reduction curves ΔPNdB on both runs indicate that there was a pure tone contribution at 5000 Hz at all other microphone locations, i.e., the lack of a peak at 45 degrees on the #32 run was anamolous. It is therefore particularly important to realize that the sound level reproducibility is limited and to compare sound emissions curves with and without foam injection for each run.

4.4.2 Sound Reduction Caused by Foam Injection

When foam was injected into the nitrogen jet, the preceived noise level was decreased in all cases. The decrease was highest for high noise emission levels and for high frequencies. This finding is in agreement with the hypothesis that foam acts as a resonating energy absorber whose absorption capability is most pronounced in the audible high frequency range (1 to 10 kHz). Foam injection flattens the sound level versus frequency curves, obliterating any pure tone components (Figures 4-19, 4-20, 4-22, and 4-26).

Observations made during the tests and the acoustic data indicate that foam injected into the jet effects noise reduction in several ways. Injected foam was broken into flakes of up to ~1/4 inch in diameter and the flakes were blown 30 or 40 feet by the jet. These flakes absorbed sound energy by resonance in the foam or served as scatterers, hence, the more effective absorption of high frequency sounds. The increase of low frequency sound emission in directions close to the jet axis, however, indicates that the ingestion of foam also influences the structure of the turbulence in the mixing region of the jet.

Ribner (Reference 59) has shown that the directivity of jet noise is governed by a factor accounting for eddy convection and for sound refraction by velocity gradients:

$$(1 + \cos^4 \theta) \left[(1 - M_c \cos \theta)^2 + \alpha^2 M_c^2\right]^{-5/2}$$

where θ is the direction angle with the jet axis, M_c the eddy convection Mach number and α a factor inversely proportional to the lifetime of an eddy. The lifetime of an eddy is short; hot wire studies show that an

eddy in a jet is convected about three times its length before decaying. The ingestion of relatively heavy foam particles may well reduce the eddy life and change the polar distribution of sound.

Polar diagrams of the sound levels with and without foam injection are shown in Figures 4-33 and 4-34. These diagrams are a composite of runs #59 and #60 in which the four microphones were located 22.5, 30, 37.5 and 45 degrees and 45, 52.5, 60 and 67.5 degrees, respectively (Figure 4-8). Five frequencies are shown on the polar diagrams. Foam injection reduced high frequency sound at all polar locations; at low frequencies the sound level was increased near the axis while it decreased somewhat at angles above 45 degrees.

A third possible type of noise reduction e.g., by attentuation of sound transmitted through an envelope of foam surrounding part of the sound-emitting zone of the jet, was not detected. The 3.1-inch diameter foam injector produced an approximately 3-inch long foam sleeve around the jet. A photograph of the foam surrounded jet, Figure 4-5, clearly shows the inward flow of foam, followed by foam backup. Thus, nearly one-half of the jet mixing region in which most of the noise was generated was enclosed in a foam sleeve. For smaller foam injector diameters the breakup of foam started quite close to the injector face as shown in Figure 4-6. Despite this difference, all foam injectors effected similar jet noise reduction levels. It may, therefore, be concluded that the foam does not act as a muffler and that only the ingested foam is effective.

The nitrogen gas jet was quite cold, near the freezing point of water upstream of the nozzle and close to -90°F (206°K) at the exit for the supersonic jet. Local foam freezing may have occurred in the jet mixing region at the interface between foam and gas, where the major noise generation occurs. (No overt evidence of freezing was found.) It is anticipated that, if freezing did occur, the response of the foam bubble matrix would be impared. In addition the shear structure of the mixing region would probably be affected differently since solid foams would not have the compliance of liquid foams. The overall absorption capability of the foam would be reduced, assuming the foam to act as a compressible, dissipating absorber. In a hot jet the problem is not present. In addition, vaporization is expected to occur and add an additional mode for energy absorption. Tests are required to confirm this conjecture.

Jets issuing from the convergent nozzle were subsonic with respect to the atmospheric speed of sound, but the jet velocity was supersonic compared to the speed of sound in the cold nitrogen. The structure of these jets was different from hot subsonic jets with regard to turbulence and the possible presence of shock waves. The cold supersonic jets also have a structure different from that of hot supersonic jets. Thus, experimentation with hot jets is needed to extend the cold jet test results.

The frequency distribution of the sound emitted by jets is known to be influenced by the jet diameter. A shift of intensity to lower frequencies is found as the jet diameter increases. Thus, foams having better absorption properties for lower frequencies need to be investigated.

4.4.3 Influence of Foam Characteristics

Two foaming agents 3 percent Regular Protein and High Expansion were tested. The Protein foam was tested at two concentrations —3 percent and 10 percent—and the High Expansion foam was tested at 6 percent. The expansion ratio could not be measured accurately because the foam injection velocity was so high as to make sample collection for weighing difficult, however, a few samples were weighed. The gas flow rate was adjusted to obtain as light a foam as possible without slug flow. It was estimated that the expansion ratio of the 6 percent concentration High Expansion foam was 15 to 17 while that of the protein base foams was 20 to 30. The sound emission of a jet with foam injection was quite independent of the type of foam injected. For instance the curves for #11, #12 and #5 (Figures 4-12, 4-13 and 4-16) were all similar. though Protein foam at two concentrations and a High Expansion foam were injected. No difference in noise level reduction because of foam type could be detected in the supprsonic jet experiments (compare #29, 32 and 33; Figures 4-21, 4-24, and 4-25).

Foam flow rate was lowered from a high value, corresponding to a liquid flow rate approximately 0.370 kg/sec (0.83 lbm/sec), until a decrease in effectiveness was noted. Generally, there was no difference between flow rates of 0.370 to 0.315 kg/sec, but a decrease of effectiveness occurred when the flow rate was dropped to 0.300 kg/sec (see #3, #4 and #5 for subsonic jets and #42, #43, and #44, #31 and #32 for supersonic jets).

4.4.4 Influence of Foam Injector Diameter and Gap Sizes

Four injector configurations were evaluated:

1.5 inch (0.0381 m) diameter, 0.050 (0.00127 m) inch gap

2.25 inch (0.0572 m) diameter, 0.050 (0.00127 m) inch gap

1.5 inch (0.0381 m) diameter, 0.100 (0.00254 m) inch gap

3.1 inch (0.0788 m) diameter, 0.050 (0.00327 m) inch gap

Comparing #24, #19, #22 and #41 (P_o = 54 psia), it is found that the preceived noise level reduction was 6 to 6.5 PNdB for all of the runs. The weak influence of foam injector configuration of foam flow rate strengthens the hypothesis that the foam ingested in the form of flakes into the mixing region of the jet, absorbs sound by resonance. The injector design and the injection velocity must only be adequate to distribute the foam in that region.

4.4.5 Experiments with a Foam Lined Exit Manifold

A rigid exit manifold was also tried in conjunction with the convergent-divergent jet nozzle and the 3.1-inch (0.0787 m) diameter foam injector. The effect of the exit pipe was to reduce thrust considerably

and to shift to slightly higher frequency the general sound level curve; the pure tone emission of the jet was also increased, thus increasing the PNdB levels. Tests #63 and #64 (Figures 4-31 and 4-32) may be compared to #59 and #60 (Figures 4-19 and 4-20). Foam injection flattened the sound level curve, decreasing the high frequencies and increasing the low frequencies. The frequency shift was more pronounced in tests with the pipe than tests without the pipe, and the PNdB reduction was somewhat lower, 6 PNdB compared to 10 PNdB.

4.5 SUMMARY OF MODEL JET TESTS

Conclusions drawn from the 1-inch diameter cold nitrogen tests are

- Foam injection results in a perceived noise level reduction in all directions.
- The higher the noise level, the greater the noise reduction.
- The effects are most pronounced at the high frequencies.
- Noise reduction increases with foam flow rate but the reduction becomes constant when a sufficient flow rate is reached.
- Directivity of sound emission is affected by foam injection. High frequency sounds are attenuated in all directions, although in some instances low frequency sound emission is increased in the direction of small angles with the jet axis.
- Foaming agent type and its concentration in the foaming solution have no detectable influence.
- The diameter of the annular foam injector had little influence in the range of diameters tested.

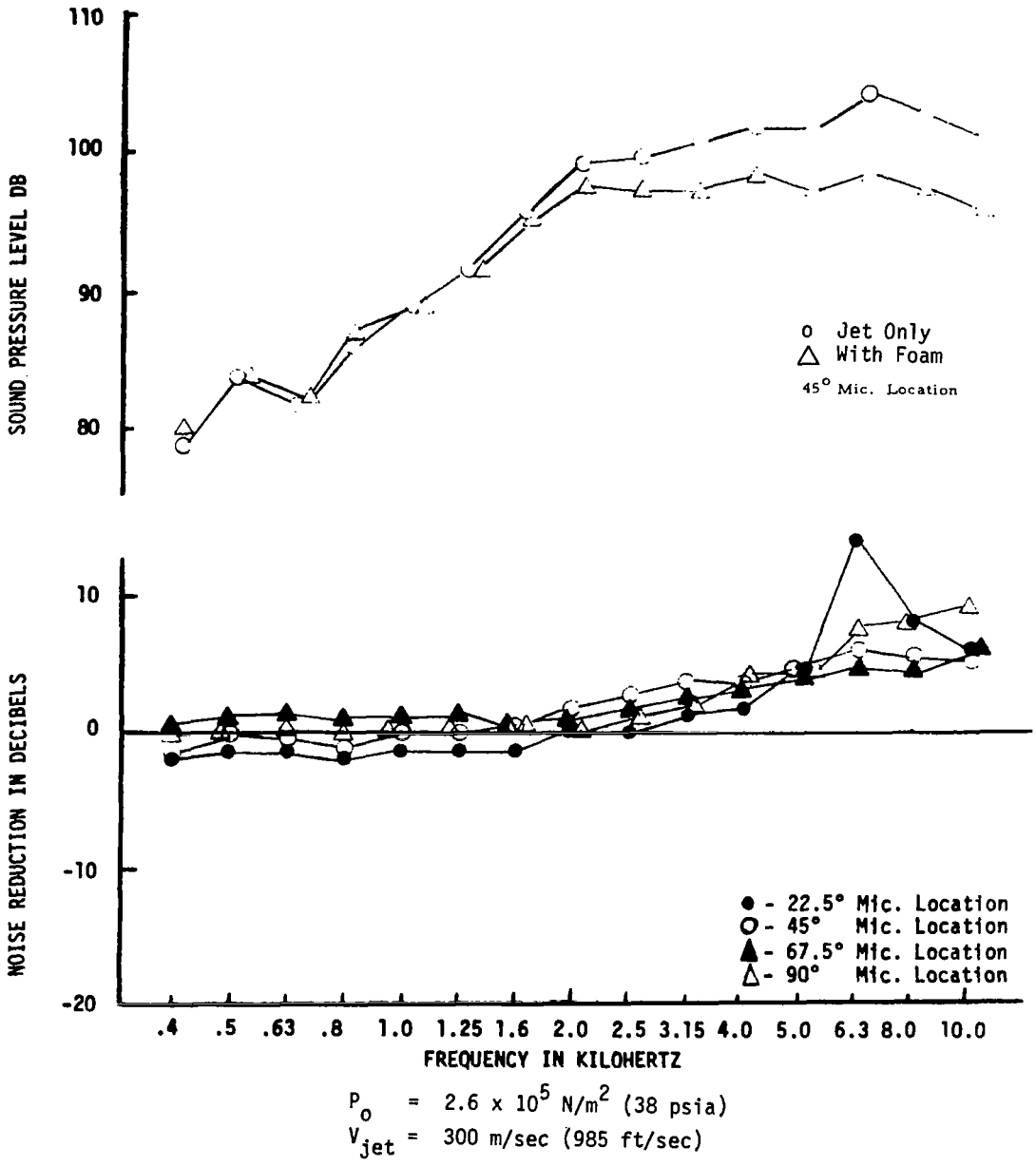

Figure 4-12. Jet Noise Reduction, Run No. 11, Convergent Nozzle

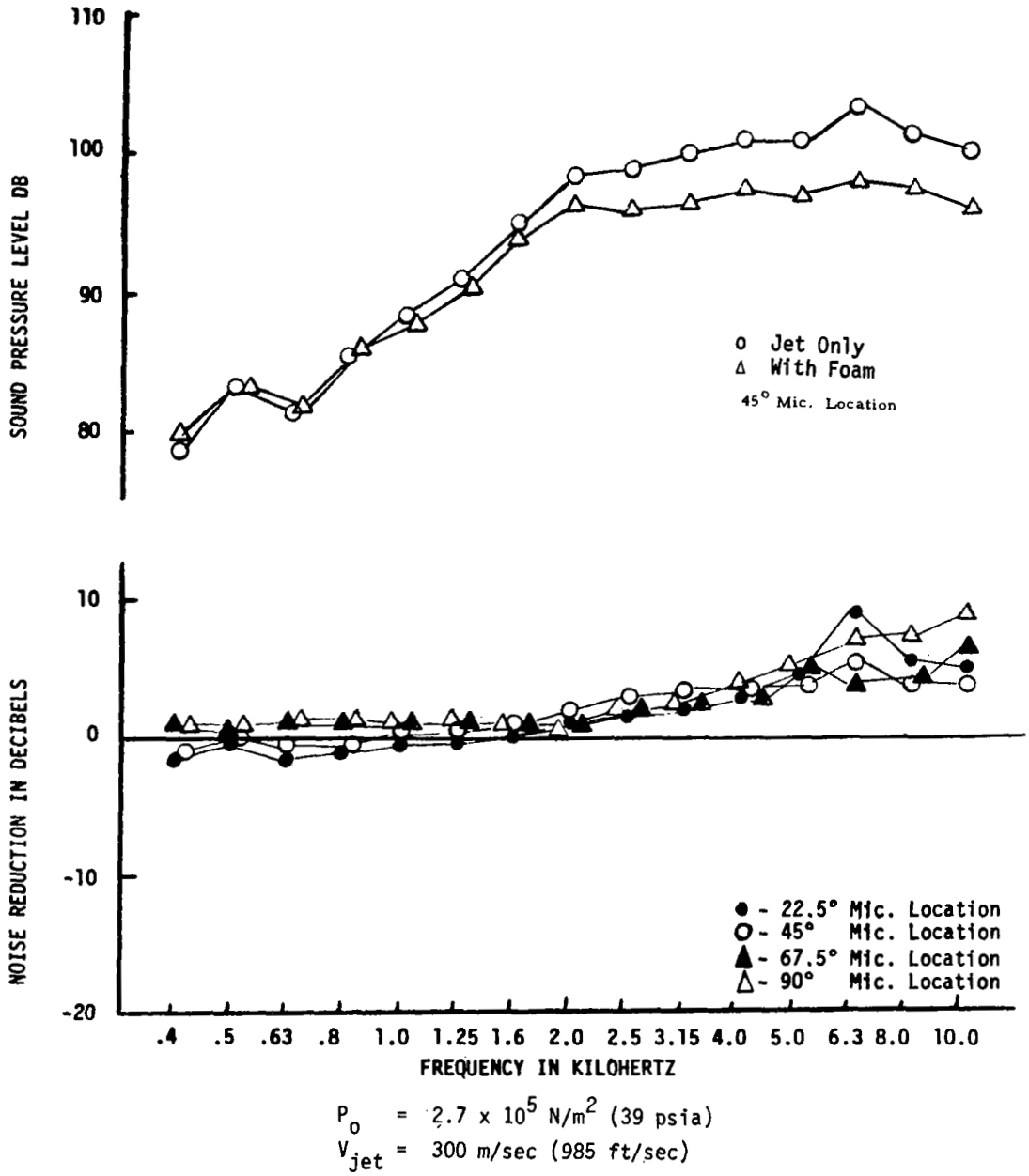

Figure 4-13. Jet Noise Reduction, Run No. 12, Convergent Nozzle

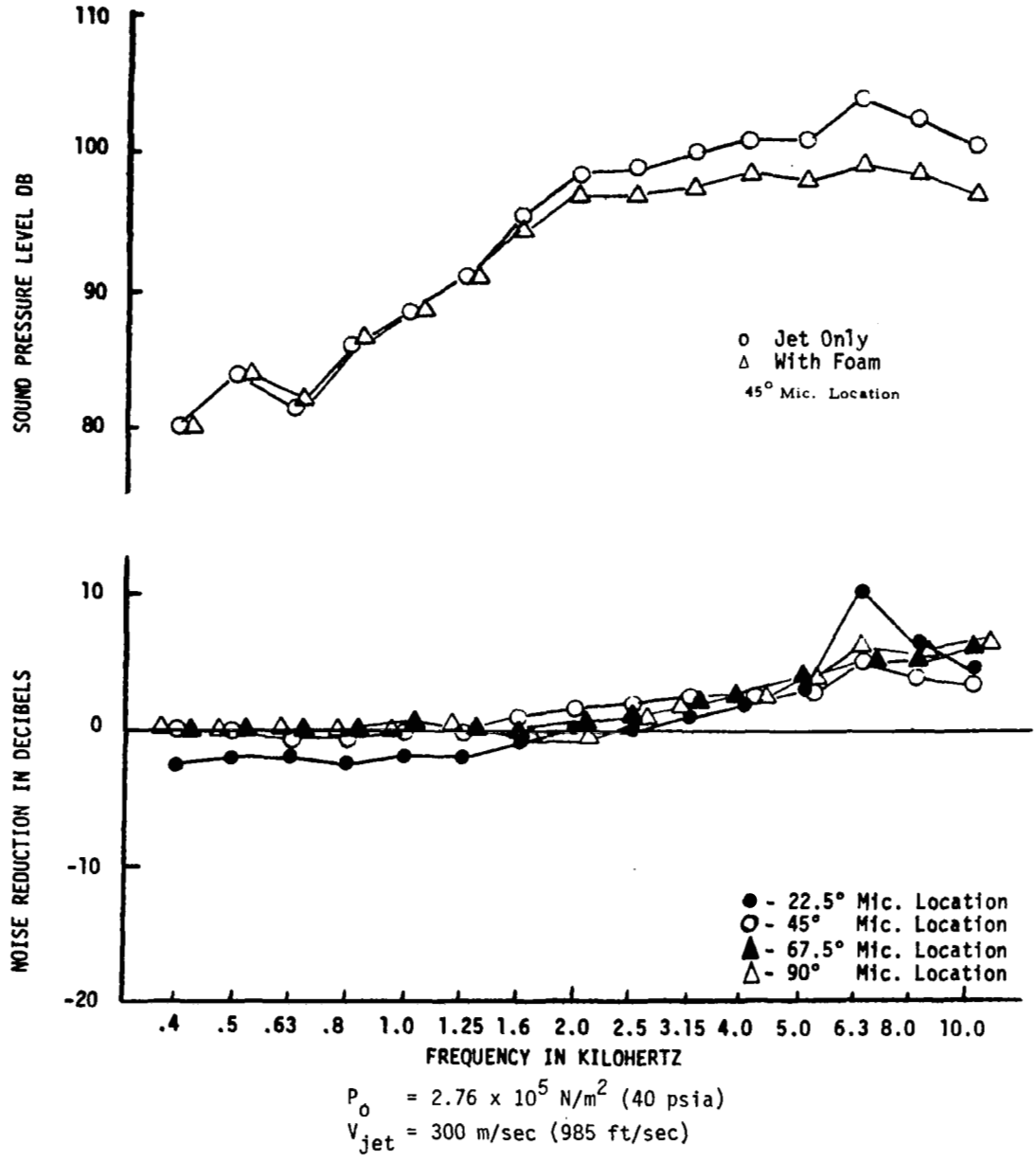

Figure 4-14. Jet Noise Reduction, Run No. 3, Convergent Nozzle

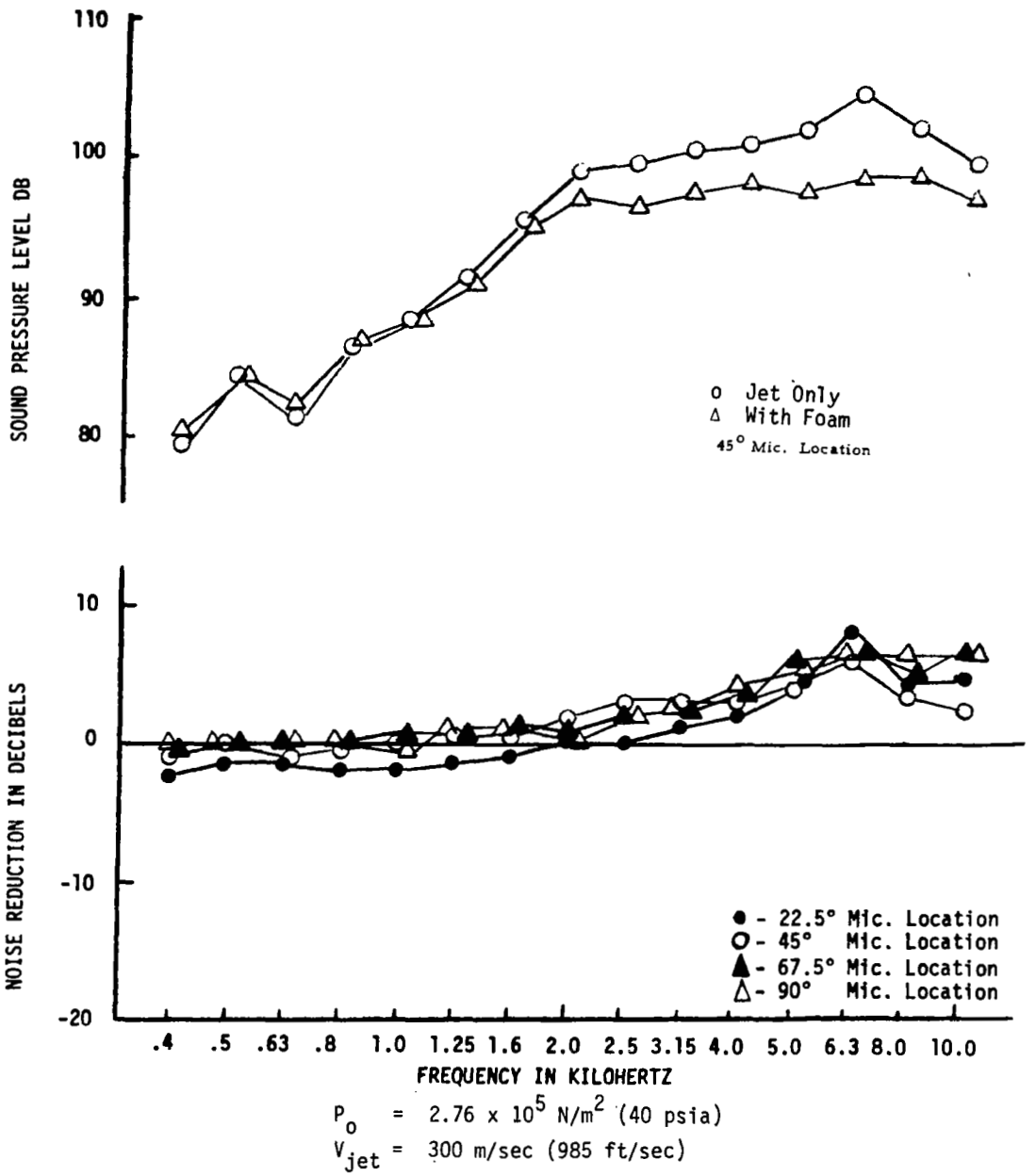

Figure 4-15. Jet Noise Reduction, Run No. 4, Convergent Nozzle

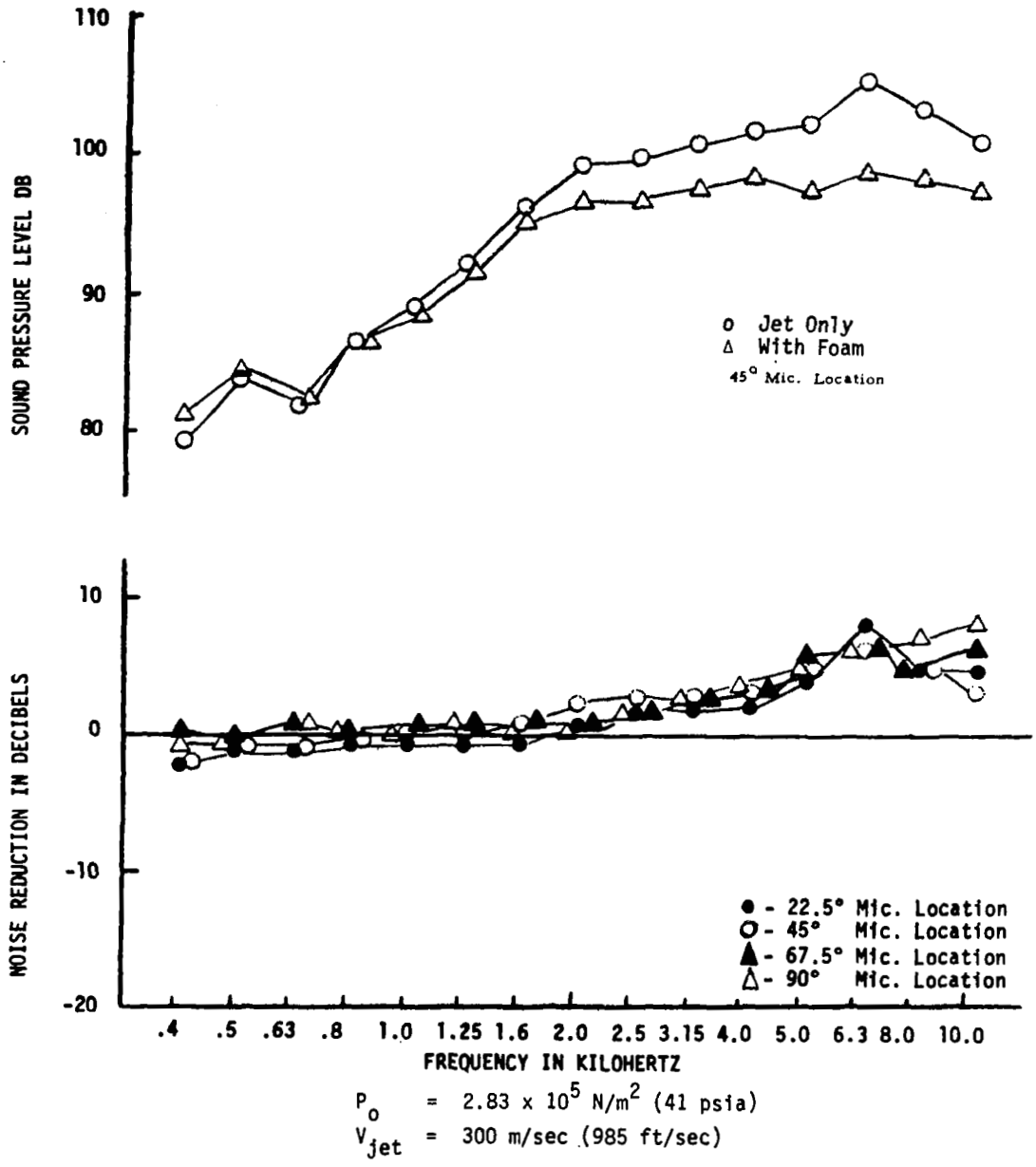

Figure 4-16. Jet Noise Reduction, Run No. 5, Convergent Nozzle

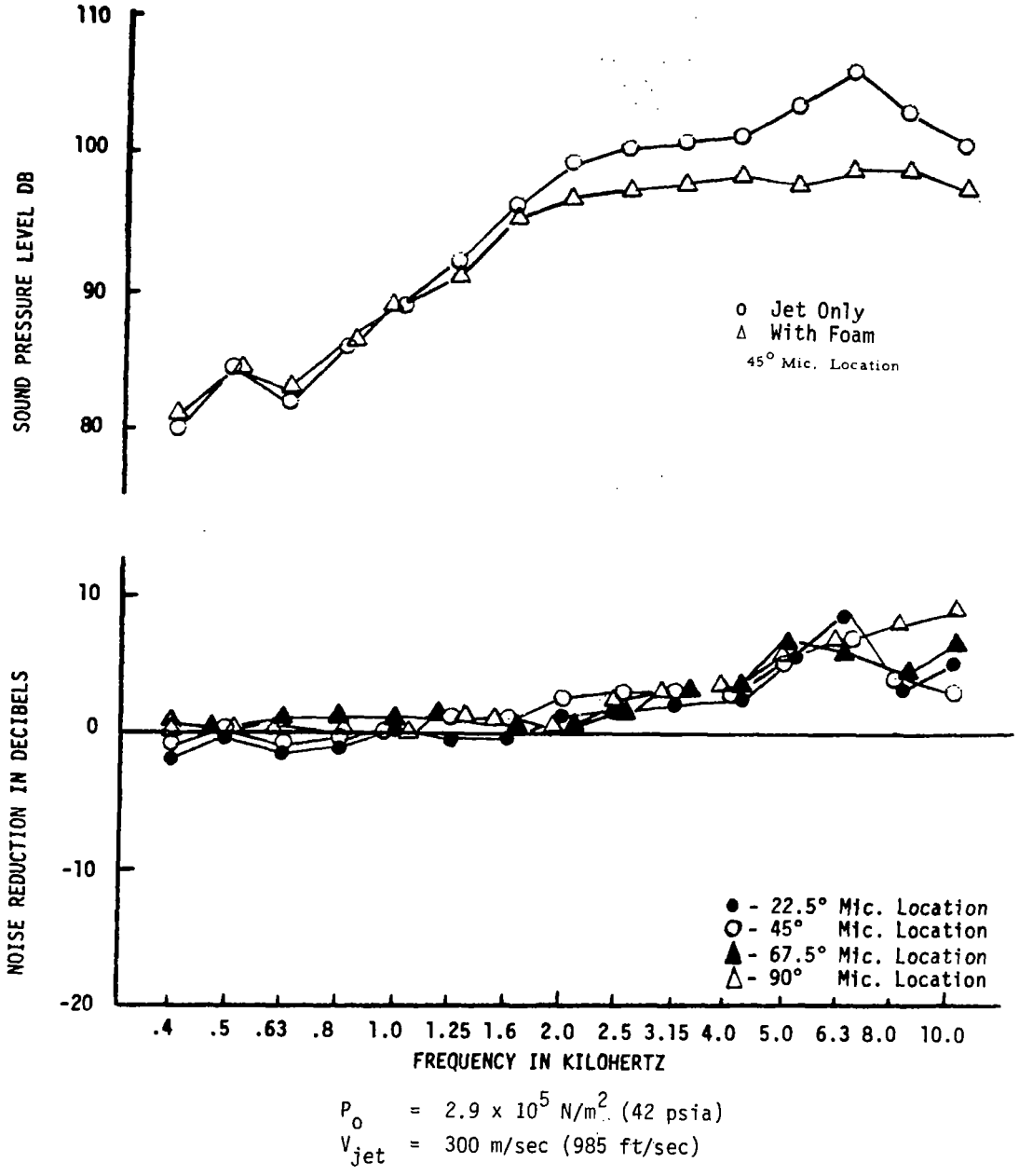

Figure 4-17. Jet Noise Reduction, Run No. 6, Convergent Nozzle

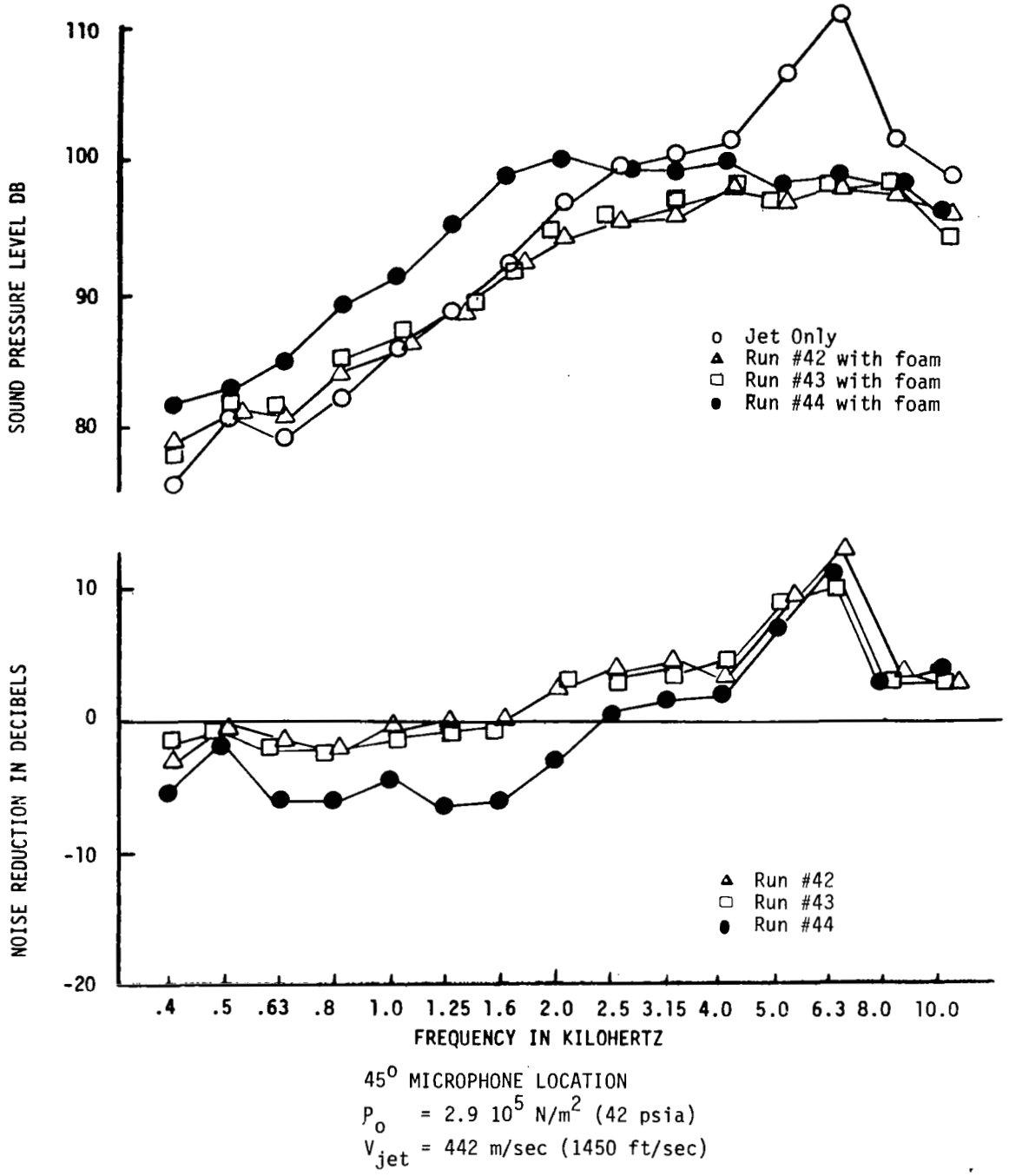

Figure 4-18. Jet Noise Reduction, Run Nos. 42, 43, 44, Convergent Divergent Nozzle. Influence of foam flow rate.

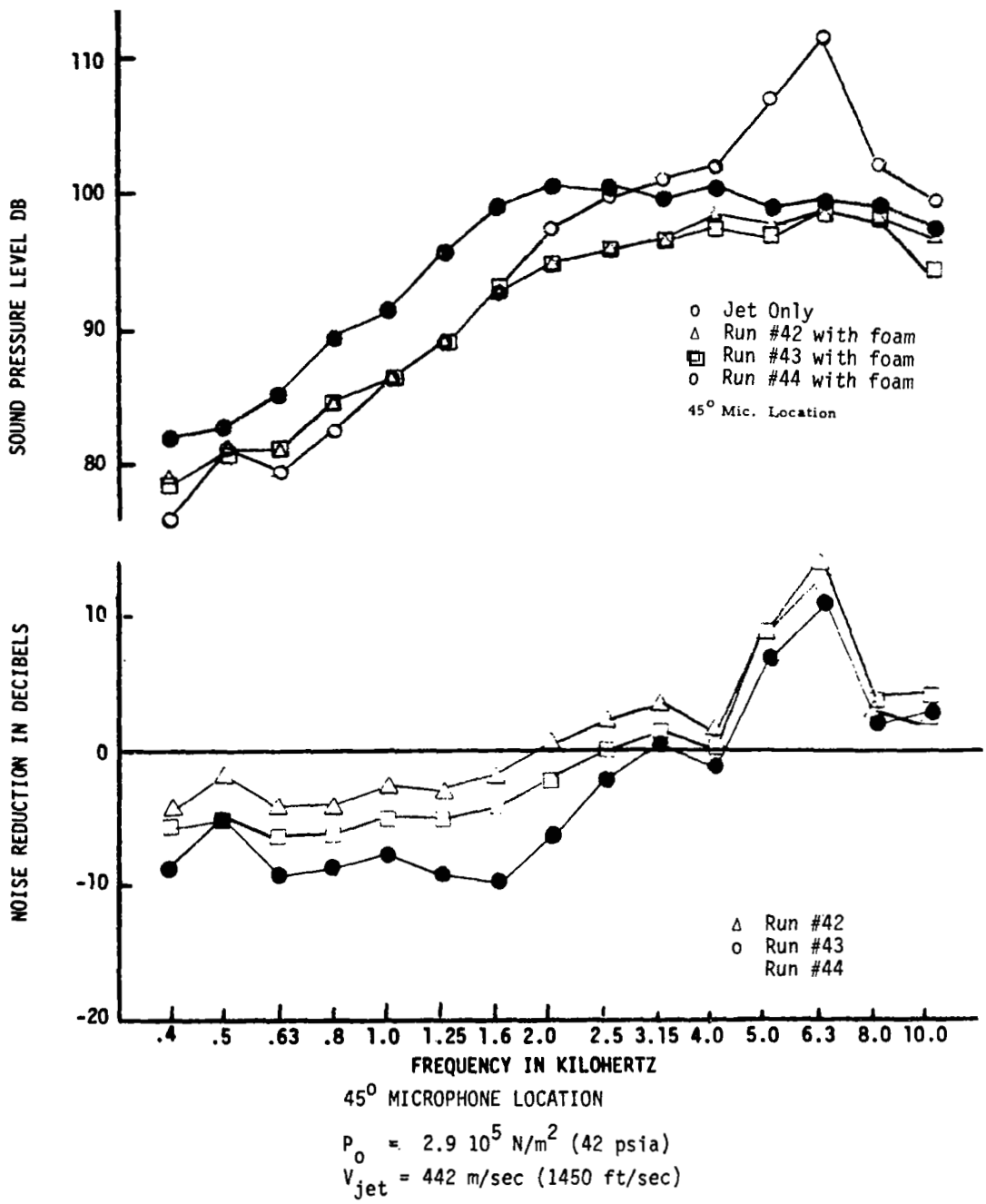

Figure 4-18. Jet Noise Reduction, Run Nos. 42, 43, 44, Convergent Divergent Nozzle

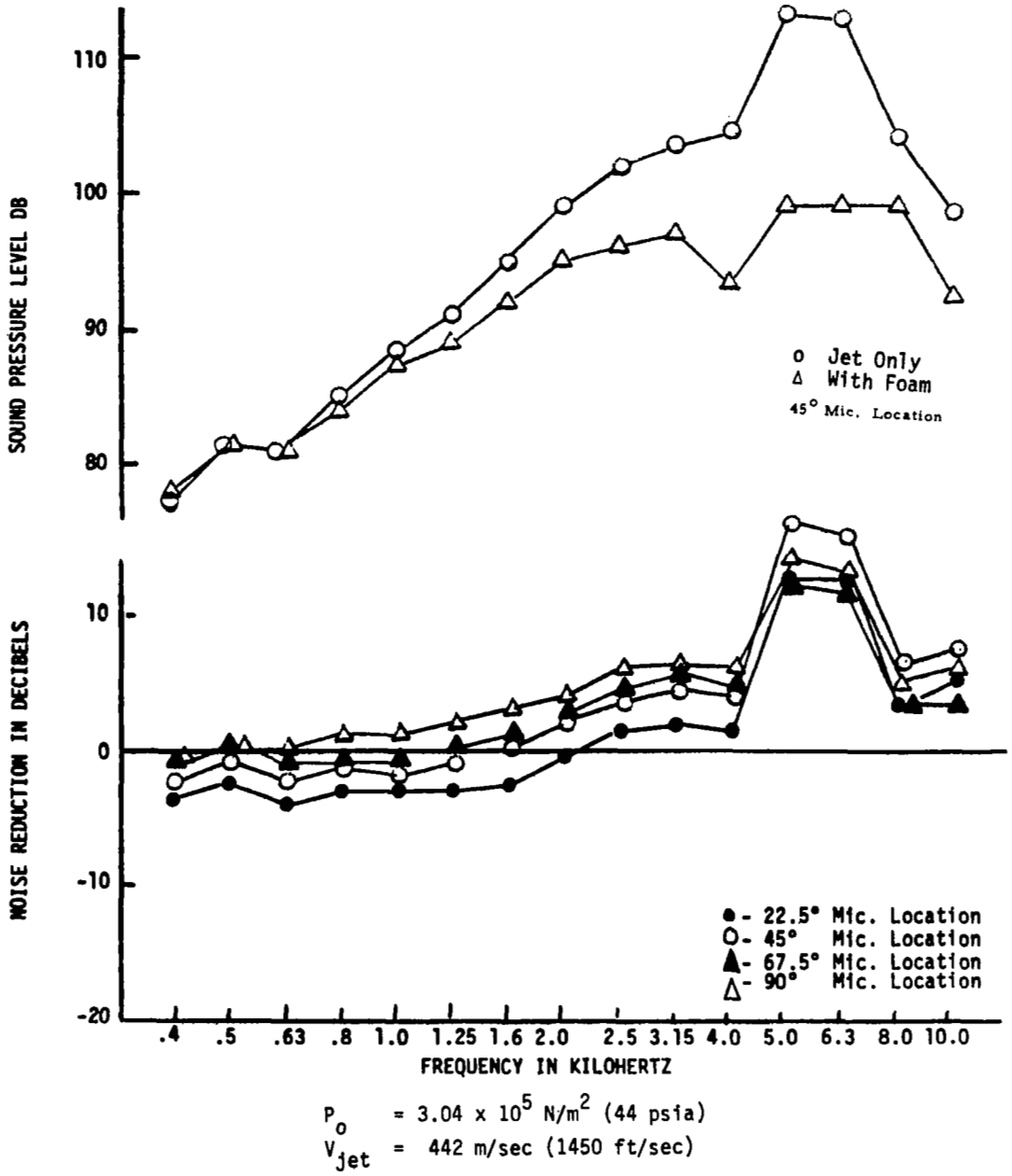

Figure 4-19. Jet Noise Reduction, Run No. 59, Convergent Divergent Nozzle

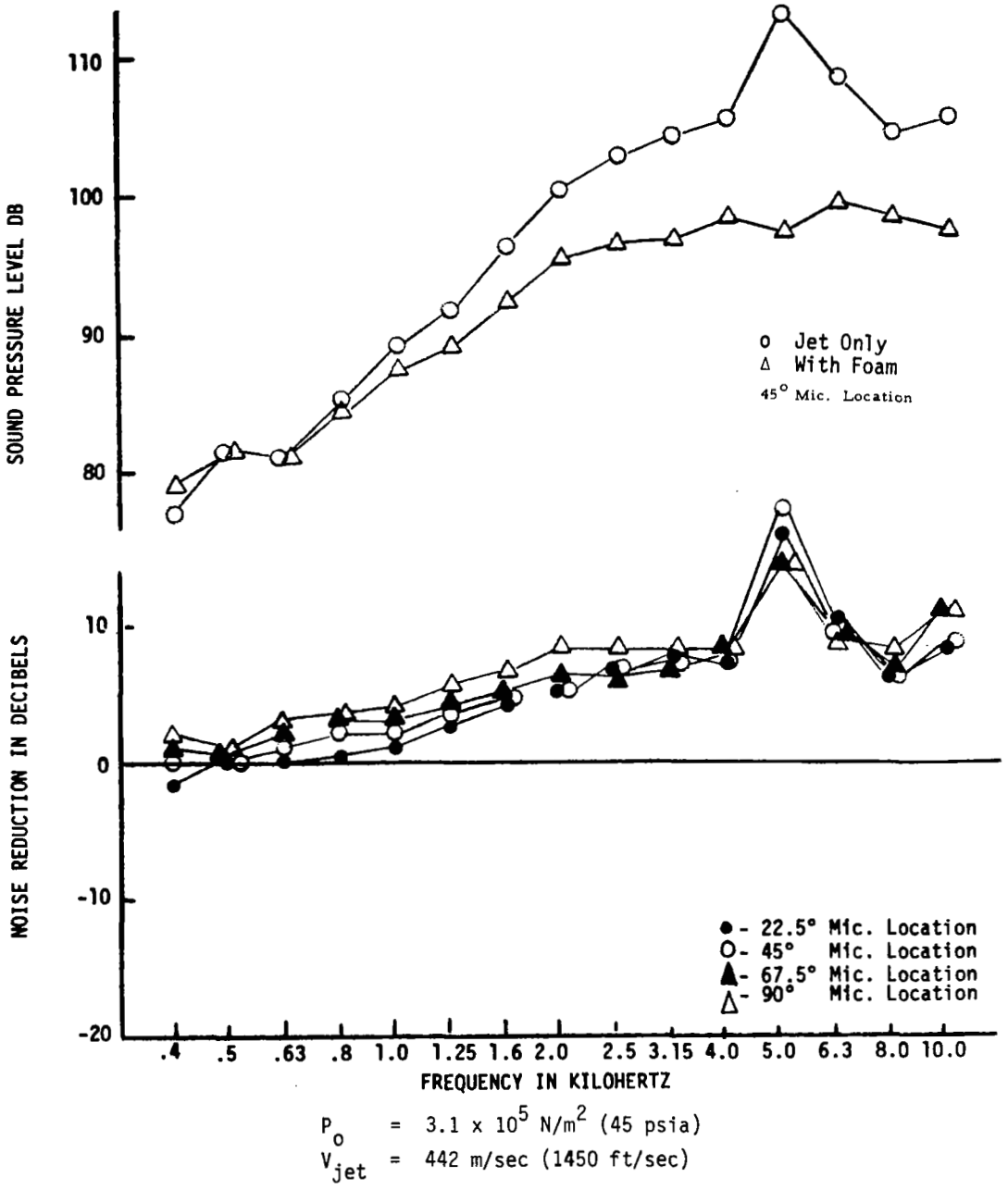

Figure 4-20. Jet Noise Reduction, Run No. 60, Convergent Divergent Nozzle

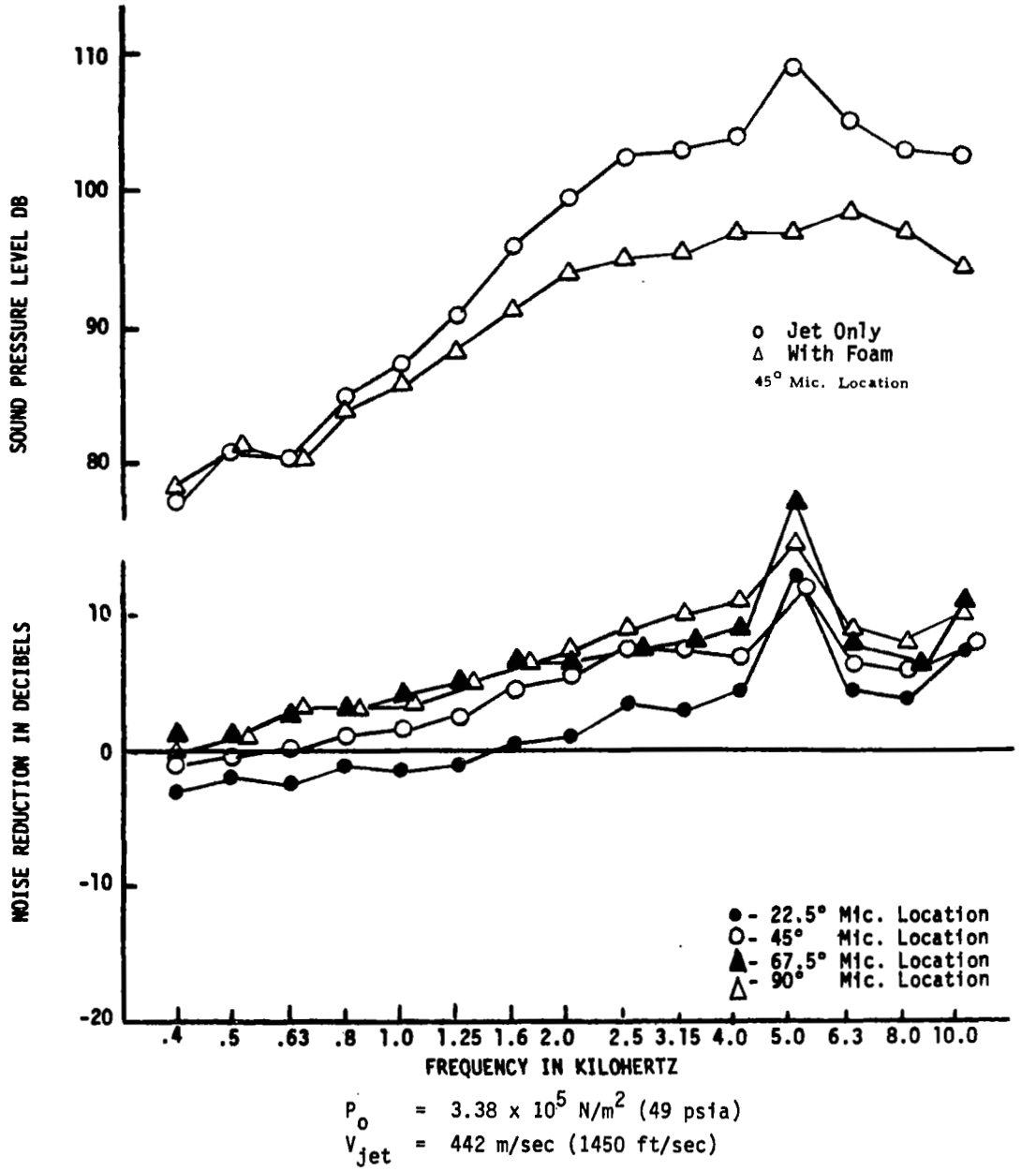

Figure 4-21. Jet Noise Reduction, Run No. 29, Convergent Divergent Nozzle

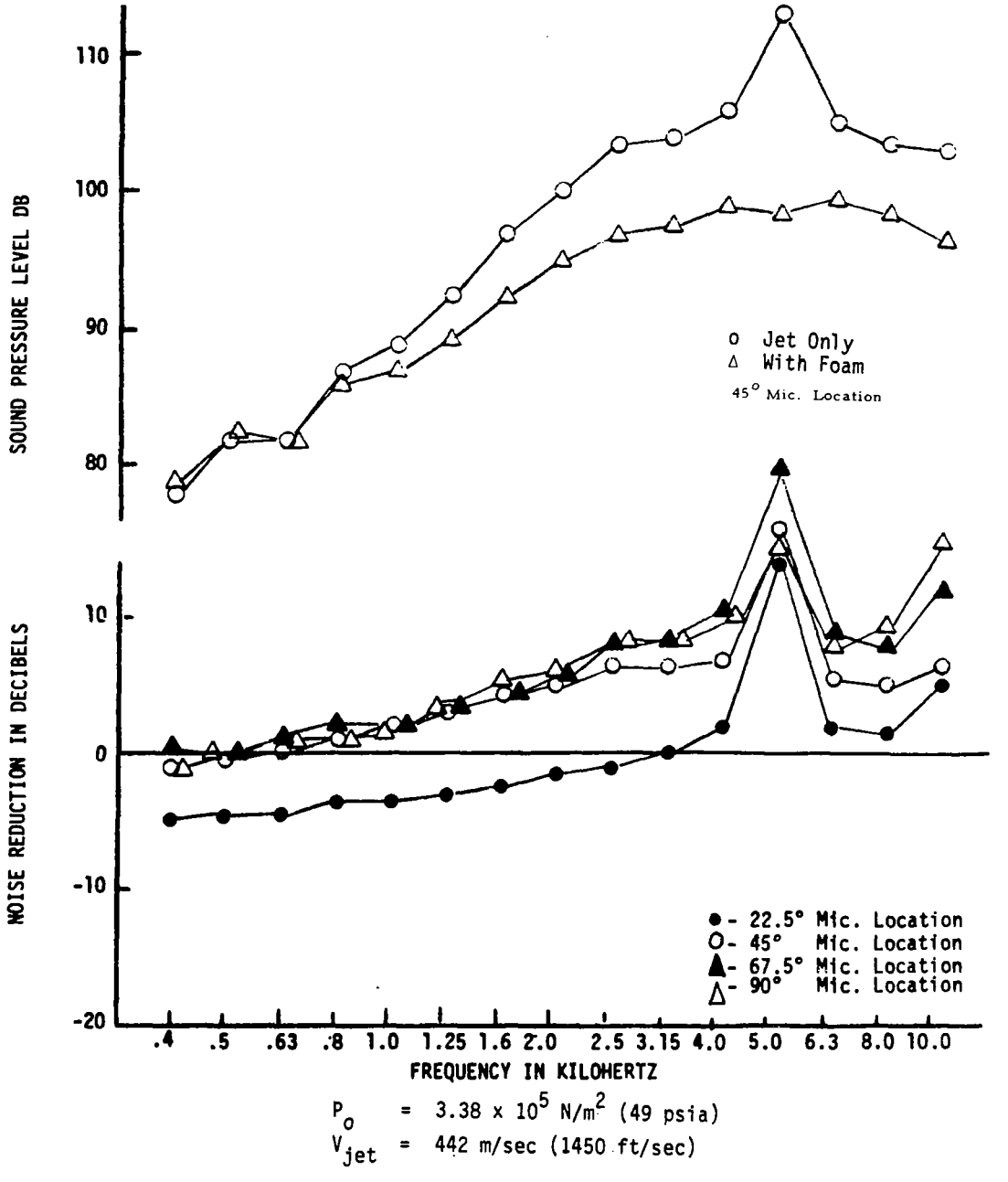

Figure 4-22. Jet Noise Reduction, Run No. 30, Convergent Divergent Nozzle

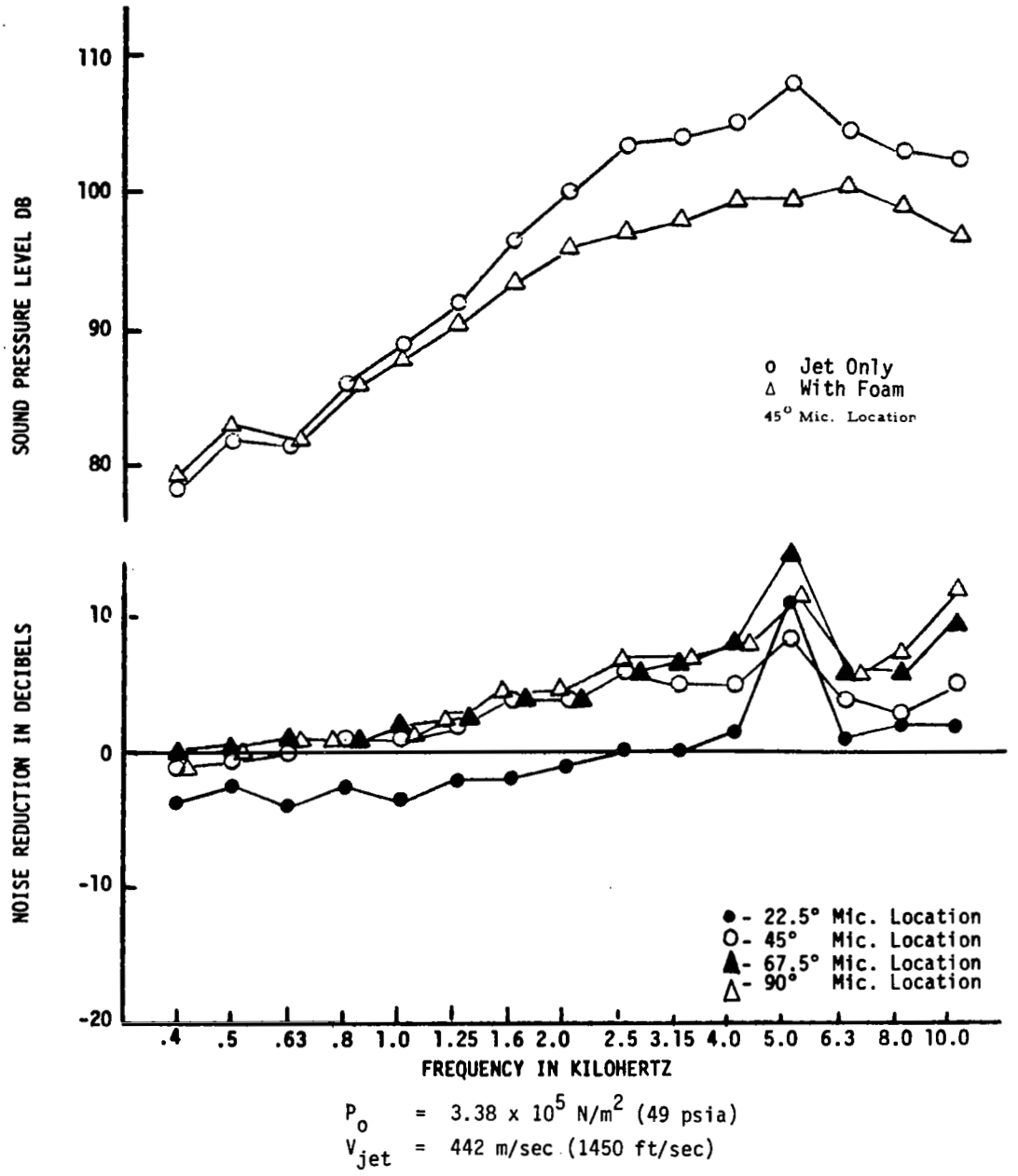

Figure 4-23. Jet Noise Reduction, Run No. 31, Convergent Divergent Nozzle

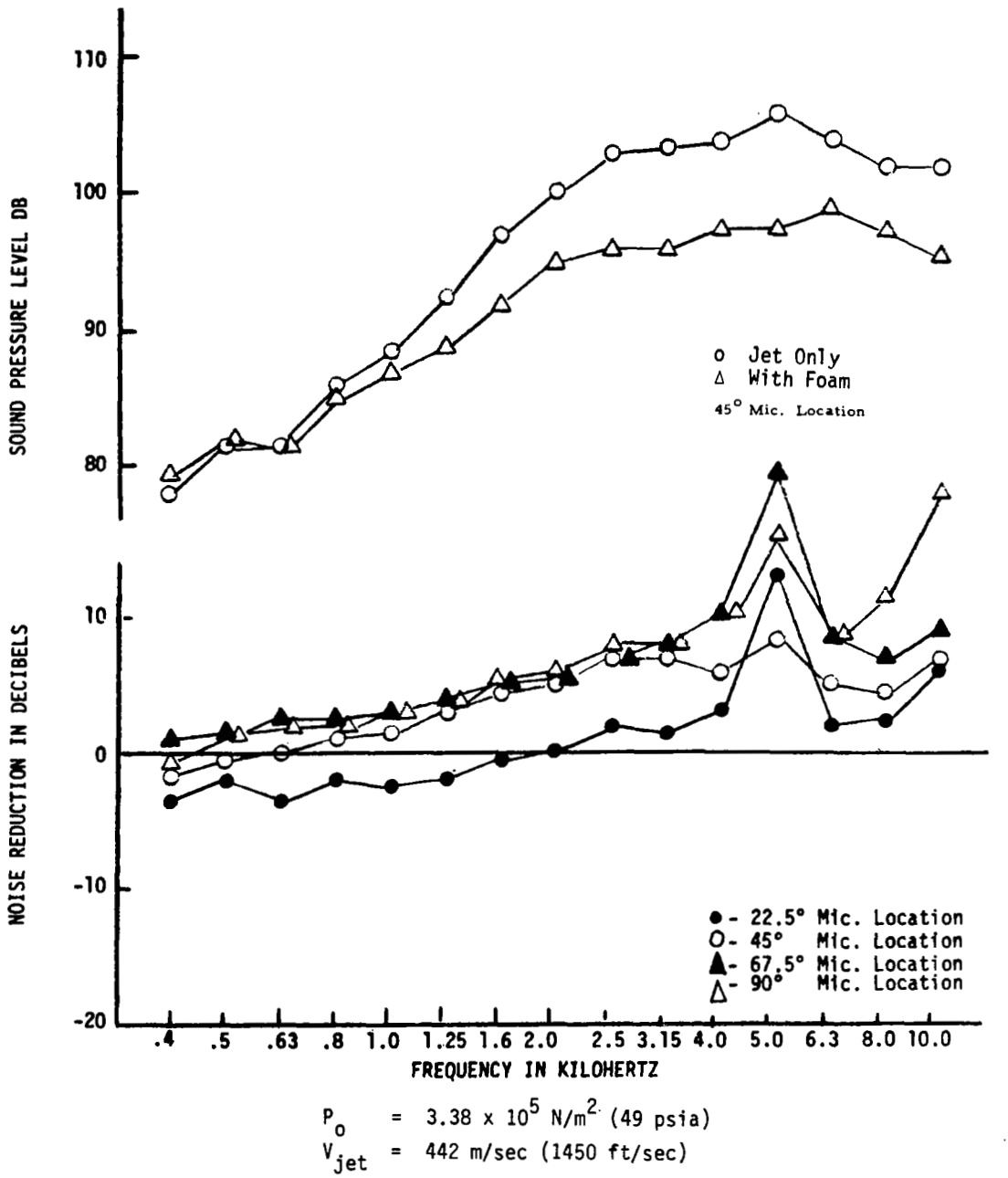

Figure 4-24. Jet Noise Reduction, Run No. 32, Convergent Divergent Nozzle

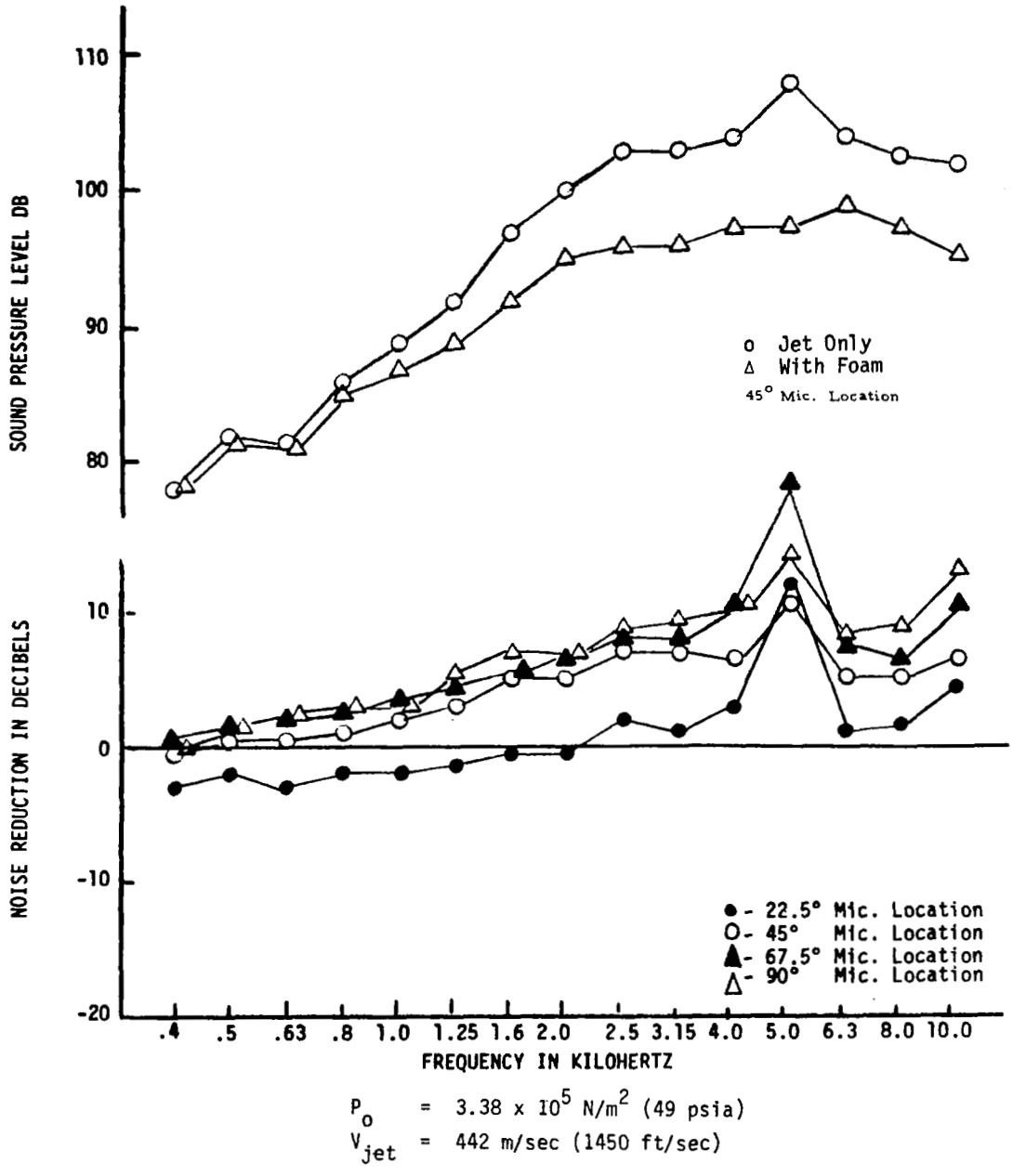

Figure 4-25. Jet Noise Reduction, Run No. 33, Convergent Divergent Nozzle

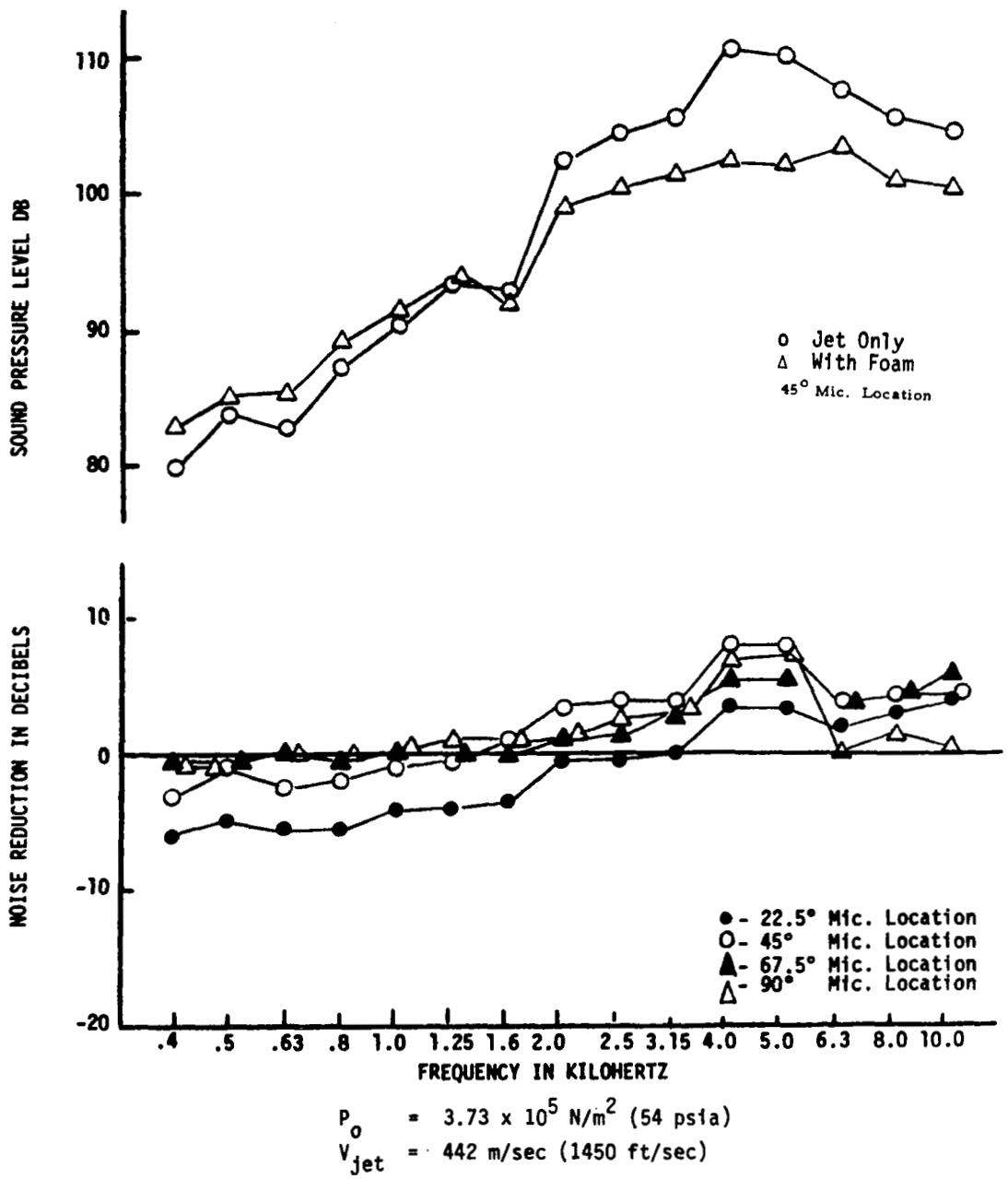

Figure 4-26. Jet Noise Reduction, Run No. 22, Convergent Divergent Nozzle

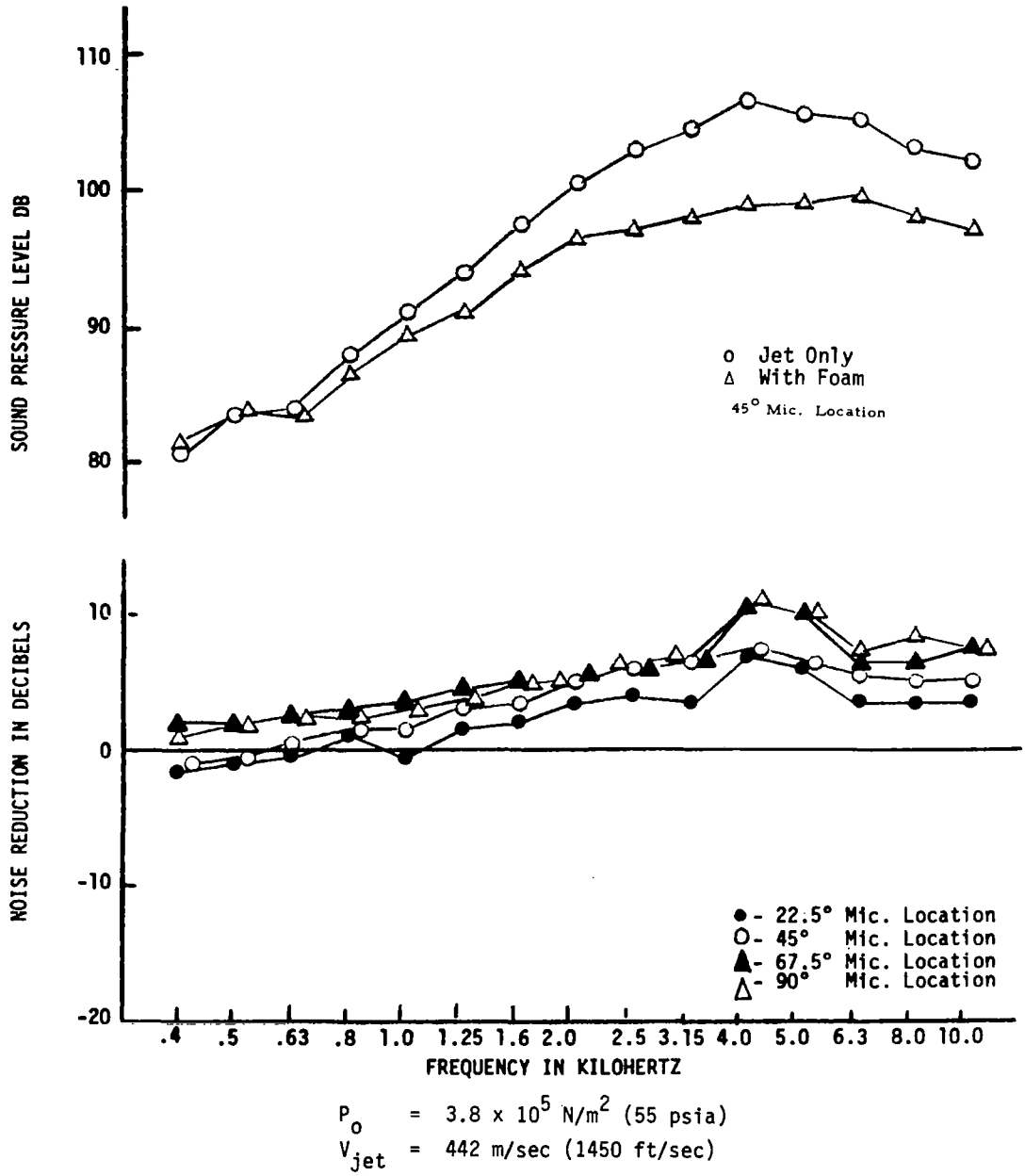

Figure 4-27. Jet Noise Reduction, Run No. 24, Convergent Divergent Nozzle

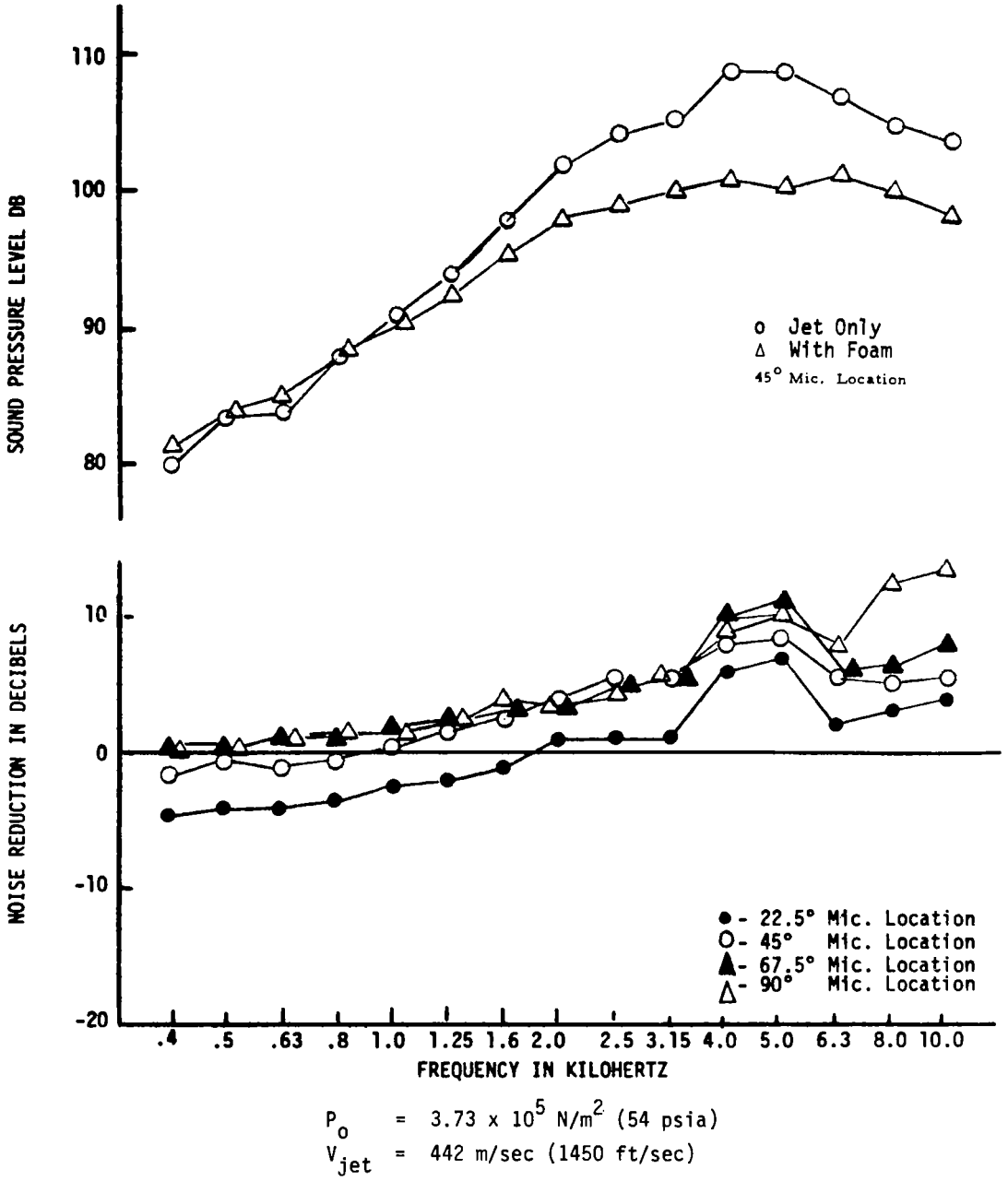

Figure 4-28. Jet Noise Reduction, Run No. 19, Convergent Divergent Nozzle

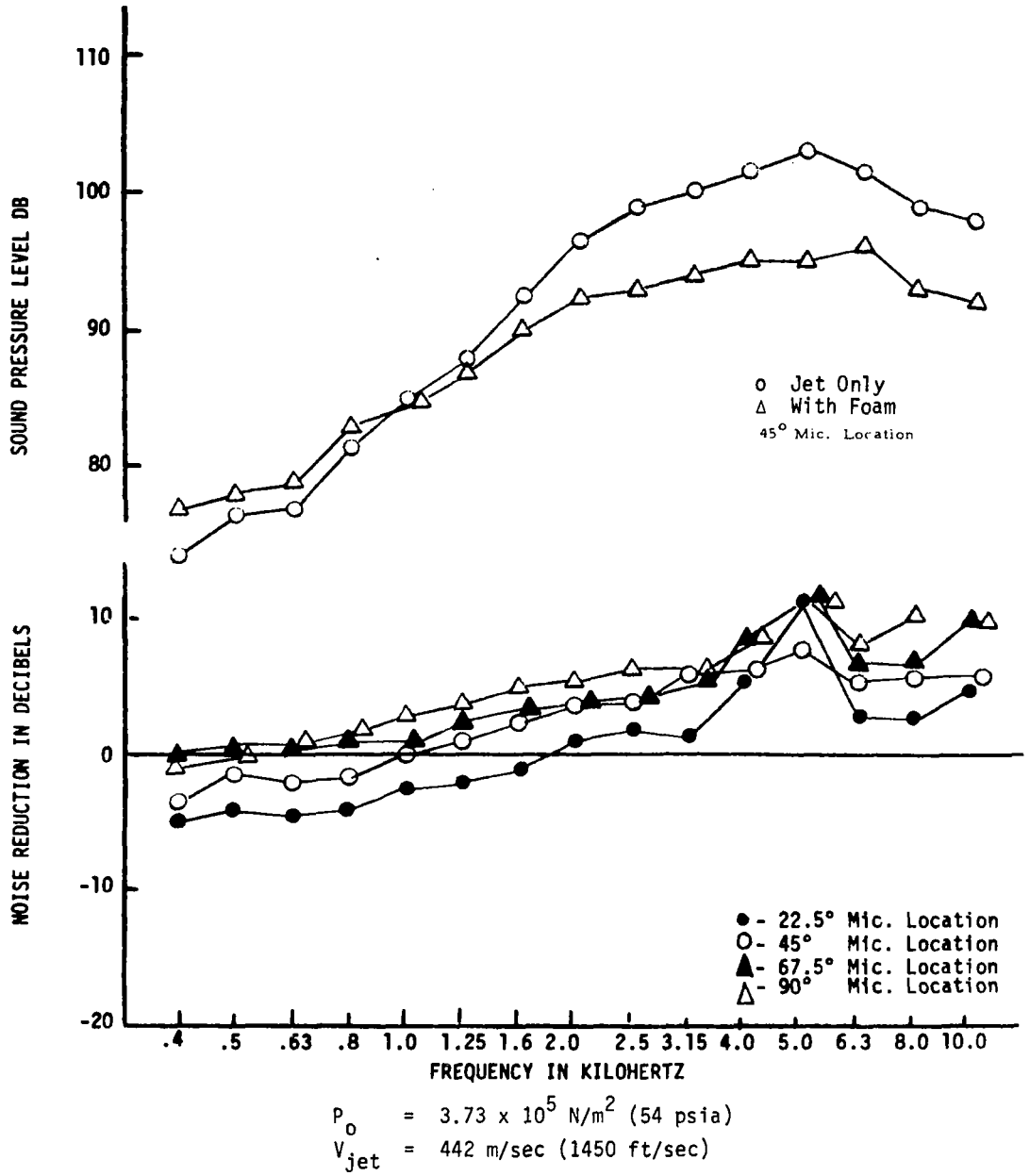

Figure 4-29. Jet Noise Reduction, Run No. 41, Convergent Divergent Nozzle

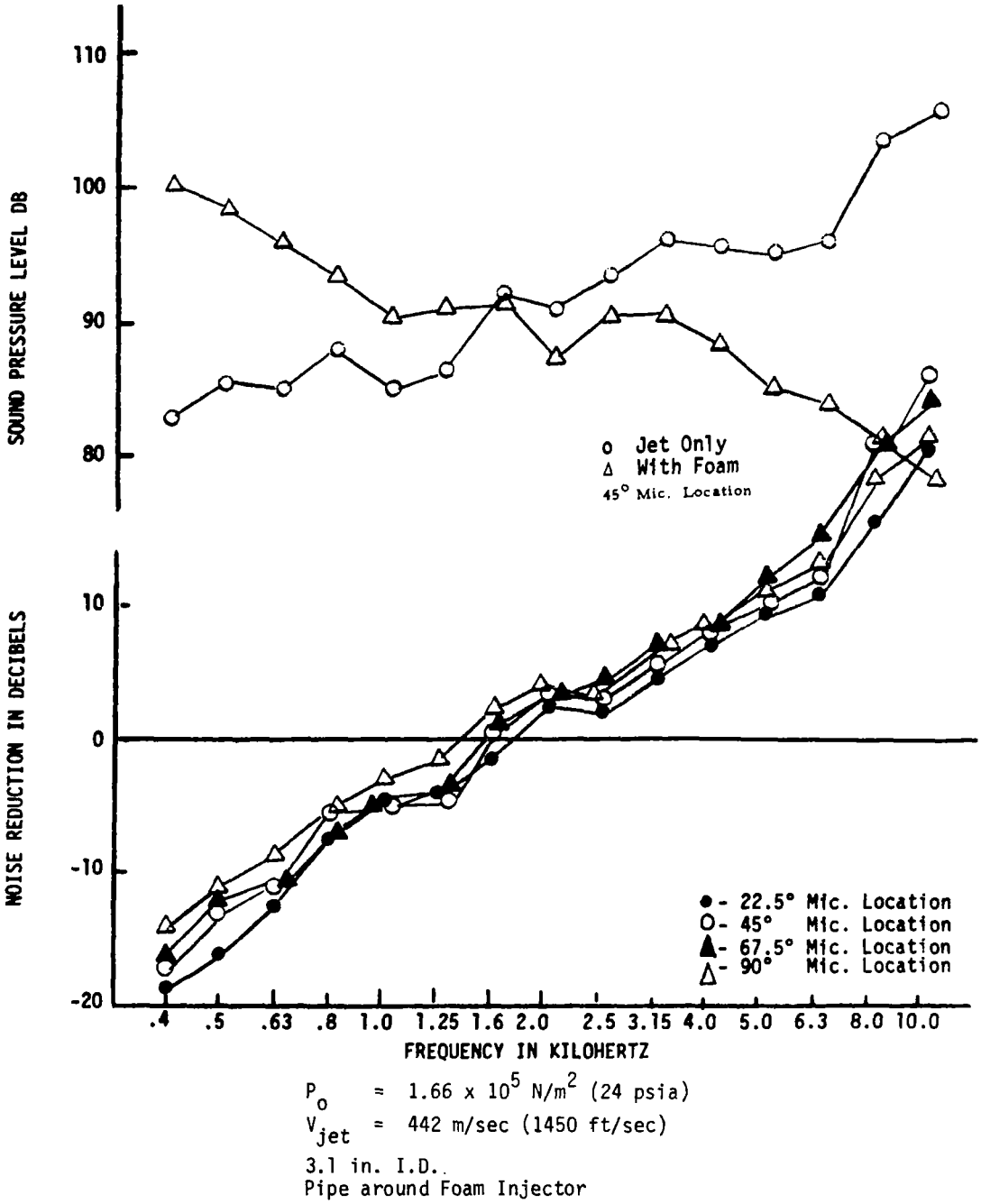

Figure 4-30. Jet Noise Reduction, Run No. 65, Convergent Divergent Nozzle

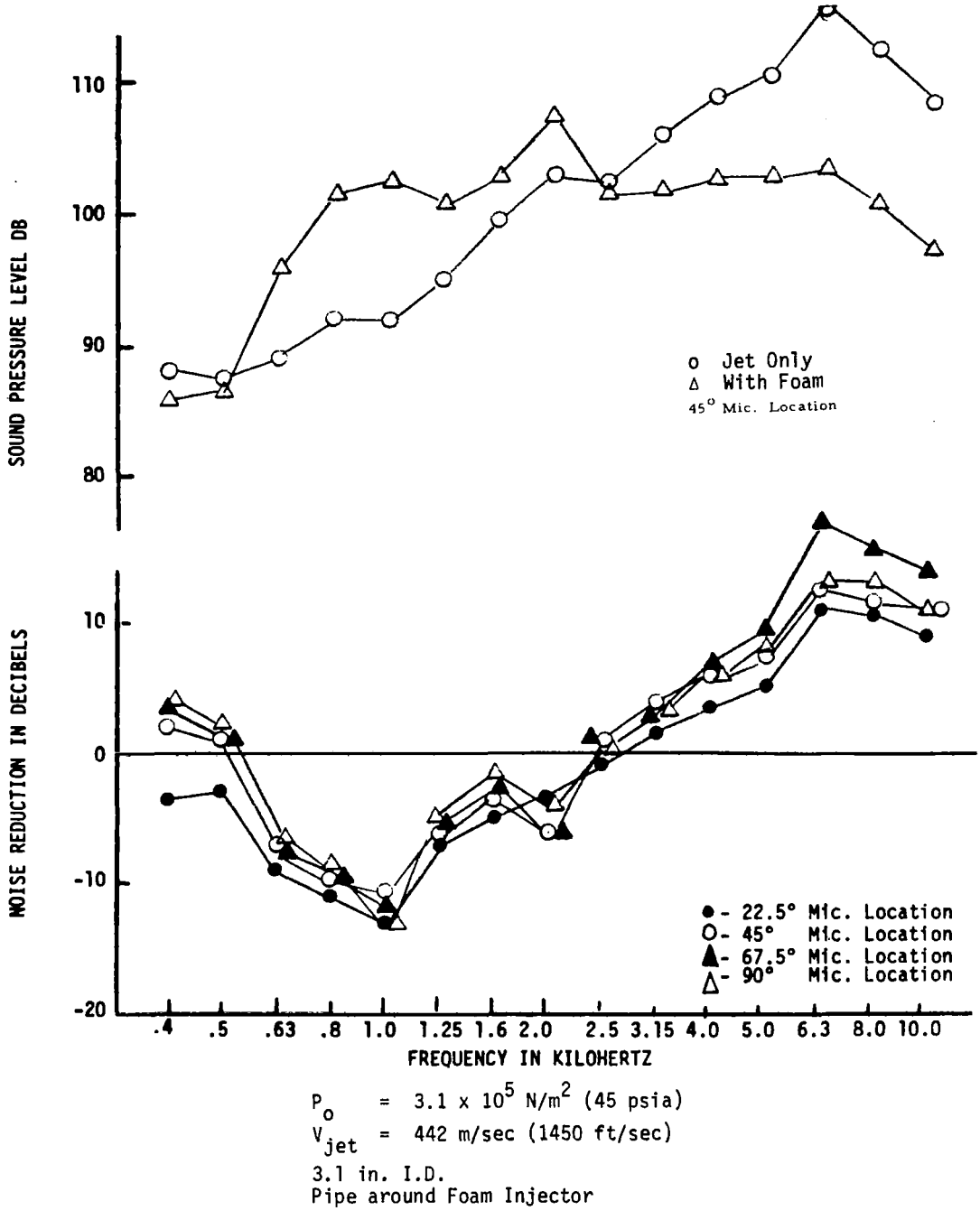

Figure 4-31. Jet Noise Reduction, Run No. 64, Convergent Divergent Nozzle

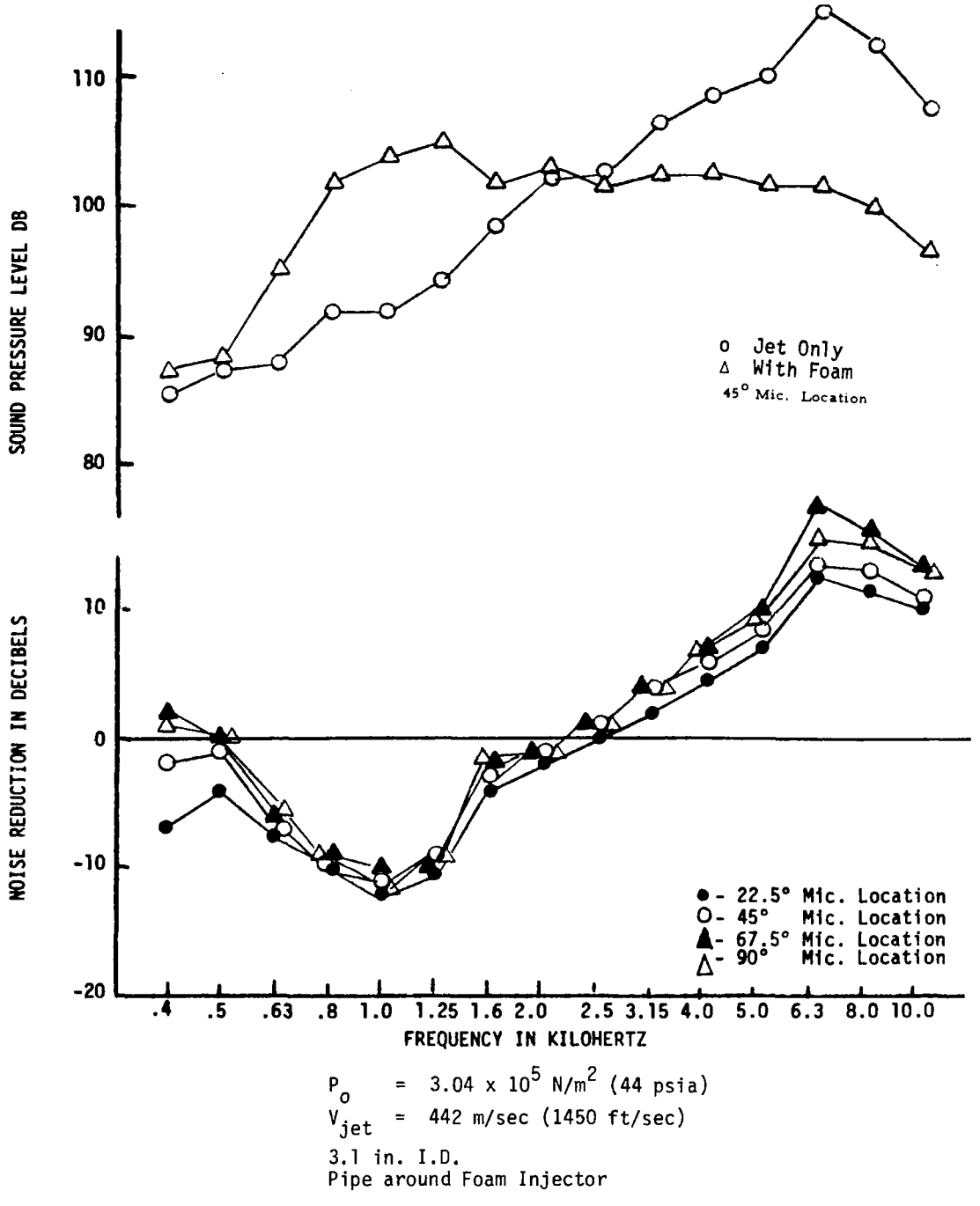

Figure 4-32. Jet Noise Reduction, Run No. 63, Convergent Divergent Nozzle

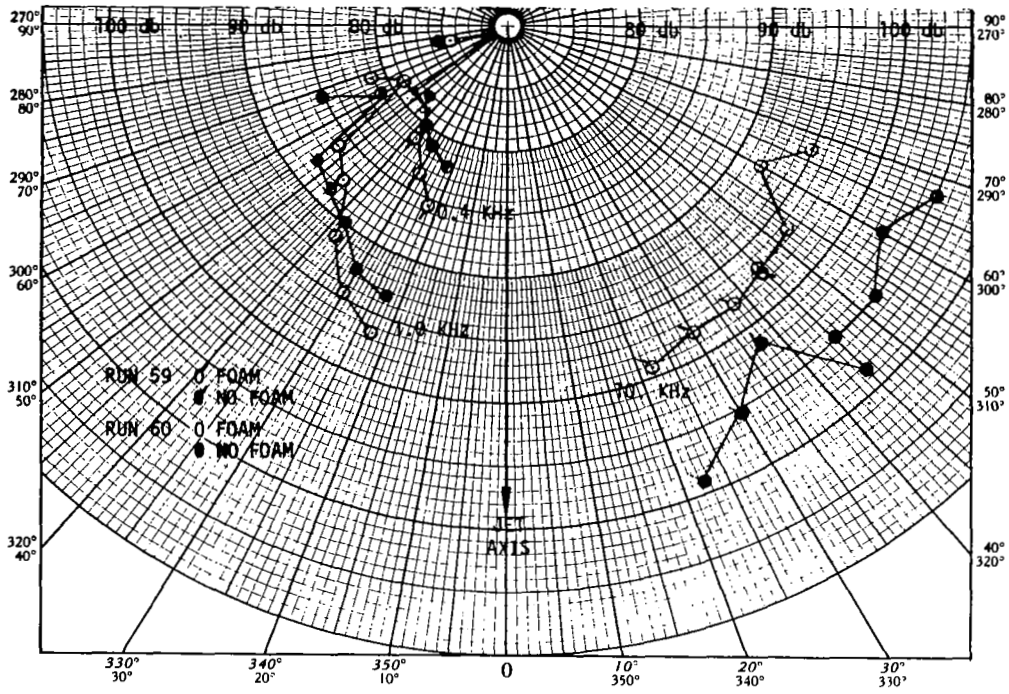

Figure 4-33. Polar Plot Sound Level Results for Runs 59 and 60, With and Without Foam, 0.4, 1.0, and 10 kHz

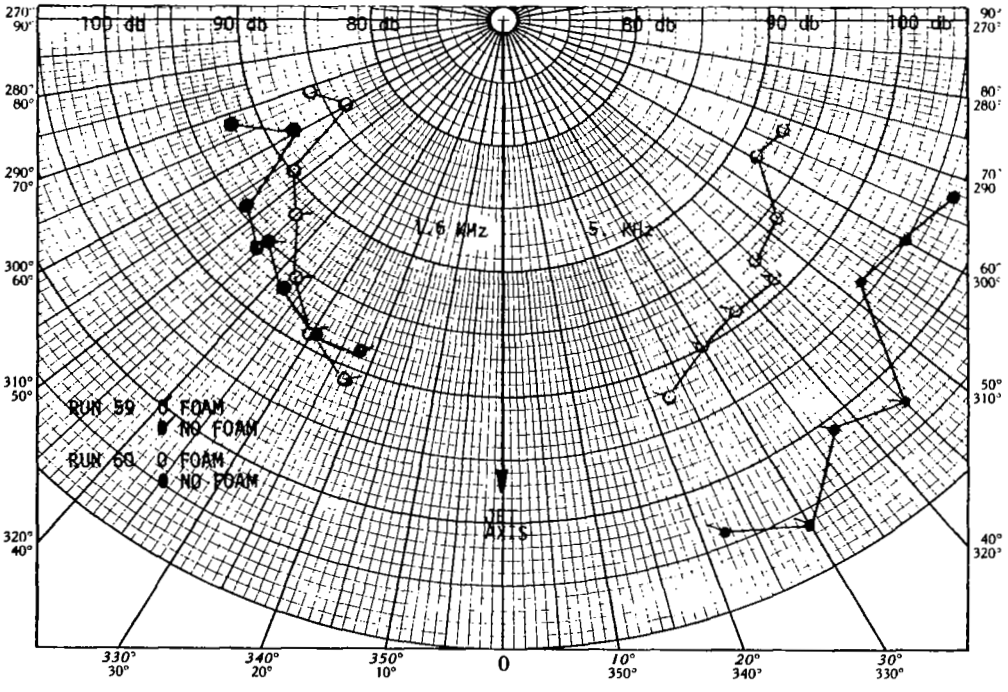

Figure 4-34. Polar Plot Sound Level Results for Runs 59 and 60, With and Without Foam, 1.6 and 5.0 kHz

Table 4-1. Model Gas Jet Noise Reduction Tests

Run	Noise		Jet			Foam				
Run #	Level PNdB Jet/ Jet + Foam	Reduction ΔPNdB	Po psia (6900psi =N/m^2)	Gas Flow kg./sec (2.2 $kg.s^{-1}$= lbs/sec.)	Thrust Jet/Jet + Foam lb_f (4.45 lb_f=N)	Injector Dia./Gap Inches	Agent	Concentration %	Liquid Flow kg/sec	Fig.
CONVERGENT NOZZLE, JET VELOCITY = 300 m/sec. (985 ft/sec)										
11	122.6/119.2	3.4	38	.352	29/31	2.25/0.050	Protein	10	.370	4-12
12	122.1/118.8	3.3	39	.347	30/32	2.25/0.050	Protein	3	.370	4-13
3	122.4/119.7	2.7	40	.347	29/30	2.25/0.050	Hi Ex	6	.300	4-14
4	122.8/119.4	3.4	40	.356	30/33	2.25/0.050	Hi Ex	6	.330	4-15
5	123.2/119.3	3.9	41	.362	31/34	2.25/0.050	Hi Ex	6	.370	4-16
6	123.5/119.4	4.1	42	.365	32/36	2.25/0.050	Hi Ex	6	.370	4-17
7	122.5/119.4	3.1	42	.365	32/35	2.25/0.050	Protein	10	.370	
9	(Max.=66dB)		Foam Only		-- --	2.25/0.050	Protein	10	.370	
CONVERGENT-DIVERGENT NOZZLE, JET VELOCITY = 442 m/sec (1450 ft/sec)										
25	113.1/107.9	5.2	27	.193	13/16	1.50/0.050	Hi Ex	6	.370	
13	111.8/111.0	.8	29	.204	13/16	2.25/0.050	Hi Ex	6	.370	
14	112.3/111.4	.9	31	.211	16/17	2.25/0.050	Hi Ex	6	.285	
44	124.5/121.3	3.2	42	.327	27/28	3.10/0.050	Protein	3	.300	4-18
43	124.6/118.4	6.2	43	.322	27/28	3.10/0.050	Protein	3	.315	4-18
42	126.6/118.7	7.9	43	.325	28/30	3.10/0.050	Protein	3	.370	4-18
59	129.3/119.2	10.1	44	.322	27/30	1.50/0.050	Protein	3	.315	4-19
60	129.3/118.9	10.4	45	.329	29/33	1.50/0.050	Protein	3	.315	4-20
54	127.9/117.7	10.2	45	.329	29/33	1.50/0.050	Protein	3	.370	
55	127.4/117.8	9.6	46	.329	29/32	1.50/0.050	Protein	3	.315	
56	126.5/118.9	7.6	46	.336	30/31	1.50/0.050	Protein	3	.300	
27	126.3/117.9	8.4	48	.360	32/38	1.50/0.050	Hi Ex	6	.370	
29	126.6/117.9	8.7	49	.360	32/36	1.50/0.050	Hi Ex	6	.370	4-21
30	129.2/119.8	9.4	49	.360	32/34	1.50/0.050	Hi Ex	6	.300	4-22
31	125.7/120.0	5.7	49	.367	31/34	1.50/0.050	Protein	3	.300	4-23
32	124.9/118.9	6.0	49	.367	33/37	1.50/0.050	Protein	3	.370	4-24
33	126.0/118.6	7.4	49	.367	32/37	1.50/0.050	Protein	10	.370	4-25
34	126.2/120.3	5.9	49	.367	33/35	1.50/0.050	Protein	10	.300	
35	123.1/114.1	9.0	48	.355	31/33	3.10/0.050	Protein	3	.370	
15	126.6/119.1	7.5	48	.354	33/36	2.25/0.050	Hi Ex	6	.370	
22	129.1/123.0	6.1	54	.395	38/40	1.50/0.100	Hi Ex	6	.370	4-26
24	126.1/120.1	6.0	55	.401	39/43	1.50/0.050	Hi Ex	6	.370	4-27
19	128.3/121.8	6.5	54	.390	37/40	2.25/0.050	Hi Ex	6	.370	4-28
41	121.7/115.9	5.8	54	.398	35/36	3.10/0.050	Protein	3	.350	4-29
57	126.4/120.1	6.3	54	.392	37/41	1.50/0.050	Protein	3	.370	
20	125.4/122.7	2.7	60	.442	43/47	2.25/0.050	Hi Ex	6	.370	
28	125.3/121.9	3.4	66	.494	49/54	1.50/0.050	Hi Ex	6	.370	
16	126.3/124.0	2.3	69	.508	52/55	2.25/0.050	Hi Ex	6	.370	
49	126.2/121.0	5.2	48	.347	31/31*	1.50.0.050	None	Water Only	.370	
65**	119.2/113.6	5.6	24	.163	5/6	Pipe* 0.050	Protein	3	.300	4-30
64	132.6/126.2	6.4	45	.324	19/25	Pipe* 0.050	Protein	3	.300	4-31
63	131.8/125.0	6.8	44	.322	19/24	Pipe* 0.050	Protein	3	.315	4-32

* Pipe - 3.1 in. inner diameter, 5 in. long

** Jet velocity subsonic

5. CONCLUDING REMARKS

The results of this first exploratory effort to determine the potential of liquid foams as a sound attenuation material are very encouraging. The program objectives have been met in the investigation described in this report. A basic understanding of the mechanisms of sound absorption in liquid foams has been reached both from the experimental phase and from the analytical model building effort.

Liquid foams have been shown to possess excellent fundamental sound absorbing characteristics. Further experimental and analytical work is needed to extend this work to flow conditions more realistically representative of future applications and to acquire sufficient insight into the sound propagation and absorption phenomena in foams.

In particular, methods more nearly adapted to the transient nature of liquid foam structures must be developed to obtain accurate measurements of their acoustic properties. Work is needed to fully understand the response of liquid foam structures to sound waves. There will be a possibility of producing foams having the desired properties for a given application when the influence of the many features of foam structures, such as bubble size distribution, liquid film thickness, surface tension and surface viscosity, etc., on the acoustic behavior of foams is understood. It is noted here that no surface chemistry work has been done so far. Existing fire-fighting foaming agents have been utilized without modification, though lighter and more shear-resistant foams were produced through a modification of the foam generators.

Jet noise abatement measurements should be made on larger and much hotter jets. The resulting low temperatures in the small cold jet experiments had the two-fold effect of presenting a totally different gas flow structure in the mixing region of the jet and of potentially freezing at least part of the ingested foam. Freezing would result in a definite deterioration of the compliance, and therefore of the sound absorption capability, of the foam. On the other hand foam destruction through bubble collapse and liquid evaporation in a hot jet will have unpredictable effects on noise abatement. Early foam destruction may be deleterious but evaporation, absorbing energy as it does, may increase sound absorption.

REFERENCES

1. H. Burge and N. Rodewald, "Advanced Rocket Engine Cooling Concept Program," TRW Systems Group, NASA CR-72594, February 1969.

2. J. S. Bikerman, Foams: Theory and Industrial Applications, Reinhold Publishing Corporation, New York, 1953.

3. S. Berkman and G. Egloff, Emulsions and Foams, Reinhold Publishing Corporation, New York, 1941.

4. A. M. Schwartz and J. W. Perry, Surface Active Agents, Vol. I, Interscience Pub. Inc., New York, 1949.

5. R. M. G. Boucher and A. L. Weiner, "Sonic Defoaming," Food Processing, October 1962.

6. Rubin and E. L. Gadden, "Foam Separation," New Chemical Engineering Separation Techniques Ch. 5, Ed. H. M. Schoen, Interscience Publ., New York, 1962.

7. C. R. Viswanadham, S. Singh, and U. Ranganathan, "Laboratory Test Methods for Foam Making Compounds Used in Fire Fighting," J. Sci. and Ind. Res, 19A, 10, October 1960.

8. D. N. Meldrum, J. R. Williams, and C. J. Conway, "Storage Life and Utility of Mechanical Fire-Fighting Foam Liquids," Fire Technology 1, 2, May 1965.

9. J. R. Williams, "A New Foam for Polar Solvents," Nat. Fire Protection Association Quarterly, 58, 1, July 1964.

10. D. N. Meldrum, J. R. Williams, and D. Gilroy, "Foam Fire Protection of Liquid Propellants," Fire Tech., 2, 3, August 1966.

11. C. S. Grove, Jr., G. E. Wise, Jr., W. C. Maish, and J. B. Gray, "Viscosity of Fire-Fighting Foam," Ind. and Eng. Chem., 43, 5, May 3, 1951.

12. R. J. French, "The Resistance of Fire-Fighting Foams to Destruction by Radiant Heat," J. Appl. Chem. 2, February 1952.

13. P. H. Thomas, "The Absorption of Radiant Heat by Fire-Fighting Foam," J. Appl. Chem., 9, Part 5, May 1959.

14. N. O. Clark, "The Electrical Conductivity of Foams," Trans. Faraday Soc., p. 13, 1948.

15. A. R. Aidun andC. S. Grove, Jr., "Novel Uses for Aqueous Foams," Che., Engr., 71, 4, 17 February 1964.

16. A. W. Adamson, Physical Chemistry of Surfaces, John Wiley Inc., 2nd Edition, p. 415, 1967.

17. N. O. Clark, "Fire-Fighting Foams," Chem. and Ind., January 10, 1948.

18. V. H. Edwards and R. K. Firm, "New Separation Techniques," AIChE Today Series 1968, Section IV.

19. L. A. Eggleston, "Fire Fighting Foam—Its Development and Progress," Fire Engineering, 118, No's 1, 2, 3, and 4, p. 38-40 January 1965; p. 34-6, February 1965; p. 46-7 and 75-6 March 1965; p. 58-9, 92-3, April 1965.

20. J. F. Fry, and R. J. French, "A Mechanical Foam-Generator for Use in Laboratories," J. Appl. Chem., 1, October 1951.

21. A, Mallock, "The Damping of Sound for Frothy Liquids," Proc. Royal Society, Series A, 84, 391-395, 1910.

22. J. Ackeret, "Experimental and Theoretical Investigations on Cavitation in Water," Tech. Mech. and Therm. 1, No. 1, Berlin, 1930.

23. L. Spitzer, Jr., NDRC Report No. 6, 1-sr 20-918, 1943.

24. L. Foldy, and E. Cartensen, J. Acoust. Soc. Am., 19, 481-501, 1947.

25. S. Gouse, "An Index to the Two Phase Gas—Liquid Flow Literature," M. I. T. Report 9, M. I. T. Press, Cambridge, Mass., 1966.

26. H. Karplus, and Clinch, Jr., "An Analytical Study of the Propagation of Pressure Waves," NASA CR 54015, May 31, 1963.

27. P. Epstein, "On the Absorption of Sound in Suspensions and Emulsions," Contributions to Applied Mechanics, Theodore von Karman Anniversary Volume, California Institute of Technology, 1941.

28. P. Epstein, and R. Carhart, "The Absorption of Sound in Suspensions and Emulsions, I. Water Fog in Air," J. Acoust. Soc. Am., Vol. 25, p. 533, 1953.

29. S. Temkin, and R. Dobbins, "Attenuation and Dispersion of Sound by Particulate Relaxation Pressures," J. Acoust. Soc. Am., Vol. 40, p. 317, 1966.

30. R. Dobbins, and S. Temkin, "Propagation of Sound in a Gas—Particle Mixture and Acoustic Combustion Instability," AIAA J., Vol. 5, p. 2182, 1967.

31. J. I. C., Lire, "Some Comments on the Use of Additives (Small Solid Particles) in the Jet Noise Problem," NASA SP-207, Basic Aerodynamic Noise Research, Conference held at NASA Headquarters, July 14-15, 1969.

32. L. Arnold, and S. Slutsky, "Attenuation of Plane Waves of Sound by Suspension of Resonating Particles," NASA SP-207, Basic Aerodynamic Noise Research, A Conference held at NASA Headquarters, July 14-15, 1969.

33. E. Silberman, "Sound Velocity and Attenuation in Bubbly Mixtures Measured in Standing Wave Tubes," J. of Acoustical Soc., 29, No. 8, p. 925, August 1957.

34. H. S. Ribner, "The Generation of Sound by Turbulent Jets," Advances in Applied Mechanics, Vol 8, Academic Press, 1969.

35. H. S. Ribner, "Jets and Noise," Canadian Aeronautics and Space Journal, October 1968.

36. H. T. Nagamatsu and R. E. Sheer, Jr., "Supersonic Jet Noise Theory and Experiments," NASA SP-207, Basic Aerodynamic Noise Research Conference, July 1969.

37. L. W. Lassiter and H. H. Hubbard, "Experimental Studies in Noise from Subsonic Jets in Still Air," NASA TN 2757, August 1952.

38. R. A. Scott, "An Apparatus for Accurate Measurement of the Acoustic Impedance of Sound Absorption Materials," Proc. Phys. Soc., Vol. 58, p. 253-264, 1940.

39. L. L. Beranek, Acoustic Measurements, John Wiley and Sons, Inc., p. 326.

40. R. A. Scott, "The Absorption of Sound in a Homogeneous Porous Medium," Proceedings of Physical Society, London. Vol. 58, 1940.

41. C. T. Molloy, "Propagation of Sound in Lined Ducts," J. of Acoustical Soc., Vol. 16, No. 1, p. 31-37, July 1944.

42. L. L. Beranek, Acoustics, Chapter 10, McGraw-Hill Book Co., 1954.

43. C. M. Harris, "Absorption of Sound in Air Versus Humidity and Temperature," NASA Contractor Report NASA CR-647, January 1967.

44. L. L. Beranek, Acoustic Measurements, John Wiley & Sons, Inc., p. 860, 1949.

45. Lord Rayleigh, Theory of Sound, Dover, 1945.

46. M. Minnaert, "On Musical Air-Bubbles and the Sounds of Running Water," Phil. Mag., 16, p. 235, 1933.

47. C. Devin, "Survey of Thermal Radiation and Viscous Damping of Pulsating Air Bubbles in Water," J. Acoustical Soc. of Am., 12, 31, December 1959.

48. M. Strasberg, "Gas Bubbles as Sources of Sound in Liquids," J. of Acoustical Soc. of A., 1, 28, January 1965.

49. H. G. Koger and G. Houghton, "Damping and Pulsation of Large Nitrogen Bubbles in Water," J. Acoustical Soc. of Am., p. 571, 43, 3, 1968.

50. G. Houghton, "Theory of Bubble Pulsation and Cavitation," J. of the Acoustical Society of America, Vol. 35, No. 9, September 1963.

51. H. Goldstein, Classical Mechanics, Addison-Wesley Publish Co., Inc., Reading Mass. p. 21, 1959.

52. T. F. Hueter and R. H. Bolt, Sonics, John Wiley and Sons, Inc., p. 402, 1955.

53. W. C. Johnson, Transmission Lines and Networks, McGraw Hill Book Company, Incorporated, p. 105.

54. W. V. Morgan, L. C. Sutherland, and K. J. Young, "The Use of Acoustic Scale Models for Investigating Near Field Noise of Jet and Rocket Engines," WADD TR 61-178, Boeing, 1961.

55. T. R. Strobridge, "The Thermodynamic Properties of Nitrogen 64 to 300°K between 0.1 and 200 Atmosphere," NBS TN 29.

56. G. P. Sutton, Rocket Propulsion Elements, Wiley and Sons, Inc., Second Edition.

57. K. D. Kryter and K. S. Pearsons, "Some Effects of Spectral Content and Duration on Perceived Noise Level," J. Acoust. Soc. Amer. 35, 866-883, 1963.

58. K. D. Kryter and K. S. Pearsons, "Modification of Noy Tables," J. Acoust. Soc. Amer., 36, 394-397, 1964.

59. H. S. Ribner, "The Generation of Sound by Turbulent Jets," Adv. in Applied Mechanics, Vol. 8, 1964.

BIBLIOGRAPHY

Acoustics

Alders, W. M., "Underwater Acoustics Handbook," 11, The Pennsylvania State University Press, University Park, Pennsylvania, 1965.

Anon., " NASA Acoustically Treated Nacelle Program," NASA SP-220, 1969.

Anon., "Progress of NASA Research Relating to Noise Alleviation of Large Subsonic Jet Aircraft," NASA SP-189, 1968.

Beltran, M., et al, " Liquid Rocket Engine Combustion Instability Studies," AFRPL-TR-66-125, Dynamic Science, A Division of Marshall Industries, July 1, 1966.

Beyer, R., " Nonlinear Acoustics," Physical Acoustics, by Warren P. Mason, Academic Press, 1965.

Chambri, P., "Speed of a Plane Wave in a Gross Mixture," J. Acoustical Soc. Am., 26, No. 3, 1954.

Davies, P. O. A. L., Fisher, M. J., and Barratt, M. J., "The Characteristics of the Turbulence in the Mixing Region of a Sound Jet," Fluid Mechanics, 15.

Deich, M., et al, "The Speed of Sound in Two-Phase Media," Teploenergetika 11, No. 8, 1964.

Eddington, R., "Investigation of Supersonic Shock Phenomena in a Two-Phase (Liquid-Gas) Tunnel," Tech. Rept. 32-1096, Jet Propulsion Laboratory, Pasadena, California, March 15, 1967.

Elder, S. A., "Cavitation Microstreaming," Acoustical Soc. of Am., 31, 1, January 1959.

Elliot, D., and Weinberg, E., "Acceleration of Liquids in Two-Phase Nozzles," Technical Report 32-987, Jet Propulsion Laboratory, Pasadena, California., July 1, 1968.

Harris, C. M., Handbook of Noise Control, Chapter 33, McGraw-Hill Book Co., Inc., New York, 1957.

Hsich, D., and Plesset, M., "On the Propagation of Sound in a Liquid Containing Gas Bubbles," Phys. of Fluids, 4, No. 8, 1961.

Karplus, H., "The Velocity of Sound in a Liquid Containing Gas Bubbles," C00-248, June 11, 1958.

Laurence, J. C., "Intensity, Scale, and Spectra of Turbulence in Mixing Region of Free Subsonic Jet," NACA Report 1292, 1956.

Levin, S. M., "Aircraft Noise—Can it be Cut," Space Aeronautics, August 1966.

Lighthill, M. J., "Jet Noise," AIAA Journal, Vol. 1, No. 7, p. 1507, 1963.

Lighthill, M. J., "On Sound Generated Aerodynamically, Part I: General Theory," Proc. Roy. Sec., London 211A, 564-87, 1107, March 20, 1952.

Mangulis, U., "Acoustic Radiation from a Piston in a Layered Medium with Application to a Layer Containing Bubbles," J. Acoustical Soc. of Am., 40, 5, p. 1083, 1966.

Mason, W. P., Physical Acoustics Principles and Methods, Vol. II, Part B—" Properties of Polymers and Nonlinear Acoustics," Academic Press, New York, 1965.

Meyer, E., and Tamm, K., "Natural Vibration and Damping of Gas Bubbles in Liquids," David Taylor Model Basin Translation 109, AD 662 651, April 1943.

Steinberg, M. S., "Resonance Scattering of Sound by a Small Gaseous Object of Arbitrary Form," J. Acoustical Soc. of Am., 41, 5, p. 1352, 1967.

Tangren, R. F., Dodye, C. H., and Seifert, H. S., "Compressibility Effects in Two-Phase Flow," J. Applied Physics, 20, 7, July 1949.

Woo, S. H., and Paslay, P. R., "Nonlinear Oscillations of a Bubble," J. Acoustical Soc. of Am., 42, 1, p. 114, 1967.

Wood, A., Textbook of Sound, the Macmillan Company, New York, 1941.

Wood, A. B., A Textbook of Sound, London, G. Bell and Sons Ltd., 1960.

Wylie, C. R., Advanced Engineering Mathematics, Chapter 4, McGraw-Hill Book Co., Inc., New York, 1951.

Young, R. W., and Peterson, A., "On Estimating Noisiness of Aircraft Sounds," J. Acoustical Soc. of Am., 45, No. 4, p. 834, 1969.

Foam

Cray, "High-Expansion Foam," NFPA Quarterly, July 1964.

Dorsey, A. E., "Control of Foam During Fermentation by the Application of Ultrasonic Energy," J. Bio, Micro. Tech. and Engr., 1, 3, p. 289, 1959.

BIBLIOGRAPHY (Continued)

Drouhin, R., "La Formation des Lits de Mousse et Leur Application au Transfert de Chaleur et de Matière," Genie Chimique, 85, 1, January 1961.

Moffitt, W. E., and Jamison, W., "Industry Uses High Expansion Foam," 118, 10 October 1965.

Sun, Shiou-Chuan, "Destruction of otation Froth with Intense High-Frequency Sound," Mining Eng. 865, 1951.

Tuve, R. L., "Light Water and Potas m Bicarbonate Dry Chemical— A New Two-Agent Extinguishing Sy tem," NFPA Quarterly, July 1964.